# Core-shell particles at fluid interfaces: Performance as interfacial stabilizers

**Christian Buchcic**

**Thesis committee**

**Promotor**

Prof. Dr M.A. Cohen Stuart
Emeritus Professor of Physical Chemistry and Colloid Science
Wageningen University

**Co-promotors**

Dr R.H. Tromp
Senior Scientist, NIZO food research, Ede
Associate Professor, Physical and Colloid Chemistry
Utrecht University

Dr M.B.J. Meinders
Senior Scientist, Food and Biobased Research
Wageningen UR

**Other members**

Prof. Dr E. van der Linden, Wageningen University

Dr M.H.G. Duits, University of Twente

Dr C. Monteux, ESPCI Paris, France

Prof. Dr R. Tuinier, Eindhoven University of Technology

This research was conducted under the auspices of the Graduate School VLAG (Advanced studies in Food Technology, Agrobiotechnology, Nutrition and Health Sciences).

# Core-shell particles at fluid interfaces: Performance as interfacial stabilizers

**Christian Buchcic**

**Thesis**

submitted in fulfilment of the requirements for the degree of doctor

at Wageningen University

by the authority of the Rector Magnificus

Prof. Dr A.P.J. Mol,

in the presence of the

Thesis Committee appointed by the Academic Board

to be defended in public

on Wednesday 14 September 2016

at 4 p.m. in the Aula.

Christian Buchcic

Core-shell particles at fluid interfaces: Performance as interfacial stabilizers,

150 pages.

PhD thesis, Wageningen University, Wageningen, NL (2016)

With references, with summary in English

ISBN 978-94-6257-896-8

DOI http://dx.doi.org/10.18174/387982

## Abstract

There is a growing interest in the use of particles as stabilizers for foams and emulsions. Applying hard particles for stabilization of fluid interface is referred to as Pickering stabilization. By using hard particles instead of surfactants and polymers, fluid interfaces can be effectively stabilized against Ostwald ripening and coalescence. A drawback of the use of hard particles as interfacial stabilizers is that they often experience a pronounced energy barrier for interfacial adsorption and that hard particles are very specific with regard to the type of fluid interface they can adsorb to. Soft particles, on the other hand, are known as good stabilizers against coalescence and they spontaneously adsorb to a variety of different fluid interfaces.

The aim of this thesis was to investigate core-shell particles comprising a hard core and soft shell with regard to their interfacial behaviour and their ability to act as sole stabilizers for foams and emulsions. We hypothesised that the presence of the soft shell allows for easier interfacial adsorption of core-shell particles compared to the hard core particles only. To test this hypothesis, we prepared core-shell particles comprising a solid polystyrene (PS) core and a soft poly-N-isopropylacrylamide (PNIPAM) shell. To ascertain the effect of shell thickness, we prepared a range of core-shell particles with different shell thicknesses, containing identical core particles. We found that core-shell particles are intrinsically surface active and can generate high surface pressures at the air-water interface and oil-water interfaces, whereas core particles seemed to experience a large energy barrier for interfacial adsorption and did not lower the surface tension. We also confirmed by microscopy that core-shell particles are actually adsorbing to the fluid interface and form densely packed interfacial layers. Further, we found that a certain critical thickness of the soft shell is necessary in order to ensure facile interfacial adsorption. If the PNIPAM shell on top of the core particles is well above 100nm thick, particle adsorption at the air-water interface was found to be diffusion limited.

By gentle hand-shaking we were able to produce dispersion of air bubbles and emulsion droplets solely stabilized by core-shell particles. The resulting bubbles still underwent Ostwald ripening, albeit slowly. For oil-in-water emulsions of hexane and toluene, both of which have a relatively high solubility in the continuous phase, we found that core-shell particles can stop Ostwald ripening. The resulting emulsion droplets adopted pronounced non-spherical shapes, indicating a high elasticity of the interface. The high stability and the remarkable non-spherical shape of the emulsion droplets stabilized by core-shell particles were features we also observed for fluid dispersion stabilized by hard particles. This shows that in terms of emulsion stability core-shell particles behave similar to hard particles as interfacial stabilizer.

As to why the differences between the stability of bubble and oil dispersions arise could not be finally answered. Yet, microscopic analysis of the interfacial configuration of core-shell particles at the air-water interface reveals some peculiar insights which may suggest that core-shell particles adsorb in a polymer-like fashion with the soft PNIPAM shells adsorbing to the air-water interface only, while the hard PS cores reside in the continuous phase.

In summary, we showed that core-shell particles with a hard core and a soft shell can indeed combine the advantageous properties of hard and soft particles. The soft shell enables spontaneous adsorption to a variety of fluid interfaces. Despite their spontaneous adsorption, core-shell particles strongly anchor and do not spontaneously desorb from the fluid interface again. Further, the hard core provides enough rigidity to the core-shell particles to allow the establishment of a stress bearing interfacial particle network. This network eventually stops Ostwald ripening in oil-in-water emulsions. Our results therefore show that in the case of oil-water interfaces, core-shell particles can perform better than solely hard particles as interfacial stabilizers.

# Table of Contents

**Chapter 1 General Introduction ..... 1**

1.1. Instabilities in foams and emulsions ..... 2

1.2. Mechanisms and actions of common interfacial stabilizers ..... 3

1.3. Particles as interfacial stabilizers ..... 5

1.3.1. Advantages of particles over other interfacial stabilizers ..... 5

1.3.2. Hard particles as interfacial stabilizers ..... 6

1.3.2.1. Characteristics of hard particles at fluid interface ..... 6

1.3.2.2. Structure bubbles & emulsion droplets stabilized by hard particles ..... 7

1.3.2.3. Formation of a colloidal amour prevents Ostwald ripening ..... 7

1.3.2.4. Capillary mechanism for thin film and coalescence stability ..... 9

1.3.3. Soft particles as interfacial stabilizers ..... 10

1.3.3.1. Characteristics of soft particles at fluid interfaces ..... 10

1.3.3.2. Structure of emulsion droplets stabilized by soft particles ..... 11

1.3.3.3. Viscoelastic properties of interfaces stabilized by soft particles ..... 12

1.3.3.4. Coalescence and thin film stability of dispersions stabilized by soft particles ..... 12

1.3.4. Kinetics of particle adsorption to the fluid interface ..... 13

1.3.5. Differences between hard and soft particles as interfacial stabilizer ..... 14

1.4. Aim and outline of the thesis ..... 16

**Chapter 2 Assembly of jammed colloidal shells onto micron-sized bubbles by ultrasound ..... 23**

2.1. Introduction ..... 24

2.2. Experimental details ..... 27

2.2.1. Materials ..... 27

2.2.2. Synthesis of colloidal particles ..... 27

2.2.3. Characterization of colloids by light scattering ..... 27

2.2.4. Electrokinetic charge of the colloidal particles ..... 28

2.2.5. Ultrasonic treatment ..... 28

2.2.6. Bubble size characterization ..... 28

2.2.7. Exposure of bubbles to surfactants ..... 29

2.2.8. Contact angle measurements ..... 29
2.2.9. Tensiometry ..... 29
2.3. Results and Discussion ..... 29
2.3.1. Colloidal Particle Synthesis & Characterization ..... 29
2.3.2. Bubble size ..... 30
2.3.3. Influence of process parameters on bubble yield ..... 32
2.3.4. Interfacial structure of the bubbles ..... 33
2.3.5. Effect of surfactant exposure on the bubble stability ..... 37
2.4. Conclusion ..... 38

**Chapter 3 Synthesis & stimuli-responsive properties of core-shell particles... 43**
3.1. Introduction ..... 44
3.2. Material & Methods ..... 44
3.2.1. Materials ..... 44
3.2.2. Synthesis Core particles ..... 45
3.2.3. Synthesis core-shell particles ..... 45
3.2.4. Electrolyte titration ..... 46
3.2.5. Dynamic Light Scattering (DLS) / Micro-electrophoresis ..... 46
3.3. Results & Discussion ..... 46
3.3.1. Influence of temperature on colloidal stability and size of core-shell particles ..... 47
3.3.2. Influence of electrolyte concentration on size and colloidal stability of core-shell particles ..... 49
3.3.3. Influence of pH on core-shell particles ..... 50
3.4. Conclusion ..... 52

**Chapter 4 Harnessing the advantages of hard and soft colloids by use of core-shell particles as interfacial stabilizers ..... 53**
4.1. Introduction ..... 54
4.2. Material & Methods ..... 56
4.2.1. Materials ..... 56
4.2.2. Synthesis core particles ..... 57
4.2.3. Synthesis core-shell particles ..... 57

4.2.4. Dynamic Light Scattering ..... 57
4.2.5. Tensiometry ..... 58
4.2.6. Light microscopy ..... 58
4.2.7. Cryo-scanning electron microscopy ..... 58
4.3. Results & Discussion ..... 59
4.3.1. Interfacial tensiometry ..... 59
4.3.2. Microscopic analysis of core-shell particles at the fluid interface ..... 62
4.3.3. Stabilization of bubbles and emulsion droplets by core-shell particles ..... 66
4.4. Conclusion ..... 68

**Chapter 5 Equation of state of core-shell particles adsorbed at the air-water interface ..... 73**
5.1. Introduction ..... 74
5.2. Material & Methods ..... 76
5.2.1. Materials ..... 76
5.2.2. Synthesis core-shell particles ..... 76
5.2.3. Size determination by dynamic light scattering ..... 77
5.2.4. Langmuir trough measurement of compression isotherm ..... 77
5.3. Results and Discussion ..... 78
5.3.1. Surface pressure-area isotherms ..... 78
5.3.2. Microscopic analysis of interfacial structure ..... 82
5.4. Conclusion ..... 89

**Chapter 6 Adsorption behaviour core-shell particles at air-water interface .... 93**
6.1. Introduction ..... 94
6.2. Materials & Methods ..... 95
6.2.1. Materials ..... 95
6.2.2. Synthesis core-shell particles ..... 95
6.2.3. Measurement of surface tension ..... 95
6.2.4. Drop-exchange experiment ..... 95
6.2.5. Cryo-scanning electron microscopy ..... 96
6.2.6. Dark field light microscopy ..... 96
6.3. Results & Discussion ..... 96

6.3.1. Assessment particle adsorption dynamics by tensiometry ..... 96
6.3.2. Assessment particle desorption by droplet profile analysis tensiometry . 103
6.3.3. Determination of the interfacial structure of core-shell particles by scanning electron microscopy (SEM) and epi-illumination dark field microscopy..... 104
6.4. Conclusion ..... 107

**Chapter 7 General Discussion..... 111**
7.1. Performance of hard particles as interfacial stabilizers..... 112
7.1.1. Sonication for assembly of particle stabilized bubbles ..... 112
7.1.2. Effect of electrolyte on the ability of hard particles to adsorb onto the fluid interface ..... 114
7.1.3. Influence of particle wettability on the adsorption of hard particles onto fluid interfaces ..... 116
7.1.4. Surface pressure development due to particles adsorption at the fluid interface ..... 118
7.1.5. Structure of bubbles/droplets stabilized by hard particles ..... 120
7.2. Performance of core-shell particles as interfacial stabilizers..... 121
7.2.1. Adsorption of core-shell particles at fluid interfaces ..... 121
7.2.2. Elastic properties of interfacial layers covered by core-shell particles.... 122
7.2.2.1. Air-water interface..... 122
7.2.2.2. Oil-water interface..... 124
7.2.3. Tuning the dilational response of particle-laden fluid interfaces ..... 124
7.2.4. Stability of particle stabilized dispersions ..... 125
7.3. Performance of core-shell particles as interfacial stabilizers in comparison to hard particles..... 125

**Summary.....129**
**Acknowledgement.....133**
**Scientific Publications .....137**
**Overview of completed training activities.....139**

Chapter1

# Introduction

## 1.1. Instabilities in foams and emulsions

Fluid interfaces are the boundaries between two different fluid phases. Examples are the boundary between a liquid and a gas, or between two immiscible liquids. The formation of such interfaces costs energy because intermolecular forces in each of the respective materials must be overcome in order to bring bulk molecules to the interface. The work which needs to be expended in order to create additional interfacial area is the surface tension (dimension of force per unit length, mN $m^{-1}$) or interfacial free energy (mJ $m^{-2}$).

The most prominent examples of systems of which the behaviour is seriously affected by the existence of an fluid interface are foams and emulsions. These are disperse systems in which the disperse phase consists of bubbles or droplets. These bubbles and droplets may be of micron-sized dimension in which case the surface-to-volume ratio of the disperse phase is very high and the resulting interfacial free energy becomes significant with respect to the internal energy of the system. One consequence is that bubbles and drops tend to be spherical, as this shape has the lowest surface area for a given volume. Further thermodynamically driven minimization of the free energy associated with the existence of the fluid interface occurs via the processes of coalescence and Ostwald ripening, both of which can ultimately lead to a complete phase separation of the different phases in contact with each other.

Ostwald ripening is the pressure-driven exchange of material between small and large bubbles or droplets of a dispersion. The process is driven by the difference in Laplace pressure $P_L$ (the pressure difference between in- and outside of the bubble/droplet) between differently sized bubbles/droplets of the dispersed phase. The Laplace pressure is given as:

$$P_L = \frac{2\sigma}{R} \qquad (1)$$

where $\sigma$ is the interfacial tension and $R$ is the radius of the bubble/droplet. Equation 1 implies that the pressure inside small drops (bubbles) is higher than inside big drops (bubbles). Thus, a transport of material from small to large bubbles or droplets takes place. The average size of the dispersed phase increases. The rate of mass transport and hence the rate of Ostwald ripening depends on several factors; a very important one is the solubility of the disperse material in the continuous phase. Higher solubility increases the rate of mass transport and accelerates Ostwald ripening.

The term coalescence refers to the merger of bubbles or droplets. Coalescence is typically preceded by gravity-induced creaming or sedimentation of the disperse phase. As a result, dispersed bubbles and droplets approach each other and a thin liquid film forms between them. Gravity-induced film drainage proceeds up to a critical film thickness, at which the thin liquid film spontaneously breaks and bubbles/droplets merge. Spontaneous rupture of the thin film is driven by attractive van der Waals forces. The exact value of the critical film thickness where rupture occurs depends on the range and magnitude of the intermolecular and surface forces involved. For a bare air-water interface at neutral pH and without added electrolyte, the critical film thickness is around 50 nm [1].

Eventually, the combined action of coalescence and Ostwald ripening leads to a minimization of the total surface area of the system, which becomes thermodynamically more stable, but comes along with foam and emulsion instability. For stabilization of foams and emulsions, additives which change the physicochemical properties of the systems must be added. The action of such additives is explained in the following section.

## 1.2. Mechanisms and actions of common interfacial stabilizers

The large interfacial free energy associated with the existence of an interface can be reduced by the addition of surface active additives. These are molecules or macromolecules which lower the interfacial tension upon adsorption to the fluid interface, thereby reducing the thermodynamic driving force for phase separation via Ostwald ripening and coalescence. Surfactants and polymers are among the most prominent examples for such surface actives molecules. Surfactants are amphiphilic molecules, bearing polar and apolar groups, and are intrinsically surface active. The surface activity of polymers is determined by the chemical composition of the polymer subunits, but in general most polymers show a certain level of surface activity.

Surface active materials lower the interfacial tension and, as a consequence, may also impart a certain elasticity to the interface. Interfaces are said to be elastic, when the surface active material does not desorb (adsorb) from (on) the interface upon decrease (increase) of the interfacial area A so that the interfacial tension changes. A measure for the elasticity of an interface is the interfacial dilational elasticity modulus E:

$$E = \frac{d\sigma}{dA/A} = \frac{d\sigma}{d\ \ln A} \qquad (2)$$

with *A* being the interfacial area and *dA* being the area change. While surfactant covered interfaces are usually not very elastic, polymers which adsorb in a train-loop configuration or which are loosely cross-linked by intermolecular covalent bonds can form elastic interfacial layers. The value of the interfacial elasticity E must depend on the timescale because (partial) desorption or adsorption lead to stress-relaxation processes in the interfacial layer. For the bespoken polymers such relaxation processes are characteristic. This means that polymer covered interfaces behave viscoelastic, the exact values of the loss and storage modulus measured are strongly frequency dependent.

Numerical calculations show that an elastic interface can substantially reduce the rate of Ostwald ripening, even though, long-term interfacial relaxation processes may continue [2, 3]. This is also confirmed by experiment where low-frequency elastic moduli could be well correlated to emulsion stability [4]. Elastic interface are also though to prevent rupture of the thin films separating individual bubbles and droplets in close contact with each other. This effect arise because surface tension gradients arising upon local stretching of the thin films are counterbalanced by transport of surface active material and simultaneous liquid flow to the thinned region. This mechanism prevents further thinning, stabilizes liquid films and is frequently denoted as Marangoni effect [5].

Next to their ability to lower the surface tension and impart elasticity to an interface, the existence of surfactants and polymers at the interface leads to the appearance of a disjoining pressure when the interfaces of two droplets or bubbles come into proximity. The disjoining pressure is a result of steric and/or electrostatic interaction between molecules adsorbed at the interface. The pressure can also be viewed as an excess osmotic pressure which arises when two interfaces which are covered by surface active material approach each other. The resistance of droplets against coalescence can be correlated to the magnitude of this disjoining pressure, given that systems of equal size are considered. Coverage of the fluid interface by molecules which can created a substantial disjoining pressure will thus lead to a good stability of the constituting dispersion against coalescence [6].

## 1.3. Particles as interfacial stabilizers

### 1.3.1. Advantages of particles over other interfacial stabilizers

Particles are a prominent alternative to surfactants or polymers for the stabilization of fluid interfaces. One usually speaks of colloidal particles when the dimension of the colloidal entity is in the size range from several tens of nm up to a few micrometres. The larger size compared to surfactants and polymers goes along with a higher adsorption energy at the fluid interface. Particles larger than about 10 nm typically possess such a large adsorption energy relative to the thermal energy $k_BT$ that they adsorb irreversibly. Adsorption of particles can therefore lead to the formation of highly elastic interfacial layers. This results in highly stable bubbles and droplets; the surface tension may become so low that deviations from spherical shape are possible, and Ostwald ripening nearly vanishes. Remarkably, even bubbles and droplets with a high solubility of the disperse material in the continuous phase are observed to be stable for months or longer.

Not least because of their excellent stability, a growing interest in particle stabilized interfaces can be observed as rated by the soaring number of scientific publication on this topic starting from the beginning of the 21st century onwards. It is not a new topic, however; the outstanding stability of particle stabilized emulsions was already noted by Ramsden and Pickering in the beginning of the 20th century [7]. Thus, it took one century for research efforts to becomes focussed on this topic. Nowadays the term “Pickering emulsion” is commonly adopted if one refers to a particle stabilized emulsion. The term is infrequently used to refer to particle stabilized foams though.

While the early research activities of Pickering were mainly focused on the use of inorganic particles for dispersion stabilization, nowadays, the focus is on the design of biodegradable and/or food-grade particles for Pickering stabilization which still appears to be a big challenge [8, 9]. An economic and robust method for design of food-grade microparticles with high interfacial activity would certainly find its application in modern food processing for the design of foams and emulsions with long shelf-life [9].

Other “modern” research activities concerned with particles at interfaces focus on particles that can respond to certain environmental stimuli, so that foam or emulsion stability can be manipulated, e.g. Pickering emulsion for controlled release [10]. One more prominent research direction is the application of non-spherical particles for Pickering stabilization. Non-spherical particles are interesting candidates for the controlled assembly of particles at interfaces via capillary interaction. Precise control over the interfacial location of colloidal particles technique may help in bottom-up

fabrication of new microstructured materials [11]. Overall it appears that for particles as interfacial stabilizers a variety of new potential application can be foreseen [10].

### 1.3.2. Hard particles as interfacial stabilizers

#### 1.3.2.1. Characteristics of hard particles at fluid interface

Traditionally most of the work on particles as interfacial stabilizers was concerned with the use of hard particles which have elastic moduli in the GPa range and, thus, do not easily deform by interfacial forces [12]. Examples are colloidal silica or PS particles. Silica particles should be hydrophobized in order to make them surface active. This is because in order for the particles to have a certain affinity for the fluid interface, they should be wetted by both of the two coexisting fluid phases. The particle wettability is usually quantified in terms of the three-phase contact angle θ between the solid and the fluid interface. For air-water or oil-water interfaces a contact angle of θ = 0° corresponds to particles being completely immersed in the aqueous phase, θ = 180° corresponds to particles completely immersed in the non-polar medium, and θ = 90° corresponds to particles which are equally wetter by each of the two continuous phases adjacent to the interface [13]. The energy of adsorption $\Delta E$ of hard particles at the fluid interface depends on the particle wettability as well as particle size and surface tension of the bare interface. For particles of radius $r$, with a contact angle $\theta$, at a fluid interface with surface tension $\sigma$, $\Delta E$ is given by the following equation 3.

$$\Delta E = \pi r^2 \sigma (1 \pm \cos\theta)^2 \qquad (3)$$

For a particle of radius $10^{-6}$ m at an air-water interface with surface tension 0.072 N $m^{-1}$ and a contact angle $\theta$ of 60° (characteristic for polystyrene particles), the energy for removal from the fluid interface is of the order of $10^7$ $k_BT$. This extremely large energy barrier in relation to the thermal energy $k_BT$ explains why particle adsorption is irreversible and particles can form highly elastic interfacial layers. We note in passing that the adsorption energy given in equation 3 is valid assuming that (1) the particle contact line is completely flat and (2) possible effects of line tension can be ignored, both of which factors may actually have strong influence on the particle adsorption strength.

#### 1.3.2.2. Structure of bubbles and emulsion droplets stabilized by hard particles

Through microscopic investigation, a lot of knowledge has been gained on the structure of bubbles and droplets stabilized by hard particles. Some authors report that no full coverage of the fluid interface with particles was necessary to obtain a stable emulsion. For oil-in-water emulsions, surface coverages in the range of 10 – 30 percent are reported to yield stable emulsion [14-16]. Another study which probed the coalescence stability of two particle covered droplets by forcing them into contact with a micromanipulation technique, also concluded that no close-packing is necessary in order to prevent coalescence [17]. Note that these studies prepared oil-in-water emulsions of long-chain hydrocarbons with low solubility in the continuous phase. The main mechanism leading to phase separation in this type of dispersion is coalescence [18].

In contrast to the results above, toluene-in-water and octanol-in-water emulsions were found to have a closed-packed interfacial layer of particles [19, 20]. Equally stable ionic liquid-in-water emulsions were also bearing a closed packed interfacial layer of particles [21]. For stabilization of aqueous dispersions of gas filled bubbles, full coverage of the fluid interface with particles was necessary to obtain a stable dispersion, in fact phase separation only stopped once a closed-packed interfacial particle layer was formed [22-25]. What all these studies had in common is the good solubility of the disperse material in water. From these studies it appears that for stabilization of disperse systems with a good solubility of the dispersed material in the continuous phase, and which are thus prone to Ostwald ripening as well as coalescence, a closed-packed interfacial layer of particles is necessary.

The discussion on the experimentally determined structure of hard particle stabilized dispersion shall be continued by a description of phenomenological models explaining their extraordinary stability.

#### 1.3.2.3. Formation of a colloidal amour prevents Ostwald ripening

The high resistance of particle stabilized dispersions against Ostwald ripening - in comparison with molecular stabilizers - can be attributed to the strong anchoring of particles at the fluid interface and the high interfacial elasticity. Even upon strong lateral compression of the interface, particles with sufficiently high adsorption energy may not desorb. A partially covered bubble/droplet will thus undergo Ostwald ripening and shrink, consequently the surface coverage will increase up to the point where particles experience strong enough mutual repulsion and shrinking stops. At this moment, a so called “colloidal amour”, a closed packed interfacial layer of particle is formed (see Fig). It is thought that due to strong lateral repulsion between interfacial

particles, the surface tension vanishes completely. As a result the shrinking due to pressure-driven mass transport of the dispersed material stops.

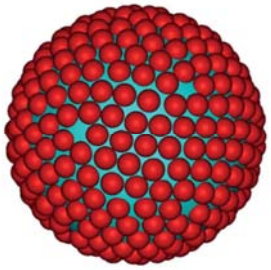

Fig. 1: Sketch of a “colloidal amour” on the bubble/droplet interface (courtesy of Dr. Ran Ni, Nanyang Technological University, Singapore)

In the previous paragraph we described how individual particle stabilized bubbles/droplets increase their surface coverage and become stable through shrinking. Ostwald ripening, however, is accompanied by mass transport from small to large bubbles/droplets of lower Laplace pressure, which hence increase in size. The surface coverage of these larger entities will decrease through Ostwald ripening and, at a certain point, make them also prone to coalescence. The merger of two partially covered bubbles/droplets will result in a higher surface coverage of the newly formed bubble/droplet and may even give them a non-spherical shape. Non-spherical bubbles and droplets are frequently observed in particle stabilized dispersions. The fact that bubbles/droplets adopt a non-spherical shape is interpreted as a sign of vanishing surface tension.

It should become clear that the strong anchoring of particles at the fluid interface leads to a very different outcome of the phase separation processes in particle stabilized dispersions: While the combined action of coalescence and Ostwald ripening normally paves the way for complete phase separation of the system, with particles at interfaces these processes may precede the formation of a stable dispersion. The process by which partially covered emulsion droplets acquire a fully covered interface through multiple events of coalescence is frequently denoted as “limited coalescence”. The same process also happens with particle stabilized bubbles, but here also Ostwald ripening can play a role in the formation of the fully covered interface.

In our discussion, we first dealt with Ostwald ripening and then with coalescence. This order is not meant to indicate that the two processes follow each other, they rather proceed simultaneously. Which process prevails depends on the physicochemical properties of the fluid dispersion. Parameters such as solubility of

the dispersed material in the continuous phase, surface tension and particle surface coverage determine the respective rates of coalescence and Ostwald ripening.

#### 1.3.2.4. Capillary mechanism for thin film and coalescence stability

Another factor which presumably contributes to the good stability of dispersions stabilized by hard particles is their resistance against rupture of the thin liquid films which are separating individual bubbles/droplets. All theoretical approaches to quantify the stability of thin films stabilized by solid particles are based on capillarity [26, 27]. These concepts can be laid out in the following way:
For rupture of the thin liquid film to occur, the two opposite interfaces must approach each other to the critical film thickness $h_{cr}$ at which point attractive van der Waals interaction causes spontaneous film rupture [28]. For the particle covered interfaces to approach each other, the fluid must be squeezed out from the thin film in between the bubbles/droplets. In foams and emulsion this process is driven by gravity and by pressure differences between thin films and Plateau borders, so called “Plateau border suction” [29]. Upon sufficient thinning of the films, the fluid interface around individual particles must deform in order to allow further liquid drainage. As a result of this unfavourable interfacial deformation, a disjoining pressure is emerging which counteracts further thinning of the thin liquid films. In order to calculate the magnitude of the disjoining pressure in particle stabilized dispersions, several assumptions must be made. Particles are assumed to homogeneously distribute over the entire interface. Particles also straddle the fluid interface and adopt a certain equilibrium position with respect to the fluid interface. Further, the liquid meniscus around individual particles is assumed to be axisymmetric and the thin film is stabilized by a bilayer of particles, meaning both interfaces adjacent to the thin film are covered with particles. These assumptions lead to the following theoretical expression for the maximum capillary pressure $P_C$ at which rupture of the thin film is occurring [27].

$$P_C = b\,\frac{\sigma\,\cos\theta}{r} \tag{4}$$

where $\sigma$ is the interfacial tension, $\theta$ is the contact angle between fluid interface and particle measured in the internal liquid of the film, $r$ is the particle radius and $b$ is the constant which depends from the surface coverage and the interfacial organization of particles. The constant b could be on the order of one for a closed-packed particle layer [27], but also higher values up to 10 are suggested in literature. According to equation 4, the disjoining pressure in particle stabilized dispersion can be in the range of 10kPa up to a few hundreds of kPa [6]. Also slightly different variations of

equation 4 are suggested in literature for different interfacial configurations of particles, but these still yield surface pressures on the same order of magnitude as equation 4 [26]. The applicability of equation 4 could be verified by few experiments [30, 31]. Tcholakova et al. conclude that the theoretically estimated high values for the disjoining pressure of particle stabilized thin films lack sufficient confirmation by experiments [6].

We would like to emphasize that the concept of thin film stability presented here is only valid for interfaces stabilized by hard particles. The calculation of disjoining pressure according to equation 4 is based on the possible shape of the liquid menisci in between the particles upon substantial thinning of the liquid films. The theoretical model is only applicable to interfacial particles that do not deform due to surface forces and that have a well-defined contact angle which results in an equilibrium shape of the interface between the particles [27].

### 1.3.3. Soft particles as interfacial stabilizers

#### 1.3.3.1. Characteristics of soft particles at fluid interfaces

"Soft" particles are a relatively new class of materials for the stabilization of fluid interfaces. These particles are characterized by a low elastic modulus in the kPa range [32]. Examples of soft particles are cross-linked polymer particles, also denoted as microgels. A very prominent example for aqueous microgels are cross-linked polymer particles based on Poly(N-isopropylacrylamide) (PNIPAM). PNIPAM undergoes a structural transition from coil-to-globule upon increasing the temperature above the lower critical solution temperature (LCST) which leads to a volume reduction of the microgel particles. Through chemical modification of the polymer, PNIPAM particles can also be made responsive to pH and electrolyte concentration.

It has been shown that microgel particle-stabilized emulsions can be broken on-command, by heating and/or pH adjustment; their content can be released and the microgels can be recycled by subsequent cooling. This stimuli-responsiveness of PNIPAM particles makes them interesting candidates for the production of controlled release systems based on particle stabilized emulsion droplets. [21, 33].

A feature which soft particles share with their hard counterparts is the strong anchoring onto fluid interfaces. The particle adsorption energy $\Delta E$ is given by:

$$\Delta E = \pi r^2 \sigma \qquad (5)$$

where $r$ is particle radius and $\sigma$ is the surface tension of the bare fluid interface. For micron-sized particles at common fluid interfaces, the adsorption energy is very high

in comparison with the thermal energy $k_BT$, which is why particles adsorb irreversibly to the fluid interface.
Due to their soft nature, microgels can be substantially deformed by interfacial forces [34, 35]. For perfectly soft particles with uniform elastic modulus of the whole particle, Deshmukh et al. use the ansatz

$$\Delta r \sim \frac{\sigma}{E_{bulk}} \quad (6)$$

to estimate a typical length scale of deformation due to surface forces [36]. Here $\Delta r$ is the magnitude of radial stretching, $\sigma$ is the surface tension and $E_{bulk}$ is the elasticity of the particle. For a system with $\sigma$ of 70 mN $m^{-1}$ and $\varepsilon$ around 50 - 100 kPa, as found for typical poly-NIPAM microgels, one obtains $\Delta r$ on the order of one micrometer. This shows that soft particles deform substantially under the influence of surface forces. The deformation of soft particles at a fluid interface can markedly increase their adsorption energy. The radius $r$ in equation 5 is in fact the radius of the particle at the fluid interface. Particles with low elastic moduli attached to a fluid interface with high surface tension will undergo pronounced radial stretching, bulk and interfacial radius will differ accordingly, and the particle adsorption energy increases strongly [34].

#### 1.3.3.2. Structure of emulsion droplets stabilized by soft particles

The majority of work on soft particles at interfaces focuses on the stabilization of emulsion droplets, here in particular on droplets stabilized by PNIPAM microgel particles. These soft particles are found to be excellent stabilizer for various types of oil-in-water emulsion [37]. There are some literature reports on water-in-oil emulsions stabilized by microgels, however, the microgels were found to be swollen by the oil phase [38, 39]. It was concluded that alteration of the interfacial properties of the microgels by solvent uptake was responsible for the microgels ability to stabilize water-in-oil emulsions [37, 38].
Emulsion droplets stabilized by microgels can be characterized by a densely packed particle monolayer at the oil-water interface [37, 38]. PNIPAM microgels, only swollen by water, are found to residue predominantly in the water phase rather than the oil phase, which seems plausible as PNIPAM below the LCST is well soluble in water. Particles at the oil-water interface are strongly flattened when observed through the non-polar phase. Furthermore, they adopt a core-corona morphology, with a core which protrudes more in the non-polar phase than the apparently softer, strongly flattened shell [40]. The appearance of this core-corona structure is associated to a

higher density of cross-links in the particle interior relative to the particles outer shell, which is explained by a faster polymerization rate of cross-linker in comparison with the NIPAM monomer [41].
Not only is there a difference between core and corona, also the periphery of the PNIPAM microgel particles is decorated with dangling chains, polymers which are only loosely cross-linked and barely connected to the rest of the polymer network. These dangling chains result in a fuzzy density profile of the microgels' periphery as measured by neutron scattering experiments in aqueous bulk solution [41]. Once the microgel is adsorbed to the fluid interface, the dangling chains are adsorbing too. Dangling chains from different microgel particles are strongly entangled and form an interconnected polymer network on the interface of emulsion droplets [37, 42, 43].

#### 1.3.3.3. Viscoelastic properties of interfaces stabilized by soft particles

The formation of a network of intertwined microgel particles seems to be a prerequisite for the stabilization of emulsion droplets. Brugger et al. could show that charged microgels can form an entangled network at the oil-water interface which yields a viscoelastic interfacial layer. Upon pH induced protonation of charged groups inside the microgels, particles became more dense as well as less connected, their performance as interfacial stabilizer deteriorated [37, 44, 45]. Upon protonation of charged groups, also the elastic response of the interface as probed by dilational rheology decreased [39]. In accordance with the latter observations, Destribats et al. have shown that by lowering the cross-linking density, one can increase the interfacial deformation and the overlap between the peripheral parts of the particles, which results in a better performance as emulsion stabilizers [43].
From these results it can be concluded that the viscoelastic response of microgel covered interfaces results from the formation of a 2D interfacial layer of microgels having their peripheral parts connected to a certain extend [37, 43, 46]. The viscoelastic properties of the microgel-covered interface seems to be a crucial factor that determines emulsion stability. This results agree with the general notion that a high value of the low-frequency elastic modulus results in a reduced rate of Ostwald ripening and better dispersion stability [2-4].

#### 1.3.3.4. Coalescence and thin film stability of dispersions stabilized by soft particles

The ability of microgels to stabilize thin liquid films against coalescence is also of importance to ensure good dispersion stability. The extraordinary stability of microgel stabilized emulsions has been demonstrated by microfluidic experiments in which

emulsion droplets of opposite charge were forced into contact, but did not coalesce. However, by protonation of either the cationic or anionic microgel-covered emulsion droplets, the droplets coalesced under the same experimental conditions [47]. This confirms that for the stabilizing properties of microgels the particle charge plays an indirect role via its influence on the extend of swelling and, hence, on the particle morphology.

The stability of microgel stabilized free standing thin films in air seems inferior to the high stability of thin films between emulsion droplets. Monteux et al. studied microgel stabilized thin films in air with a Sheludko cell and found relative fast drainage and film rupture. However, microgels were observed to aggregate at the air-water interface, resulting in regions deprived of microgels. The authors concluded that the particle-depleted regions of the film are the weak spots causing film rupture. Control over particle aggregation and formation of a homogenously covered film of soft particles was suggested to markedly improve thin film stability [48].

The above results highlight the peculiar properties of microgels as interfacial stabilizers. It becomes clear that soft particles behave distinctly differently from hard particles and that their exact morphology plays an important role with respect to their ability to stabilize fluid interfaces [37].

### 1.3.4. Kinetics of particle adsorption to the fluid interface

A property which qualitatively distinguishes hard particles from soft particles is their adsorption behaviour onto fluid interfaces. Hard particles, in particular when negatively charged, do not adsorb easily at the fluid interface. This is often attributed to repulsive interaction between the particles and the fluid interface [6]. Air-water and oil-water interfaces adopt a negative charge due to spontaneous adsorption of hydroxyl-ions, which in turn repels anionic particles [49-51]. Repulsive interaction between particle and interface can also arise for cationic particles, due to image charge effects [52]. To enable its adsorption onto fluid interfaces, a hard particle must be endowed with sufficient kinetic energy to overcome possible energy barriers. A suitable way to do this is high-shear mixing.

For soft particles such as PNIPAm based microgels, interfacial adsorption occurs spontaneously [53]. Deshmukh et al. could show that microgel adsorption to the air-water interface is diffusion limited [36]. Another study concluded that adsorption to the oil-water interface is diffusion limited as well [54]. The absence of considerable energy barriers for interfacial adsorption at fluid interfaces seems a generic property of soft particles [55].

### 1.3.5. Differences between hard and soft particles as interfacial stabilizer

In the previous two sections we highlighted the ability of soft particles to act as dispersion stabilizers. In terms of coalescence stability hard and soft particles seem to perform equally well. The next question which arises concerns the ability of soft particles to stop Ostwald ripening. The question can be rephrased into how adsorbed microgels react to bubble/droplet shrinkage. As soft particles of micron-sized dimension are thought to irreversibly adsorb to the fluid interface, reduction of the interfacial area will lead to a transition from a fluid-like interfacial layer to a solid-like layer which shows a certain elastic response [37]. In this limit dangling chains on the particles periphery may perhaps share excluded volume, but they are not really compressed yet [48]. Further reduction of the interfacial area though, will lead to pronounced lateral compression of the soft particles attached to the fluid interface. The compressive strain response to this stress is largely dependent on the elastic modulus of the particles. For an estimation one can assume the following:
According to Roark, the lateral stress *s* in the shell with thickness *d* of a hollow sphere with radius *R* under pressure *P* equals [56]:

$$s = \frac{P\,R}{2d} \tag{7}$$

The pressure acting on the shell of a bubble/droplet is the Laplace pressure given as

$$P_L = \frac{2\sigma}{R} \tag{8}$$

Then it follows that the lateral stress *s* in the particle covered bubble/droplet shell is

$$s = \frac{\sigma}{d} \tag{9}$$

The strain response $\varepsilon$ of the shell is given as

$$\varepsilon = \frac{s}{E_{bulk}} \tag{10}$$

If one assumes a shell thickness on the order of $d=10^{-6}$ m and surface tension $\sigma$=70mN $m^{-1}$, equation 9 yields a lateral stress of 7E+04 N $m^{-2}$. With a bulk modulus for PNIPAM based soft particles of E=10E+03 N $m^{-2}$ this gives according to equation 10 a strain $\varepsilon>>1$. Hence, one would expect that the soft particles/microgels

adsorbed to the fluid interface undergo strong lateral compression during the course of Ostwald ripening, the particle covered bubbles/droplets would shrink accordingly. Shrinking of the bubble/droplet and compression of the soft particles could stop only, if a high surface pressure develops during interfacial compression and the high Laplace pressure vanishes. This, however, supposes that the soft particles do not desorb from the fluid interface before the high surface pressure can develop. Otherwise bubble/droplet shrinkage continues, accompanied by particle desorption from the interface.

The exact response of a particle laden interface to compression depends on the physicochemical parameters of the systems. For PNIPAM microgels at the air-water interface Cohin et al. found that the interfacial dilational elasticity modulus E (for a definition see equation 2) adopts very small values, on the order of several mN $m^{-1}$ [48]. From the data of Deshmukh et al. we estimate that E could be on the order several tens of mN $m^{-1}$, but E declines already when the surface tension σ is still relative high [36]. Similar behaviour was observed for PNIPAM particles at the oil-water interface [57]. The latter results seem to indicate that PNIPAM-based microgels desorb from the fluid interface at a finite surface tension rather than developing high surface pressures; however, the authors of the mentioned studies did not elaborate on that.

From this argumentation it appears that the PNIPAM microgel systems studied so far cannot completely stop Ostwald ripening. PNIPAM microgels can only impart certain viscoelastic properties to the interface which retards Ostwald ripening and provides kinetic stability to microgel stabilized emulsions. In fact, there are no literature references on the stabilization of gas bubbles by PNIPAM microgels, and only a few reports on the stability of emulsions prepared with polar oils which, however, lack data on the long-term stability. We want to stress that the behaviour described here is not generic for all soft particles, but system-specific. Other soft particle types, with higher adsorption strength to the respective fluid interface, may be able to stop Ostwald ripening.

## 1.4. Aim and outline of the thesis

The aim of this work was to gain an insight into how efficient adsorption of colloidal particles onto fluid interfaces could be achieved in order to obtain aqueous gas or oil dispersions solely stabilized by the particles. In the first instance we wanted to identify suitable processes which yield particle stabilized dispersion. Furthermore, we wanted to compare different types of colloidal particles, from simple to more complex ones, and to assess their ability to adsorb onto fluid interfaces and to stabilize fluid or liquid dispersions against phase separation. This work is structured as follows:

**Chapter 2** describes the application of ultrasound as a technique for the production of particle-stabilized air bubbles. We prepare bubble dispersions (foams) solely stabilized by solid polystyrene particles of different charge and different surface functional groups. We also examine the interfacial structure of the particles on the surface of these bubbles by microscopy. Finally, we show that surfactant addition can lead to dissolution of otherwise very stable particle stabilized bubbles. This is explained by the influence of surfactants on the capillary interaction (contact angle) by which the particles are bound to the fluid interface.

The rest of the thesis concerns the application of core-shell particles for stabilization of fluid interfaces in bubble dispersions and emulsions. These core-shell particles consist of a hard, polystyrene core and a soft poly-NIPAM based shell, and were designed with the aim to combine the advantageous properties of hard and soft particle for stabilization of fluid interfaces. We presumed that the soft, polymeric nature of the particle periphery would impart the ability to spontaneously adsorb to fluid interfaces, in the same way as pure soft particles do. The solid PS core, on the other hand, should possess a high enough elastic modulus not to be substantially deformed under the influence of compressive stresses arising from Ostwald ripening. In this way, the rigid cores should be able to establish a stress-bearing network that can stop Ostwald ripening. At the same time, the core-shell particles were designed to be rather large. Due to their micron-sized dimensions, particles are expected to possess a high adsorption energy, which should prevent particle desorption even at high surface pressures.

In summary the respective core-shell particles shall combine the following properties:

1) Ability to spontaneously adsorb to fluid interfaces
2) Ability to develop high surface pressures without desorbing from the fluid interface
3) Particles shall be able to effectively stop Ostwald ripening

In **Chapter 3** we report on the preparation of core-shell particles with varying thickness of the soft shell. We characterize these core-shell particles with respect to their responsiveness to temperature, pH and electrolyte concentration.

In **Chapter 4** we first compare core-shell particles with different thickness of the soft shell as to their ability to adsorb on the air-water interface. We do this by evaluating the surface pressure development over time, by tensiometry. From this we establish a critical thickness for the soft shell below which particles seem to experience a certain energy barrier for interfacial adsorption, but above which particles easily enter the air-water interface. As tensiometry is an indirect method to ascertain particle adsorption, we also use light microscopy to confirm that the core-shell particles are readily populating different kinds of fluid interfaces.
Finally, we prepare air bubbles and different kinds of emulsions stabilized by core-shell particles and evaluate the stability of the respective fluid and liquid dispersions.

In **Chapter 5** we describe the experimentally determined 2D equation of state for various core-shell particles adsorbed at the air-water interface. Core-shell particles with different thickness of the soft shell, as well as the actual core particles are compared with each other. With the help of optical microscopy we also assess the interfacial structure adopted by the various particle types on a flat air-water interface.

In **Chapter 6** we quantify the adsorption rate of core-shell particles onto the air-water interface. By tensiometry we first measure the surface pressure development of core-shell particles with a large shell and with the help of the 2D equation of state established in chapter 3, we are able to convert these data into particle adsorption rates. We describe the adsorption of core-shell particles onto the air-water interface by an appropriate model. After this we investigate by drop shape analysis tensiometry, using a special droplet liquid exchange set-up, whether the adsorption of core-shell particles onto the air-water interface is a reversible or an irreversible process.
In order to answer the question how core-shell particles adsorb onto the air-water interface, as to their ability to breach the air-water interface, we perform cryo-scanning electron microscopy and light microscopy. We explain the observations on the structure of core-shell particles at the fluid interface by the elasto-capillary deformation of the particle's soft shell.

In **Chapter 7** we conclude this thesis by a general discussion, and give a summary.

## References


1. Lech, F.J., et al., Stability Properties of Surfactant-Free Thin Films at Different Ionic Strengths: Measurements and Modeling. Langmuir, 2015. **31**(9): p. 2777-2782.
2. Kloek, W., T. van Vliet, and M. Meinders, *Effect of Bulk and Interfacial Rheological Properties on Bubble Dissolution.* J Colloid Interface Sci, 2001. **237**(2): p. 158-166.
3. Meinders, M.B.J. and T. van Vliet, *The role of interfacial rheological properties on Ostwald ripening in emulsions.* Advances in Colloid and Interface Science, 2004. **108–109**(0): p. 119-126.
4. Georgieva, D., et al., On the Possible Role of Surface Elasticity in Emulsion Stability. Langmuir, 2009. **25**(10): p. 5565-5573.
5. Rosen, M.J. and J.T. Kunjappu, Foaming and Antifoaming by Aqueous Solutions of Surfactants, in Surfactants and Interfacial Phenomena. 2012, John Wiley & Sons, Inc. p. 308-335.
6. Tcholakova, S., N.D. Denkov, and A. Lips, *Comparison of solid particles, globular proteins and surfactants as emulsifiers.* Physical Chemistry Chemical Physics, 2008. **10**(12): p. 1608-1627.
7. Pickering, S.U., *CXCVI.-Emulsions.* Journal of the Chemical Society, Transactions, 1907. **91**(0): p. 2001-2021.
8. Lam, S., K.P. Velikov, and O.D. Velev, *Pickering stabilization of foams and emulsions with particles of biological origin.* Current Opinion in Colloid & Interface Science, 2014. **19**(5): p. 490-500.
9. Berton-Carabin, C.C. and K. Schroen, Pickering Emulsions for Food Applications: Background, Trends, and Challenges, in Annual Review of Food Science and Technology, Vol 6, M.P. Doyle and T.R. Klaenhammer, Editors. 2015, Annual Reviews: Palo Alto. p. 263-297.
10. Tang, J., P.J. Quinlan, and K.C. Tam, *Stimuli-responsive Pickering emulsions: recent advances and potential applications.* Soft Matter, 2015. **11**(18): p. 3512-3529.
11. Cavallaro, M., et al., *Curvature-driven capillary migration and assembly of rod-like particles.* Proceedings of the National Academy of Sciences of the United States of America, 2011. **108**(52): p. 20923-20928.
12. Tan, S., R.L. Sherman, and W.T. Ford, *Nanoscale Compression of Polymer Microspheres by Atomic Force Microscopy.* Langmuir, 2004. **20**(17): p. 7015-7020.
13. Binks, B.P., *Particles as surfactants - similarities and differences.* Current Opinion in Colloid & Interface Science, 2002. **7**(1-2): p. 21-41.
14. Midmore, B.R., *Preparation of a novel silica-stabilized oil/water emulsion.* Colloids and Surfaces a-Physicochemical and Engineering Aspects, 1998. **132**(2-3): p. 257-265.

15. Vignati, E., R. Piazza, and T.P. Lockhart, Pickering Emulsions: Interfacial Tension, Colloidal Layer Morphology, and Trapped-Particle Motion. Langmuir, 2003. **19**: p. 6650.
16. Tarimala, S. and L.L. Dai, *Structure of Microparticles in Solid-Stabilized Emulsions.* Langmuir, 2003. **20**(9): p. 3492-3494.
17. Pawar, A.B., et al., *Arrested coalescence in Pickering emulsions.* Soft Matter, 2011. **7**(17): p. 7710-7716.
18. Walstra, P., *Physical chemistry of foods*. Food science and technology : 121. 2003, New York [etc.]: Marcel Dekker.
19. Dinsmore, A.D., et al., Colloidosomes: Selectively permeable capsules composed of colloidal particles. Science, 2002. **298**(5595): p. 1006-1009.
20. Velev, O.D., K. Furusawa, and K. Nagayama, Assembly of Latex Particles by Using Emulsion Droplets as Templates. 1. Microstructured Hollow Spheres. Langmuir, 1996. **12**(10): p. 2374-2384.
21. Monteillet, H., et al., *Multi-responsive ionic liquid emulsions stabilized by microgels.* Chemical Communications, 2014. **50**(81): p. 12197-12200.
22. Subramaniam, A.B., M. Abkarian, and H.A. Stone, *Controlled assembly of jammed colloidal shells on fluid droplets.* Nat Mater, 2005. **4**(7): p. 553-556.
23. Buchcic, C., et al., Assembly of jammed colloidal shells onto micron-sized bubbles by ultrasound. Soft Matter, 2015. **11**(7): p. 1326-34.
24. Abkarian, M., et al., *Dissolution arrest and stability of particle-covered bubbles.* Phys Rev Lett, 2007. **99**(18): p. 188301.
25. Park, J.I., et al., Titelbild: A Microfluidic Approach to Chemically Driven Assembly of Colloidal Particles at Gas–Liquid Interfaces (Angew. Chem. 29/2009). Angewandte Chemie, 2009. **121**(29): p. 5321-5321.
26. Denkov, N.D., et al., *A Possible Mechanism of Stabilization of Emulsions by Solid Particles.* Journal of Colloid and Interface Science, 1992. **150**(2): p. 589-593.
27. Kruglyakov, P.M., A.V. Nushtayeva, and N.G. Vilkova, *Experimental investigation of capillary pressure influence on breaking of emulsions stabilized by solid particles.* Journal of Colloid and Interface Science, 2004. **276**(2): p. 465-474.
28. Vrij, A. and J.T.G. Overbeek, *Rupture of thin liquid films due to spontaneous fluctuations in thickness.* Journal of the American Chemical Society, 1968. **90**(12): p. 3074-3078.
29. Prud'homme, R.K. and S.A. Khan, *Foams : theory, measurements, and applications*. Surfactant science series;vol. 57. 1996, New York [etc.]: Dekker.
30. Nushtayeva, A.V. and P.M. Kruglyakov, *Capillary pressure in a thinning emulsion film stabilised by spherical solid particles.* Mendeleev Communications, 2001. **11**(6): p. 235-236.

31. Binks, B.P. and S.O. Lumsdon, Influence of particle wettability on the type and stability of surfactant-free emulsions. Langmuir, 2000. **16**(23): p. 8622-8631.
32. Abate, A.R., et al., *Measuring the elastic modulus of microgels using microdrops.* Soft Matter, 2012. **8**(39): p. 10032-10035.
33. Ngai, T., S.H. Behrens, and H. Auweter, *Novel emulsions stabilized by pH and temperature sensitive microgels.* Chemical Communications, 2005(3): p. 331-333.
34. Style, R.W., L. Isa, and E.R. Dufresne, *Adsorption of soft particles at fluid interfaces.* Soft Matter, 2015. **11**(37): p. 7412-7419.
35. Mehrabian, H., J. Harting, and J.H. Snoeijer, *Soft particles at a fluid interface.* Soft Matter, 2016. **12**(4): p. 1062-1073.
36. Deshmukh, O.S., et al., Equation of state and adsorption dynamics of soft microgel particles at an air-water interface. Soft Matter, 2014. **10**(36): p. 7045-7050.
37. Richtering, W., Responsive Emulsions Stabilized by Stimuli-Sensitive Microgels: Emulsions with Special Non-Pickering Properties. Langmuir, 2012. **28**(50): p. 17218-17229.
38. Destribats, M., et al., Water-in-Oil Emulsions Stabilized by Water-Dispersible Poly(N-isopropylacrylamide) Microgels: Understanding Anti-Finkle Behavior. Langmuir, 2011. **27**(23): p. 14096-14107.
39. Brugger, B., B.A. Rosen, and W. Richtering, *Microgels as stimuli-responsive stabilizers for emulsions.* Langmuir, 2008. **24**(21): p. 12202-8.
40. Geisel, K., L. Isa, and W. Richtering, Unraveling the 3D Localization and Deformation of Responsive Microgels at Oil/Water Interfaces: A Step Forward in Understanding Soft Emulsion Stabilizers. Langmuir, 2012. **28**(45): p. 15770-15776.
41. Stieger, M., et al., Small-angle neutron scattering study of structural changes in temperature sensitive microgel colloids. The Journal of Chemical Physics, 2004. **120**(13): p. 6197-6206.
42. Brugger, B., et al., *The Colloidal Suprastructure of Smart Microgels at Oil-Water Interfaces.* Angewandte Chemie-International Edition, 2009. **48**(22): p. 3978-3981.
43. Destribats, M., et al., Soft microgels as Pickering emulsion stabilisers: role of particle deformability. Soft Matter, 2011. **7**(17): p. 7689-7698.
44. Brugger, B., J. Vermant, and W. Richtering, Interfacial layers of stimuli-responsive poly-(N-isopropylacrylamide-co-methacrylicacid) (PNIPAM-co-MAA) microgels characterized by interfacial rheology and compression isotherms. Phys Chem Chem Phys, 2010. **12**(43): p. 14573-8.
45. Massé, P., et al., Impact of Electrostatics on the Adsorption of Microgels at the Interface of Pickering Emulsions. Langmuir, 2014. **30**(49): p. 14745-14756.
46. Schmidt, S., et al., Influence of Microgel Architecture and Oil Polarity on Stabilization of Emulsions by Stimuli-Sensitive Core–Shell Poly(N-

isopropylacrylamide-co-methacrylic acid) Microgels: Mickering versus Pickering Behavior? Langmuir, 2011. **27**(16): p. 9801-9806.
47. Liu, T., et al., *Non-coalescence of oppositely charged droplets in pH-sensitive emulsions.* Proceedings of the National Academy of Sciences, 2012. **109**(2): p. 384-389.
48. Cohin, Y., et al., Tracking the interfacial dynamics of PNiPAM soft microgels particles adsorbed at the air–water interface and in thin liquid films. Rheologica Acta, 2013. **52**(5): p. 445-454.
49. Graciaa, A., et al., *The ζ-Potential of Gas Bubbles.* Journal of Colloid and Interface Science, 1995. **172**(1): p. 131-136.
50. Nguyen, A.V., P. George, and G.J. Jameson, *Demonstration of a minimum in the recovery of nanoparticles by flotation: Theory and experiment.* Chemical Engineering Science, 2006. **61**(8): p. 2494-2509.
51. Marinova, K.G., et al., Charging of Oil–Water Interfaces Due to Spontaneous Adsorption of Hydroxyl Ions. Langmuir, 1996. **12**(8): p. 2045-2051.
52. Wang, H., V. Singh, and S.H. Behrens, *Image Charge Effects on the Formation of Pickering Emulsions.* The Journal of Physical Chemistry Letters, 2012. **3**(20): p. 2986-2990.
53. Zhang, J. and R. Pelton, *Poly(N-isopropylacrylamide) Microgels at the Air−Water Interface.* Langmuir, 1999. **15**(23): p. 8032-8036.
54. Li, Z., et al., Poly(N-isopropylacrylamide) microgels at the oil-water interface: adsorption kinetics. Soft Matter, 2013. **9**(41): p. 9939-9946.
55. Deshmukh, O.S., et al., *Hard and soft colloids at fluid interfaces: Adsorption, interactions, assembly & rheology.* Advances in Colloid and Interface Science, 2015. **222**: p. 215-227.
56. Roark, R.J. and W.C. Young, *Formulas for stress and strain*. 1975, Tokyo: McGraw-Hill.
57. Geisel, K., et al., Hollow and Core–Shell Microgels at Oil–Water Interfaces: Spreading of Soft Particles Reduces the Compressibility of the Monolayer. Langmuir, 2015. **31**(48): p. 13145-13154.

## Chapter 2

# Assembly of jammed colloidal shells onto micron-sized bubbles by ultrasound

Stabilization of gas bubbles in water by applying solid particles is a promising technique to ensure long-term stability of the dispersion against coarsening. However, the production of large quantities of particle stabilized bubbles is challenging. The delivery of particles to the interface must occur fast compared to the typical time scale of coarsening during production. Furthermore, the production route must be able to overcome the energy barriers for interfacial adsorption of particles. Here we demonstrate that ultrasound can be applied to agitate a colloidal dispersion and supply sufficient energy to ensure particle adsorption onto the air-water interface. With this technique we are able to produce micron-sized bubbles, solely stabilized by particles. The interface of these bubbles is characterized by a colloidal shell, a monolayer of particles which adopt a hexagonal packing. The particles are anchored to the interface owing to partial wetting and experience lateral compression due to bubble shrinkage. The combination of both effects stops coarsening once the interface is jammed with particles. As a result, stable bubbles are formed. Individual particles can desorb from the interface upon surfactant addition, though. The latter fact confirms that the particle shell is not covalently linked due to thermal sintering, but is solely held together by capillary interaction. In summary, we show that our ultrasound approach allows for the straightforward creation of micron-sized particle stabilized bubbles with high stability towards coarsening.

This Chapter is based on: C Buchcic, RH Tromp, MBJ Meinders and MA Cohen Stuart, Assembly of jammed colloidal shells onto micron-sized bubbles by ultrasound, Soft Matter, 2015

## 2.1. Introduction

Bubbles are gas filled entities which can be dispersed in a aqueous medium. Because of their high internal pressure, they are intrinsically unstable. The Laplace pressure $P_L$, the excess pressure inside such a gas bubble, is given by the Young-Laplace-equation

$$P_L = \frac{2\sigma}{R} \quad (1)$$

where σ is the liquid/gas interfacial tension and R is the radius of the bubble. For a micron-sized bubble bounded by a pristine air-water interface, the excess pressure is about one and a half fold the standard atmospheric pressure. Owing to the high pressure difference between the in- and outside of the bubble, the contained gas readily dissolves in the surrounding liquid phase. Due to the dependence of Laplace pressure on bubble size, a concentrated system of polydisperse bubbles will undergo mass transport from small to large bubbles. This process, known as disproportionation or Ostwald ripening, together with the coalescence of individual gas bubbles eventually leads to a complete phase separation into liquid and gas phase [1].

An elastic shell around the bubbles can slow down these processes and impart kinetic stability. Lipids, proteins, surfactants or mixtures thereof are commonly used shell materials for bubble stabilization. The longevity of such bubbles depends on the rheological properties of the interface, but usually does not exceed several hours [2, 3]. An alternative to the application of these molecular stabilizers is the use of colloidal particles that are able to adsorb at the bubble surface. The stabilization of disperse systems via accumulation of particles at the phase boundary is commonly referred to as Pickering stabilization. The prevention of coalescence and disproportionation is thought to be due to a combination of electrostatic and steric effects: once a sufficient number of particles is adsorbed at the air-water interface, the shrinking of bubbles due to capillary pressure differences is arrested as soon as the particles at the interface repel each other sufficiently strongly. Further shrinking is energetically unfavourable because particles would have to leave the interface for that to occur. This will not take place owing to the large adsorption energy, which is typically orders of magnitude larger than $k_BT$. At the same time, coalescence is impeded as the liquid film in between two adjacent bubbles cannot rupture because of steric hindrance. The result is a stable suspension of bubbles, which is homogenous under gravity when the bubbles are smaller than typically 1 µm.

A prerequisite for colloidal particles residing in the bulk to adsorb at an interface is that they are partially wetted by both coexisting fluid phases. The particle wettability is usually quantified in terms of the three-phase contact angle $\theta$ between the solid and the fluid interface. For air-water interfaces contact angle values above 90° indicate that the particle is being preferentially wetted by air, whereas values below 90° indicate preferential wetting by water. The energy of adsorption $\Delta E$ depends on the particle wettability as well as particle size and surface tension of the bare air-water interface. For particles of radius $r$, with a contact angle $\theta$, at an air-water interface with surface tension $\sigma$, $\Delta E$ is given by equation 2.

$$\Delta E = \pi r^2 \sigma (1 \pm \cos\theta)^2 \qquad (2)$$

For a particle of radius $10^{-6}$ m at an air-water interface with surface tension 0.072 N $m^{-1}$ and a contact angle $\theta$ of 60° (characteristic for polystyrene particles), the energy for removal from the air-water interface is of the order of $10^7$ $k_BT$. This extremely large energy barrier relative to the thermal energy explains why such particles are practically irreversibly attached to the interface and remain stuck there although bubble shrinkage would be a driving force for them to leave the interface [4]. Due to the high energy barrier for desorption of particles from the interface, one would expect a long term stability of particle covered bubbles. Experiments confirm this and it has been shown that particle decorated interfaces can stop disproportionation and coalescence on very long time scales, up to several months [5, 6]. We note in passing that the contact line on the particle surface may not reach an instant equilibrium position [7]. The fact that particles are not at their equilibrium position may affect the exact value of the adsorption energy, but does not invalidate the argument that micron-sized particles are irreversibly attached to the fluid interface due to partial wetting. Furthermore, the contact line may be pinned due to surface roughness. This in turn may have repercussion for the effective adsorption energy and the effective particle-particle interaction [8].

The longevity of particle stabilized systems have sparked the idea to exploit Pickering stabilization of bubbles for a range of applications. Controlled assembly of such bubbles into three dimensional scaffolds may be of use in material science for the design of ultra-light weight materials or acoustic insulators [9]. Another possible area of use, on the border between material science and biomedicine, is the application of particle stabilized micron-sized bubbles as contrast agent in ultrasound based medical imaging. It was shown that bubbles having surfaces covered with nanoparticles showed pronounced non-linear behaviour under ultrasound, a property which is a prerequisite for the use of these entities in biomedical imaging [10]. Apart

from these applications one might also envision the use of particle stabilized bubbles as functional ingredient in consumer goods. Certain food products for instance owe their desired textural perception to the presence of disperse gas bubbles [11]. Incorporation of particle stabilized gas bubbles into food products might therefore enable to control the rheological properties of bubble containing products. Another interesting idea is the inclusion of micron-sized bubbles in packaging materials and coatings, in order to impart certain permeability properties to the material.

Each of the applications mentioned above may require a different level of polydispersity in the bubble size distribution. An equally important parameter for the industrial scale application of particle stabilized bubbles is the yield of the production method. Polydispersity and yield are therefore the criteria which need to be taken into account when choosing a bubble production method. Moreover, it has been recognized that for solid particles mere diffusion is not an efficient mechanism for bringing particles into the air-water interface. For production of significant quantities of particle-decorated bubbles the particles must be deliberately delivered to the interface. This requires shear forces or other forms of active transport to the interface present in the production process. The necessity for an input of energy to assemble particles at the interface can be explained by electrostatic effects between particle and interface. In addition the penetration of particles into the interface involves draining and breaking of the liquid film between particle and interface. As a result it is a difficult target to ensure fast particle absorption to the air-water interface [12].

In the scientific literature merely a few attempts to produce micron sized bubbles stabilized with colloidal particles have been reported. Manual shaking, intuitively an easy method to create bubbles, results in macroscopic, millimetre sized bubbles of high polydispersity [13-15]. As an alternative, a few authors report on the successful use of microfluidic methods for assembly of particle covered, micron-sized bubbles. The resulting bubbles show low levels of polydispersity and high stability towards coarsening. A drawback of the microfluidic methods is their low yields [9, 16].

In this work we studied the use of ultrasound for creation of particle stabilized, micron-sized bubbles. Our interest in the ultrasound technique was motivated by its possible implementation in an industrial-scale, continuous flow-through production process. The model particles of our choice were polystyrene particles with sizes of around one micrometre in diameter. We chose this size in order to allow for microscopic observation of individual particles on the bubble surface. The material polystyrene was chosen as it is partially wetted by water and air, a prerequisite to assemble particles made up of this material at the interface [17]. We investigated the efficiency of ultrasound to assemble micron-sized colloidal particles onto air-water interfaces. In addition, we studied properties of the bubbles obtained with this technique. Furthermore, we checked if the interfacial particles can be displaced from

the interface by surfactant addition. In this way we tested particle assembly onto the bubble interface is reversible.

## 2.2. Experimental details

### 2.2.1. Materials

Hydrochloric acid, sodium hydroxide, styrene, methanol, the initiators 2,2'-Azobis(isobutyramidine) dihydrochloride (AIBA) and Azo-bis-(isobutyronitril) (AIBN) as well as the co-monomer Sodium p-styrenesulfonate (NaSS) were purchased from Sigma-Aldrich (Germany). Carboxyl charge-stabilized polystyrene microspheres (Molecular Probes Inc.) with the catalogue number C37274 were purchased from Fisher Scientific, The Netherlands. The particle surfaces are claimed to be hydrophobic. The water used during this study was purified with a Milli-Q water purification system (Thermo Scientific) after passing an ion-exchanger. The obtained water had a typical resistivity of 18.2 MΩ.

### 2.2.2. Synthesis of colloidal particles

Polystyrene (PS) particles stabilized by the charged co-monomer p-styrenesulfonate (NaSS) and further on denoted as NaSS-PS particles have been synthesized by dispersion polymerization in methanol according to a procedure of Zhang et al. [18]. A round-bottomed flask was filled with 75 ml methanol, 20 ml water, 10 ml styrene, and 0.023 g of the anionic co-monomer p-styrene sulfonate (NaSS). The reaction mixture was purged with nitrogen and heated to 70°C. An amount of 0.195g AIBN was dissolved in 5 ml methanol and injected into the flask to start the reaction. Polymerization continued for 24 hours. Particles were purified by repeated centrifugation-redispersion cycles in water and subsequent dialysis against water.
PS particles stabilized by the charge which stems from the initiator 2,2'-Azobis(isobutyramidine) dihydrochloride (AIBA) and further on denoted as AIBA-PS particles have been synthesized by dispersion polymerization in methanol. A round-bottomed flask was filled with 170 ml methanol and 20 ml styrene. The reaction mixture was purged for 30 min with nitrogen and subsequently heated to 70°C where after 0.2 g of the initiator AIBA (dissolved in 20 ml Methanol) was injected. Polymerization continued for 24 hours. Particles were purified by repeated centrifugation-redispersion cycles in water and subsequent dialysis against water.

### 2.2.3. Characterization of colloids by light scattering

Particle size and polydispersity were analysed by light scattering. Measurements were performed on a ALV apparatus with a DPSS laser (Cobolt Samba 300 mW at 532 nm), ALV 50/100/200/400/600 µm Pinhole system, a Thorn RFIB263KF Photo

Multiplier Detector, ALV7002 external correlator and a ALV-SP/86 Goniometer. The scattering intensity of the particle dispersion was measured at scattering angles between 40° ≤ α ≤ 130° at 1° intervals. The resulting scattering curves were fitted to a theoretical form factor for polydisperse hard spheres from which we obtained information about particle size and polydispersity. For multimodal particle dispersions a first order autocorrelation function was generated and data were analysed by the CONTIN algorithm.

### 2.2.4. Electrokinetic charge of the colloidal particles

The electrokinetic charge of the synthesized particles was analysed with a Malvern Nanosizer S apparatus. Prior to analysis the particle dispersion was diluted with water. Adjustment of the pH was done through dropwise addition of 0.1 M hydrochloric acid respectively 0.1 M sodium hydroxide with an autotitration unit under exclusion of air. About 750 µl of particle dispersion was filled into a disposable folded capillary cell. The applied electrical current was automatically regulated by the in-built software algorithm.

### 2.2.5. Ultrasonic treatment

Ultrasonic treatment was performed with a Bandelin Sonoplus ultrasonic homogenizer operating at 20 kHz, equipped with a MS 73 ultrasound needle. A cylindrical glass vessel (2.8-cm inner diameter) with a total volume of 20 mL was used for ultrasonic irradiation. Prior to ultrasound treatment the particle stock dispersion was diluted with water to the desired concentration and about 2ml of the dispersion were transferred into the glass vessel. The ultrasound needle was placed just below the upper surface of the particle dispersion. The vessel was closed and the sample was sonicated for 15 seconds.

### 2.2.6. Bubble size characterization

A small amount of bubble suspension was diluted with water in a volume ratio 1:20. The size of the bubbles was assessed by observing the diluted samples on an upright Olympus BX 50 light microscope, equipped with long working distance objectives and operated in transmission mode. For low magnification imaging we avoided the use of a cover slide in order not to cause confinement and bubble deformation. The resulting pictures were recorded on a digital high resolution microscope camera of type Olympus DP70.

Additionally, a concentrated bubble dispersion was imaged using X-Ray Tomography on a Phoenix v[tome]x m equipped with a 180kV/15 W nanofocus X-ray tube (General Electric, US). The sample was placed in a small plastic tube for imaging. The reconstruction of the 3D structure was performed using the built-in Phoenix

software. Image analysis was done with custom-written routines using Avizo (VSG) and Matlab (Mathworks).

### 2.2.7. Exposure of bubbles to surfactants

A diluted dispersion of bubbles were introduced into a home-made glass capillary cell with a height of 100 micrometre, after which the non-ionic surfactant Triton X-100 was added in order to yield a surfactant concentration of 1mM in the bulk aqueous phase. The structure of the bubbles after surfactant exposure was observed via microscopy on an upright Olympus BX 50 light microscope.

### 2.2.8. Contact angle measurements

To determine the effect of surfactant addition on the wettability of the colloidal particles, contact angle measurement in the sessile drop conformation were performed. For this purpose colloidal particles were oven dried and dissolved in chloroform to yield a concentration around 1 % w/v. The resulting solution was spin cast at 1500 rpm on a plasma cleaned silicon wafer. Aliquots of polystyrene solution were deposited in order to yield a polymer layer of approximately 200nm thickness. Contact angle measurements were performed on these polystyrene surfaces. Contact angles on the polystyrene surfaces were determined for a sessile drop of pure water and for Triton X-100 surfactant solution of 1 mM concentration.

### 2.2.9. Tensiometry

In order to investigated if small-molecular-weight, surface-active species are present in the particle dispersions, equilibrium surface tension of the supernatant after centrifugation of the particle dispersion was measured on a Drop Tensiometer PAT-1 (Sinterface, Germany).

## 2.3. Results and Discussion

### 2.3.1. Colloidal Particle Synthesis & Characterization

For the colloid synthesis we opted for a dispersion polymerization of styrene in alcoholic solvent. This polymerization method was chosen as it allows for obtaining micron-sized particles, in a one-shot synthesis without the addition of surfactant, like in emulsion polymerization [19]. We wanted to avoid surface active additives because surfactants that are present in the polymerization process might physically adsorb to the particle surface and alter their wettability [4]. Despite the absence of surfactant present in the polymerization process, there might be surface active species in the form of oligomers formed as a by-product of the polymerization reaction [20]. The

chosen cleaning procedure with repeated centrifugation- redispersion cycles turned out to be sufficient to remove potentially present low molecular weight surface active entities. This was concluded from capillary pressure tensiometry of the supernatant after centrifugation for which a surface tension of 72 mN $m^{-1}$, equal to a pure air-water interface, was measured.

Our polymerization scheme resulted in particles with a diameter of around 1 micrometre (s. Tab. 1). The size of these particles makes them well suited for observation via standard light microscopy techniques. The cationic particles used in this study showed a bimodal size distribution which probably is due to some kind of secondary nucleation process [21].

Tab. 1: Size and polydispersity of the colloidal particles used during this study

| Particle type, electric charge | Diameter / Polydispersity index |
|---|---|
| NaSS-PS, 0.25%(w/w) NaSS, anionic | 946 nm / PDI 1.01 |
| COOH-PS, anionic | 1080 nm / PDI 1.02 |
| AIBA-PS, cationic | 1280 nm, 244 nm (bimodal) |

In Tab. 1 also the charge the particles carry is specified. For COOH-PS particles and NaSS-PS particles a negative electrokinetic charge over the whole pH range could be ascertained. Concerning the charge of the AIBA-PS particle we observed that the zeta potential reversed from positive to negative upon increasing pH. This charge reversal may be attributed to the hydrolysis of surface amidine groups into negatively charged carboxyl groups [22]. In all our experiment AIBA-PS particles were set to a pH value around 3. At this pH AIBA-PS particles showed a positive electrokinetic charge during electrophoresis. Hence, these particles are assumed to be cationic.

### 2.3.2. Bubble size

Microscopic analysis of the particle dispersion after sonication revealed the formation of micron-sized bubbles with a typical size around 10-100 µm. Fig. 1 shows a population of bubbles stabilized by the cationic polystyrene particles. A lognormal distribution was fitted to the resulting size distribution; a log mean diameter of 25 µm was found (Fig. 1).

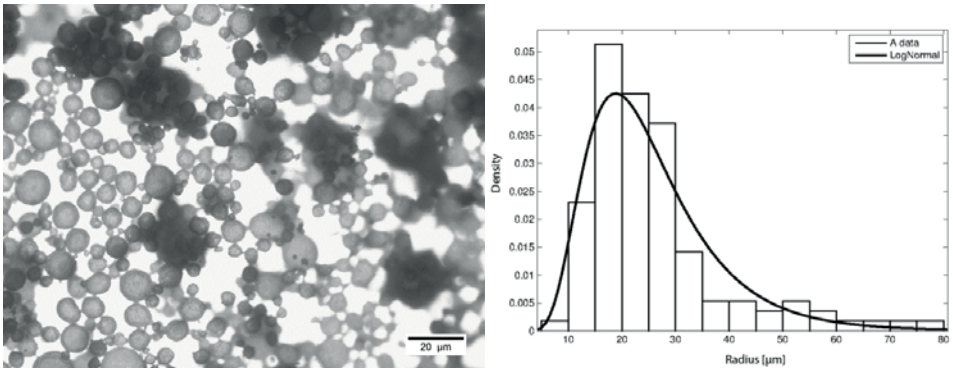


Fig. 1: (a) Population of bubbles stabilized by cationic polystyrene Latex (b) Size distribution of the bubbles with a lognormal distribution fitted to it

In order to confirm the results of the microscopic analysis, a concentrated particle dispersion containing bubbles was imaged by X-Ray tomography directly after ultrasound treatment. As seen in Fig. 2 the strong contrast between air and water allows to observe individual bubbles with a typical size of a few micrometre or larger, while sub-micron-sized PS particles are too small to be resolved at the used experimental resolution. Image analysis yielded a mean bubble volume of $10^{-5}$ $mm^3$, which corresponds to a diameter of around 27 µm and is consistent with our results from microscopic analysis. This bubble size distribution did not change during a prolonged storage period up to three months, which illustrates the excellent stability of the particle stabilized bubble dispersion.

Fig. 2: Polydisperse sample of particle stabilized bubbles imaged by XRT

### 2.3.3. Influence of process parameters on bubble yield

One parameter which strongly influenced the yield of the production method was the particle concentration. We started to test for bubble formation with diluted samples of 1% w/w particles. At these concentrations only a few particle stabilized bubbles could be made. Increasing the particle concentration clearly yielded higher numbers of particle stabilized bubbles. A particle concentration around 5% w/w ensured a good yield. The necessity for high particle concentration indicates a low efficiency of particle adsorption to the air-water interface. In other words, there is a low probability for particles to adsorb at the interface. This is most probably caused by an energy barrier to be overcome by particles entering the interface [12]. Air-water interfaces are reported to possess a negative surface potential. This negative surface potential poses an energy barrier for anionic particles to reach the interface [23-26]. Besides, other effects, such as image charge effects may cause a barrier for interfacial adsorption. This may be the case, e.g., for cationic particles dispersed in the polar phase adjacent to the interface [27]. Energy barriers may be lowered by screening of the particle surface charge [26]. In principle, this can be achieved by adjustment of the pH as well as via salt addition. As some colloids, like particles charge-stabilized with styrenesulfonate groups, have a very low pKa [28], salt addition constitutes a more generic way of charge screening. By addition of 0.1M monovalent salt charges can be efficiently screened, which postulates itself by a qualitative observed better particle adsorption to the interface; meaning more bubbles are formed.

To test the influence of ultrasound parameters, we varied ultrasound power and duty cycle. The power input was varied continuously between 10 – 100 % of the maximum capacity. In all cases we observed the formation of particle stabilized bubbles. The energy input during sonication appeared not to be a limiting factor and strong enough to overcome barriers for interfacial adsorption of particles. Ultrasound treatment may be considered as a turbulent mixing process, in which hydrodynamic forces pushing the particles towards the interface compete with repulsive forces counteracting particle adsorption to the interface. The hydrodynamic force $F$ occurring during ultrasound treatment may be estimated as [12]:

$$F \sim r^2 \rho\, \omega^{\frac{2}{3}} R^{\frac{2}{3}} \qquad (3)$$

where $r$ is the particle radius, $\rho$ the dispersion density, $\varepsilon$ the energy dissipation rate during ultrasound treatment and $R$ the droplet radius. With a particle radius $r=5*10^{-7}$ m, a typical bubble radius of $R=1.25*10^{-5}$ m, a typical density $\rho= 1000$ kg m$^{-3}$ and an energy dissipation rate $\omega \sim 10^5$ J kg$^{-1}$ s$^{-1}$ we estimate the hydrodynamic forces $F$ to be around 0.5 nN. The typical range of repulsive forces measured by Atomic Force

Microscopy for interaction of spherical particles with bare air-water interfaces are around a few hundred to a few thousand pN, depending on particle size and wettability [29]. The repulsive forces present in the systems investigated in this study are probably lower than the hydrodynamic force of 0.5 nN so that particles are able to adsorb at the air-water interface during ultrasound treatment.

### 2.3.4. Interfacial structure of the bubbles

A feature of all of the bubbles produced in the context of this work is a densely packed layer of colloidal particles on the surface (Fig. 3). Particles at the interface are jammed. Thus, it is concluded that only a densely packed particle layer at the interface is able to stop coarsening of the bubbles. Similar jammed structures have been reported for particle stabilized bubbles produced by microfluidics [9, 16].

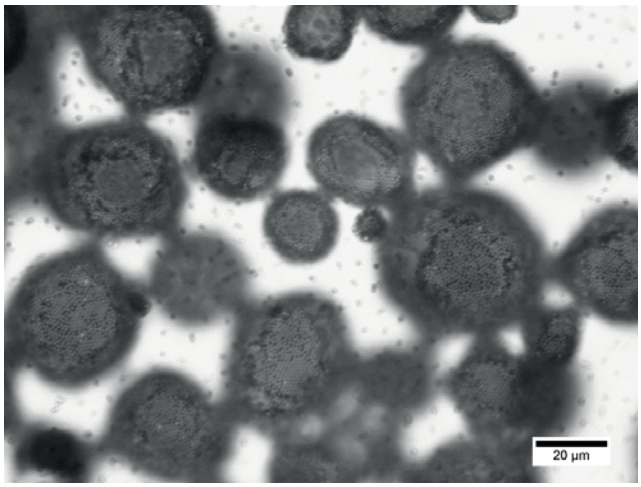


Fig. 3: Microscopic picture of bubbles stabilized by cationic Latex particles

The fully particle covered surfaces that we observe are in contrast with some reports on the interfacial structure in particle stabilized emulsions, where long term (meta)stable interfaces decorated with patches of particles separated by particle free domains were observed [30-32]. We attribute this fundamental difference to the different solubility of the dispersed materials in the aqueous phase and to a difference in the interfacial tension. Pickering emulsions containing highly apolar oils mainly phase separate via coalescence of individual oil droplets within the time scale of the experiments. Bubbles, however, contain air or other well water-soluble gases that phase separate both via Ostwald ripening and coalescence. One might argue that in the former case an incomplete surface coverage is sufficient to inhibit contact of individual oil droplets by steric interaction and therewith impart kinetic stability

against coalescence. In the case of particle stabilized bubbles on the other hand, the dispersed gas can diffuse through the aqueous phase, from small bubbles to large bubbles, and give rise to phase separation via Ostwald ripening. In order to stop coarsening, the high Laplace pressure which is the driving force for Ostwald ripening must be suppressed. As pointed out by Kam and Rossen this can be achieved via a jammed interfacial layer of colloidal particles which are interacting via capillary interaction [33]. With such a closed packed interfacial layer of particles in place, further bubble shrinkage causes the air-water interface in between the particle to change its curvature. According to their model, the air-water interface in between the particles can flatten which implies zero Laplace pressure. Further bubble shrinkage may even result in a concave interface and a net inward force which can drive the particles into hard sphere contact and could perhaps lead to sintering of the particles at the interface [33]. Although the curvature of the interface between particles residing on the interface of a bubble is difficult to assess experimentally, the proposed model can explain our experimental observation of closed packed particle monolayers on the surface of stable bubbles.

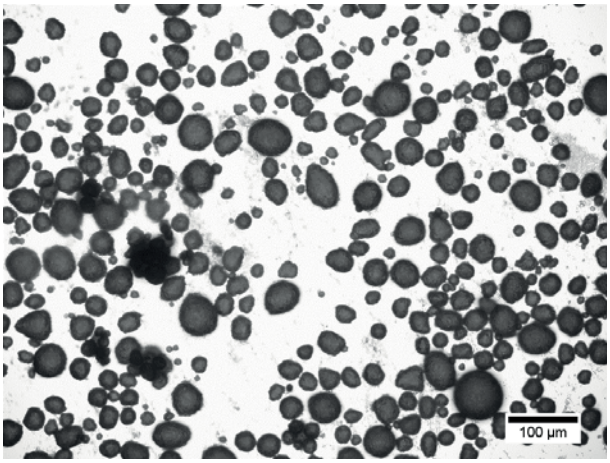


Fig. 4: Microscopic picture of bubbles stabilized by Latex particles. Pronounced non-spherical shapes can be observed.

Another feature of the bubbles prepared during this work is their non-spherical shape (see Fig. 4). This implies that particle stabilized interfaces can support non-isotropic stresses. An anisotropic shape confirms that the interfacial properties of the bubbles are no longer determined by the surface tension of the air-water boundary, because a non-zero interfacial tension would not permit any non-minimal, i.e. non-spherical shapes. Non-spherical bubbles can only exist if particles on the interface are jammed. A solid-like response to non-isotropic stresses has been identified as a generic property of jammed interfaces and was used to create non-spherical bubbles

similar to the ones we observe [34]. Non-spherical bubbles, although much larger than the ones prepared during this work, are also encountered after manual shaking a particle dispersion, and can also be attributed to crowding of particles at the interface [5, 35].

We would like to stress that for the formation of a rigid colloidal shell which is able to support non-isotropic stresses, the particles must be strongly bound to the interface. Such a strong attraction to the interface can arise if particles are partially wetted by both phases adjacent to the interface. In this case their adsorption energy is high enough to prevent desorption from the interface when interfacial particles start to interact due to bubble shrinkage. This allows for the establishment of a tight particle network which can bear non-isotropic stresses and therewith acts like a solid-like material [33]. This situation is fundamentally different from the system described by Irvine et al. [36]. These authors also observe a crystalline layer of particles at the interface of an emulsion droplet. However, these particles are attracted to the interface solely by image charge effects. Particles attracted to the interface solely by image charge effects may also be able to form a stress bearing network. Theoretical calculation predict adsorption energies up to $10^5$ $k_BT$ for particles attracted to the interface by image charge effects [37]. However, image charge effects can only be harnessed for Pickering emulsions, in cases were the particle can be dispersed in the non-polar phase.

In the case of particle stabilized bubbles produced in this work, the colloidal particles are made up of polystyrene, a material which shows partial wettability by water as well as air. These particles are expected to be strongly bound to the air-water interface and fulfil the characteristics of a Pickering stabilized system [38]. It is also interesting to note that particles do not have to be equally wetted by both phases to allow the establishment of a stress bearing network. Partial wettability is sufficient to allow the formation of a dense particle layer, providing stability against coarsening of the bubbles. From equation 2 it should become clear that for micron-sized, non-interacting particles, even a contact angle in the range of 5°-10° should be sufficient for the particles to be irreversibly adsorbed to the interface.

In order to elucidate the interfacial structure in more detail, we observed bubbles at high magnification by oil immersion microscopy. From Fig. 5 it is evident that structural order over distances larger than a few particle diameter exists. The pair correlation function indicates that a two dimensional quasi crystalline network on the bubble interface is created. Distinct peaks around 1, $\sqrt{3}$, 2, $\sqrt{8}$ and 3 times the nearest neighbour distance show that a 2D hexagonal structure is present. This is in accordance with earlier observations of such structures on the interface of micron-sized bubbles [16]. Microscopic observation of the bubble interface furthermore

revealed that thermal motion of the particles as observed in the bulk water phase is arrested.

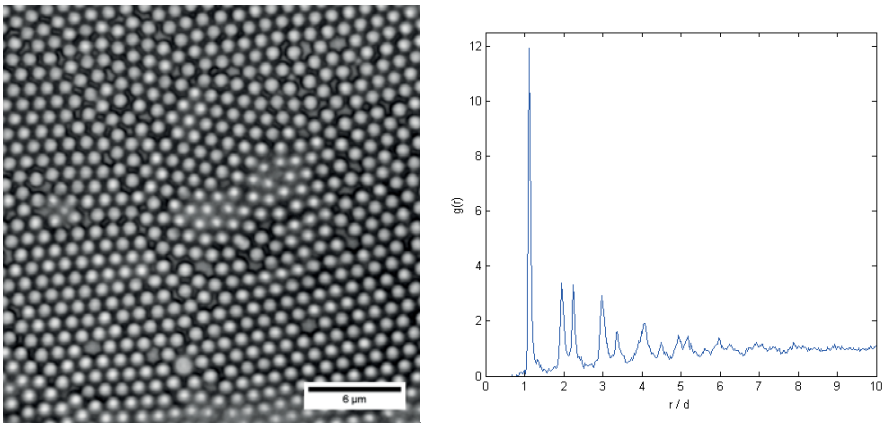


Fig. 5: Microscopic structure of the interface of a particle stabilized bubble and the resulting pair correlation function g(r).

In contrast to the particle monolayer observed in Fig. 5, salt addition to the aqueous phase for screening of surface charges can alter the interfacial structure. A side effect of salt addition is aggregation of particles at the interface. As a result a multilayer structure, shown in Fig. 6, is obtained.

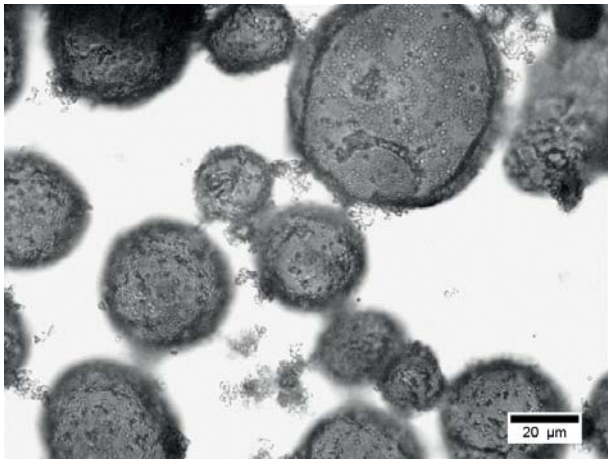


Fig. 6: Bubbles stabilized by anionic particles whose charges are screened by addition of 0.1M sodium chloride

### 2.3.5. Effect of surfactant exposure on the bubble stability

The surfactant Triton X-100 was used to investigate the interaction between particles residing on the bubble surface and surfactants added to the bulk aqueous phase. A non-ionic surfactant was chosen in order to avoid electrostatic interaction between surfactant and colloidal particles. The surfactant concentration was chosen so as to be above the critical micelle concentration of 0.22 to 0.24 mM given by the supplier [39]. In this concentration regime, the air-water interface as well as the polystyrene-water interface are expected to be completely covered with surfactant.

After the bubbles have been brought into contact with surfactant solution, it can be observed that particles are desorbing from the bubble interface (Fig. 7), the remaining particles are no longer jammed and bubbles shrink over time. This has been earlier reported in literature, and was attributed to a change in particle wettability. It was assumed there that surfactant molecules adsorb onto the particle surface with the hydrophobic tail towards and the hydrophilic head away from the particle surface, thereby causing the particles to be become more hydrophilic and consequently desorb from the air-water interface [39]. Indeed, it is well known that Triton X-100 adsorbs readily onto PS particles [40].

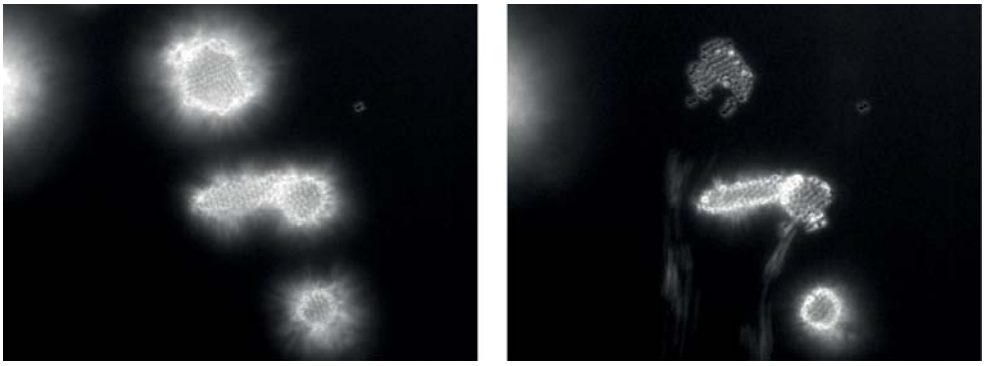

Fig. 7: Particle stabilized bubbles exposed to Triton X100, particles are expelled from the interface after surfactant addition

In order to quantify the change of particle wettability due to addition of surfactant, we measured the contact angles of a sessile drop of pure water, and surfactant solution respectively, on a flat polystyrene interface. The polystyrene surface was prepared by spin-coating and consisted of the same material the colloidal particles are made up of. Although this method does not determine the wettability of a colloidal particle itself, the method should give an estimate of the particle contact angle with the air-water interface. The method is easy to implement and is thus frequently used in practice [41]. For pure water on polystyrene, a contact angle of 87° was determined. This contact angle value indicates that polystyrene is partially wetted by water and

air, the particles made of this material should therefore strongly anchor to the bare air-water interface [42]. Contact angle measurements with a surfactant solution containing Triton X-100 in a concentration of 1mM were performed on the same polystyrene surface. For the drop of surfactant solution on the flat polystyrene surface we measured a contact angle of 12°. This strong decrease in contact angle in comparison with pure water can be attributed to the adsorption of surfactant on air-water as well as the polystyrene-water interface.

We did not measure contact angles of zero. However, we presume that the prepared polystyrene surfaces could be somehow more hydrophobic than the actual colloidal polystyrene particle. This can be because during spin-coating of polystyrene, hydrophilic groups may be buried inside the coated layer. On the colloidal particle, these hydrophilic groups are expected to be predominantly on the particle surface, making the particle more hydrophilic than a pure polystyrene layer. Thus, we assume that in the here tested surfactant concentration regime the actual colloidal particles might be completely wetted by the aqueous surfactant solution. For the behaviour of particles adsorbed to the air-water interface this means that surfactant addition causes the particles to desorb from the interface. As a result the colloidal armour loses its integrity, and the bubble is no longer protected against shrinkage due to dissolution of enclosed air. We therefore conclude, that the observed destabilization of particle stabilized air-bubbles can be explained solely by detergency. The dissolution of particles in this way also shows that no sintering takes place between the particles. Sintering of particles at the interface might have been considered as a possible mechanism for the appearance of stable bubble. This is because during ultrasound treatment the temperature can be locally very high, which might have caused the glassy polystyrene particles to sinter with each other.

## 2.4. Conclusion

We have shown that colloidal particles can be assembled at the air-water interface by means of ultrasonic treatment. With this method we were able to produce diluted bubble dispersions. We observe that the interface of stable air bubbles is covered with a jammed layer of colloidal particles. This closed packed shell emerges during shrinking of bubbles with initially partial particle coverage. Movement of particles at the interface is largely arrested, which makes the whole structure appear like a solid shell that protects the gas bubbles against dissolution. The stability of the shell can be attributed to the high desorption energy of the polystyrene polymer particles. These possess partial wettability for water and are thus practically irreversibly attached to the interface. The assembly of colloidal particles at the bubble interface

acts as a stress bearing network that inhibits the tendency of bubbles to shrink further.

The stability of the resulting structures is remarkable; particle stabilized bubbles are stable up to several weeks of storage. However, bubble stability is affected by the addition of surface active substances. Upon addition of surfactant, particles are ejected from the air-water interface. We explain that by a change in particle wettability owing to the adsorption of amphiphilic surfactant molecules on the hydrophobic polystyrene particle surface. As a result, the particle contact angle changes. This seems to favour the formation of a surfactant stabilized bubble which readily dissolves owing to the high Laplace pressure associated with their micron-sized dimension. The fact that particles can desorb as individual entities from the interface confirms that the particles do not sinter at the interface. Even though there might have been local heating during ultrasonic treatment, the particle shell seems to be solely hold together by capillary interaction.

In this study we only used a batch process to assemble particle stabilized bubbles. The implementation of a continuous ultrasound process can be easily envisaged. Altogether, ultrasound treatment seems to be a valuable method for straightforward creation of particle stabilized bubbles with the inherent exceptional stability.

## References


1. Prud'homme, R.K. and S.A. Khan, *Foams : theory, measurements, and applications*. Surfactant science series;vol. 57. 1996, New York [etc.]: Dekker.
2. Kloek, W., T. van Vliet, and M. Meinders, *Effect of Bulk and Interfacial Rheological Properties on Bubble Dissolution.* J Colloid Interface Sci, 2001. **237**(2): p. 158-166.
3. Meinders, M.B.J. and T. van Vliet, *The role of interfacial rheological properties on Ostwald ripening in emulsions.* Advances in Colloid and Interface Science, 2004. **108–109**(0): p. 119-126.
4. Binks, B.P., *Particles as surfactants - similarities and differences.* Current Opinion in Colloid & Interface Science, 2002. **7**(1-2): p. 21-41.
5. Binks, B.P. and T.S. Horozov, *Aqueous foams stabilized solely by silica nanoparticles.* Angew Chem Int Ed Engl, 2005. **44**(24): p. 3722-5.
6. Du, Z., et al., *Outstanding Stability of Particle-Stabilized Bubbles.* Langmuir, 2003. **19**(8): p. 3106-3108.
7. Kaz, D.M., et al., Physical ageing of the contact line on colloidal particles at liquid interfaces. Nature Materials, 2012. **11**(2): p. 138-142.
8. Yao, L., et al., *Near field capillary repulsion.* Soft Matter, 2013. **9**(3): p. 779-786.

9. Park, J.I., et al., Titelbild: A Microfluidic Approach to Chemically Driven Assembly of Colloidal Particles at Gas–Liquid Interfaces (Angew. Chem. 29/2009). Angewandte Chemie, 2009. **121**(29): p. 5321-5321.
10. Stride, E., et al., *Increasing the nonlinear character of microbubble oscillations at low acoustic pressures.* Journal of The Royal Society Interface, 2008. **5**(24): p. 807-811.
11. Campbell, G.M. and E. Mougeot, *Creation and characterisation of aerated food products.* Trends in Food Science & Technology, 1999. **10**(9): p. 283-296.
12. Tcholakova, S., N.D. Denkov, and A. Lips, *Comparison of solid particles, globular proteins and surfactants as emulsifiers.* Physical Chemistry Chemical Physics, 2008. **10**(12): p. 1608-1627.
13. Binks, B.P., M. Kirkland, and J.A. Rodrigues, *Origin of stabilisation of aqueous foams in nanoparticle-surfactant mixtures.* Soft Matter, 2008. **4**(12): p. 2373-2382.
14. Alargova, R.G., et al., *Foam superstabilization by polymer microrods.* Langmuir, 2004. **20**(24): p. 10371-10374.
15. Cui, H.T., et al., Aqueous foams stabilized solely by CoOOH nanoparticles and the resulting construction of hierarchically hollow structure. Journal of Nanoparticle Research, 2013. **15**(8).
16. Subramaniam, A.B., M. Abkarian, and H.A. Stone, *Controlled assembly of jammed colloidal shells on fluid droplets.* Nat Mater, 2005. **4**(7): p. 553-556.
17. Li, Y., et al., Contact Angle of Water on Polystyrene Thin Films: Effects of CO2 Environment and Film Thickness. Langmuir, 2007. **23**(19): p. 9785-9793.
18. Zhang, F., L. Cao, and W. Yang, Preparation of Monodisperse and Anion-Charged Polystyrene Microspheres Stabilized with Polymerizable Sodium Styrene Sulfonate by Dispersion Polymerization. Macromolecular Chemistry and Physics, 2010. **211**(7): p. 744-751.
19. Vincent, B., The synthesis of functional colloids, in International School of Physics “Enrico Fermi”, Volume 184 : Physics of Complex Colloids, C. Bechinger, F. Sciortino, and P. Ziherl, Editors. 2013.
20. Goodwin, J.W., et al., The preparation and characterisation of polymer latices formed in the absence of surface active agents. British Polymer Journal, 1973. **5**(5): p. 347-362.
21. Herrera-Ordonez, J. and R. Olayo, Methyl methacrylate emulsion polymerization at low monomer concentration: Kinetic modeling of nucleation, particle size distribution, and rate of polymerization. Journal of Polymer Science Part a-Polymer Chemistry, 2001. **39**(14): p. 2547-2556.
22. Elaiessari, A., et al., Adsorption and Desorption Studies of Polyadenylic Acid onto Positively Charged Latex Particles. Langmuir, 1995. **11**(4): p. 1261-1267.

23. Takahashi, M., ζ Potential of Microbubbles in Aqueous Solutions: Electrical Properties of the Gas–Water Interface. The Journal of Physical Chemistry B, 2005. **109**(46): p. 21858-21864.
24. Graciaa, A., et al., *The ζ-Potential of Gas Bubbles.* Journal of Colloid and Interface Science, 1995. **172**(1): p. 131-136.
25. Pushkarova, R.A. and R.G. Horn, *Bubble−Solid Interactions in Water and Electrolyte Solutions.* Langmuir, 2008. **24**(16): p. 8726-8734.
26. Beattie, J.K., A.M. Djerdjev, and G.G. Warr, *The surface of neat water is basic.* Faraday Discussions, 2009. **141**(0): p. 31-39.
27. Israelachvili, J.N., Chapter 13 - Van der Waals Forces between Particles and Surfaces, in Intermolecular and Surface Forces (Third Edition). 2011, Academic Press: San Diego. p. 253-289.
28. Haynes, W.M., D.R. Lide, and T.J. Bruno, *CRC handbook of chemistry and physics*. 2012, Boca Raton, Fla [etc.]: CRC.
29. Englert, A.H., et al., Interaction forces between a deformable air bubble and a spherical particle of tuneable hydrophobicity and surface charge in aqueous solutions. Journal of Colloid and Interface Science, 2012. **379**(1): p. 121-129.
30. Tarimala, S. and L.L. Dai, *Structure of Microparticles in Solid-Stabilized Emulsions.* Langmuir, 2003. **20**(9): p. 3492-3494.
31. Gautier, F., et al., *Pickering emulsions with stimulable particles: from highly- to weakly-covered interfaces.* Physical Chemistry Chemical Physics, 2007. **9**(48): p. 6455-6462.
32. Binks, B.P., et al., Naturally occurring spore particles at planar fluid interfaces and in emulsions. Langmuir, 2005. **21**(18): p. 8161-7.
33. Kam, S.I. and W.R. Rossen, *Anomalous Capillary Pressure, Stress, and Stability of Solids-Coated Bubbles.* Journal of Colloid and Interface Science, 1999. **213**(2): p. 329-339.
34. Subramaniam, A.B., et al., *Mechanics of Interfacial Composite Materials.* Langmuir, 2006. **22**(24): p. 10204-10208.
35. Jin, H., et al., Super stable foams stabilized by colloidal ethyl cellulose particles. Soft Matter, 2012. **8**(7): p. 2194-2205.
36. Irvine, W.T.M., M.J. Bowick, and P.M. Chaikin, *Fractionalization of interstitials in curved colloidal crystals.* Nature Materials, 2012. **11**(11): p. 948-951.
37. Danov, K.D., et al., Particle-interface interaction across a nonpolar medium in relation to the production of particle-stabilized emulsions. Langmuir, 2006. **22**(1): p. 106-115.
38. Paunov, V.N., Novel Method for Determining the Three-Phase Contact Angle of Colloid Particles Adsorbed at Air–Water and Oil–Water Interfaces. Langmuir, 2003. **19**(19): p. 7970-7976.

39. Subramaniam, A.B., et al., Microstructure, Morphology, and Lifetime of Armored Bubbles Exposed to Surfactants. Langmuir, 2006. **22**(14): p. 5986-5990.
40. Romero-Cano, M.S., A. Martín-Rodríguez, and F.J. de las Nieves, *Adsorption and Desorption of Triton X-100 in Polystyrene Particles with Different Functionality: I. Adsorption Study.* Journal of Colloid and Interface Science, 2000. **227**(2): p. 322-328.
41. Gillies, G., et al., *Contact angles and wetting behaviour of single micron-sized particles.* Journal of Physics-Condensed Matter, 2005. **17**(9): p. S445-S464.
42. Aveyard, R., B.P. Binks, and J.H. Clint, *Emulsions stabilised solely by colloidal particles.* Advances in Colloid and Interface Science, 2003. **100**: p. 503-546.

## Chapter 3

# Synthesis and stimuli-responsive properties of core-shell particles

We here report on the preparation of micron-sized core-shell particles comprising a solid polystyrene (PS) core and a soft poly-N-isopropylacrylamide (PNIPAM) shell functionalized with methacrylic-acid. By varying the number of seed particles during the precipitation polymerization of NIPAM, we could obtain core-shell particles with varying core/shell size ratios (radius core/radius shell) in the range of 0.04 up to 1.33. The resulting core-shell particles are monodisperse and remain colloidal stable even at a very high electrolyte concentration of 300 mM NaCl, while the polystyrene core particles tend to aggregate at such a high electrolyte concentration. This demonstrates that the soft shell provides a steric barrier against aggregation. The synthesized core-shell particles exhibit responsiveness to temperature, pH and electrolyte concentration. The lower critical solution temperature (LCST) of the core-shell particles is markedly increased in comparisons with pure PNIPAM-polymers and was found to be around 45 °C - 50 °C. Increasing the temperature up to 60 °C leads to a pronounced collapse of the soft shell, core-shell particles attain a size which is only slightly larger than the core particles.

This Chapter is based on: C Buchcic, RH Tromp, MBJ Meinders and MA Cohen Stuart, Characterization of the multi-stimuli-responsive properties of polystyrene-poly(N-isopropylacrylamide) core-shell particles, Manuscript in preparation

## 3.1. Introduction

As the name indicates, core-shell particles are a class of particles comprising a core and a shell. Core and shell can consist of different materials, often referred to as composite particles, or of the same material with a different kind of structure differentiating both parts. Synthesis of core-shell particles is often done to combine different material properties into the same entity in order to obtain new functional properties [1]. The choices regarding core and shell material are numerous. A prominent choice is to coat a polymer particle with a silica shell. The silica shell can serve for further chemical modification via the rich silane chemistry [2]. Another prominent example are core-shell particles with a polystyrene (PS) core and a poly-N-isopropylacrylamide (PNIPAM) shell [3]. PNIPAM has a lower critical solution temperature (LCST) around 32°C, below this temperature the polymer exists in a well-hydrated state and above this temperature most water is released and the polymer chain collapses. PNIPAM containing core-shell particles have gained great interest for controlled release of biomolecules [4], because of the stimuli-responsive rheological properties of the respective particle dispersions [5], and due to their tunable optical properties [6].

Polymeric core-shell structures can be created in a one-step procedure by using monomers with different polymerization rates [7]. The synthesis of core-shell particles is, however, often done via a two-step or multi-step procedure [6]. PS-PNIPAM core-shell particles can be made by synthesis of PS core particles and subsequent precipitation polymerization of PNIPAM. The polymerization reaction starts with a dilute solution of NIPAM-monomer and initiator at a temperature well above the lower critical solution temperature (LCST) of PNIPAM. The resulting polymers are insoluble and thus precipitate on top of the PS cores. Further growth of the PNIPAM shell proceeds by capture of monomers, oligomers and initiator from solution [8]. The size of the resulting shell can be controlled by the amount of seed particles present during precipitation polymerization [6]. While most reports on core-shell particles focus on core-shell particles with either a very thin shell relative to the core or vice versa, we here report on the preparation of core-shell particles which are multi-responsive and where the size ratio core/shell can be easily varied over a relative large range of values.

## 3.2. Material & Methods

### 3.2.1. Materials

Styrene, itaconic acid (IA), initiator 4,4′-azobis(4-cyanovaleric acid) (ACVA), N-isopropylacrylamide (NIPAM), N,N′-methylbisacrylamide (BIS), methacrylic acid

(MA), potassium peroxodisulfate (KPS) and sodium chloride (NaCl) are purchased from Sigma-Aldrich. Ready-to-use dialysis device Float-A-Lyzer G2 with molecular weight cut-off (MWCO) of 1000 KDa (Spectrum, US). Deionized (DI) water with a resistance of 18.2 MΩ.cm is used for all measurements.

### 3.2.2. Synthesis Core particles

Polystyrene particles are prepared by surfactant free emulsion polymerization. 20 g Styrene, 0.5 g itaconic acid and 180 g DI water are charged to a round-bottom flask sealed by a rubber septum. The flask is placed in an oil bath and heated to 80°C under sparging with nitrogen gas for the duration of 20 minutes. 220 mg of the initiator 4,4′-azobis(4-cyanovaleric acid) dissolved in 5 ml of 0.2 M sodium hydroxide solution is added to the reaction mixture. The reaction proceeds for the duration of 18 hours at 80°C under stirring at 200rpm. After filtering through glass wool, the resulting particle dispersion is centrifuged at 2500g for 3h. The supernatant is removed and the precipitate is re-dispersed in DI water. This centrifugation-redispersion cycle is repeated until the surface tension of the supernatant measured by tensiometry is 72 mN $m^{-1}$. The solid content of the final core particle dispersion was adjusted to 125 g $L^{-1}$.

### 3.2.3. Synthesis core-shell particles

Core-shell particles are prepared by precipitation polymerization. 90 g DI water, 0.5 g NIPAM, 20 mg BIS, 50 µl MA and varying amounts of core particle dispersion with a solid content of 125 g $L^{-1}$ (for CS15: 12.5g, CS167: 10g, CS230: 5g, CS530: 2.5g, for sample code see Tab. 1) are charged to a round-bottom flask sealed by a rubber septum. The flask is placed in an oil bath and heated to 80°C under sparging with nitrogen gas for the duration of 20 minutes. 50 mg of the initiator potassium persulfate dissolved in 5 ml of DI water is added to the reaction mixture. The reaction proceeds for the duration of 2 hours at 80°C under stirring at 200rpm. At the end of the reaction the resulting product is filtered through glass wool and the resulting particle dispersion is centrifuged at 2500g and a temperature of 20°C for 2h. The supernatant is removed and the precipitate is re-dispersed in DI water. Subsequent centrifugations steps are carried out at 5°C, 2500g for 24 hours. The centrifugation-redispersion cycles are typically repeated six times until the surface tension of the supernatant measured by tensiometry is 72 mN $m^{-1}$.

### 3.2.4. Electrolyte titration

Measurements are performed on a ALV apparatus with a DPSS laser (Cobolt Samba 300 mW at 532 nm), ALV 50/100/200/400/600 µm Pinhole system, a Thorn RFIB263KF Photo Multiplier Detector, ALV7002 external correlator and a ALV-SP/86 Goniometer. 3 ml of diluted particle dispersion is filled in a titration vessel. At discrete time intervals 400 mM sodium chloride solution is added under stirring. The measuring time until a sodium chloride concentration of 300 mM is reached usually amounts to a period of 24 hours.

### 3.2.5. Dynamic Light Scattering (DLS)/ Micro-electrophoresis

Size and electrokinetic charge of the colloidal particles are determined by performing dynamic light scattering and micro-electrophoresis on a Malvern Nanosizer S apparatus. Prior to analysis the particle dispersion is diluted. Were necessary, adjustment of the pH is done by dropwise addition of 0.1 M hydrochloric acid or 0.1 M sodium hydroxide. Temperature sweeps are performed in a quartz cuvette. Micro-electrophoresis is performed in a disposable folded capillary cell.

## 3.3. Results & Discussion

An overview of the synthesised core-shell particles together with their dimension is given in Tab. 1. Size determination was done by DLS. Note, that the particle size of the core-shell particles is a function of temperature $T$, salt concentration $c_s$ and $pH$. Particle sizes given are measured at 20 °C, pH 6 and in the presence of 20 mM NaCl as background electrolyte; the number contained in the sample code refers to the thickness of the soft shell under these condition. The radius of the polystyrene (PS) core particles is for all particles between 360 and 400 nm. The main source of variation in particle size is the variation in shell thickness.

Tab. 1 Overview core-shell particles dimension as measured by DLS at 20 °C, pH 6 and in the presence of 20 mM NaCl as background electrolyte

| Sample code (number indicates shell thickness in nm) | Particle radius [nm] / PDI [-] | Shell thickness [nm] |
|---|---|---|
| core | 368 / 0.08 | 0 |
| CS15 | 383 / 0.07 | 15 |
| CS167 | 567 / 0.07 | 167 |
| CS230 | 630 / 0.07 | 230 |
| CS530 | 930 / 0.09 | 530 |

### 3.3.1. Influence of temperature on colloidal stability and size of core-shell particles

The temperature response of the synthesized core-shell particles is assessed using DLS. With this technique the hydrodynamic diameter of the particles is obtained. Note that the particle dimension as apparent from Fig. 1 are measured for core-shell particles dispersed in DI water. The particle sizes are accordingly larger than the dimension given in Tab. 1 which are valid at 20 °C, pH 6 and in presence of 20 mM NaCl. If we dispersed the particles in 20 mM NaCl instead of DI water, the core-shell particles showed a tendency for aggregation upon increasing the temperature, as indicated by a soaring polydispersity index. The differences in phase behaviour below and above the particles LCST can be explained in the following way: below the LCST, when the particle shell is highly swollen, van der Waals attraction between the PNIPAM based particle shell are considered to be negligible. At temperatures well above the LCST, water is expelled and van der Waals attraction becomes important [6]. Furthermore, dangling PNIPAM chains which are present on the particle surface and give rise to steric stabilization, collapse at elevated temperatures. This leads to a vanishing steric stabilization, so that the core-shell particles are left with ionizable groups that can impart electrostatic stabilization. Some ionizable groups may be buried under the collapsed shell which may than prevent them from dissociating. Altogether, attractive van der Waals interaction, vanishing steric stabilization and decreasing electrostatic interaction seem to give rise to an attractive interaction potential at elevated temperatures. This manifests itself by the core-shell particle's tendency to aggregate upon heating to 60 °C when 20 mM NaCl as background electrolyte is present.

As core-shell particles dispersed in DI water did not show any signs of aggregation upon heating, we infer that a highly swollen PNIPAM shell can grant good colloidal stability to the core-shell particles even at elevated temperatures. The plot of the temperature dependent particle diameter reveals the distinct temperature response of the synthesized core-shell particles, while the size of the core particles is not affected by temperature (see Fig. 1). The largest particles CS530 can reduce their radius to about 65 percent of their initial size upon heating. Core-shell particles CS167 still reduce their radius to about 25 percent of their initial size. By comparing particles sizes at 60°C and 20°C, a very small but significant size reduction can be ascertained for the smallest core-shell particles CS15. The most salient feature of these data are that at temperatures of 60 °C the radius of the core-shell particles is only slightly larger than the radius of the core particles. This highlights that at temperature below the LCST the shell is highly swollen with water, as cold water is a good solvent for PNIPAM. However, by heating the core-shell particle dispersion well

above their LCST temperature, all water seem to be expelled from the PNIPAM shell. Our results are in accordance with reports in literature whereupon PNIPAM microgels contain 97 percent water by weight [9]. The expulsion of most water from the particle shell seem therefore be a plausible cause for the strong particle size reduction observed upon heating.

Noteworthy in Fig. 1 is the broad range of temperatures over which deswelling of the particle shell takes place. While pure PNIPAM polymers show a sudden volume collapse when heated above their LCST of 32 °C, the deswelling of our PNIPAM-co-MA based particle shell seem to occur gradually over a range of temperatures. Taken the steepest slope in the size-temperature curve depicted in Fig. 1 as a measure for the typical volume phase transition temperature, the core-shell particles synthesized in this study show a volume-phase transition temperature between 45°C and 50°C. The distinct increase in the particles LCST compared to pure PNIPAM polymers can be attributed to strong electrostatic interaction between ionised groups in the particle shell. Their mutual repulsion impedes conformational changes of the polymer chain upon increasing the temperature. As the result, the LCST of the copolymer-based particle shell is shifting towards higher temperatures compared to pure PNIPAM. Similar observation on the effect of charges on the LCST are made by other authors [9, 10].

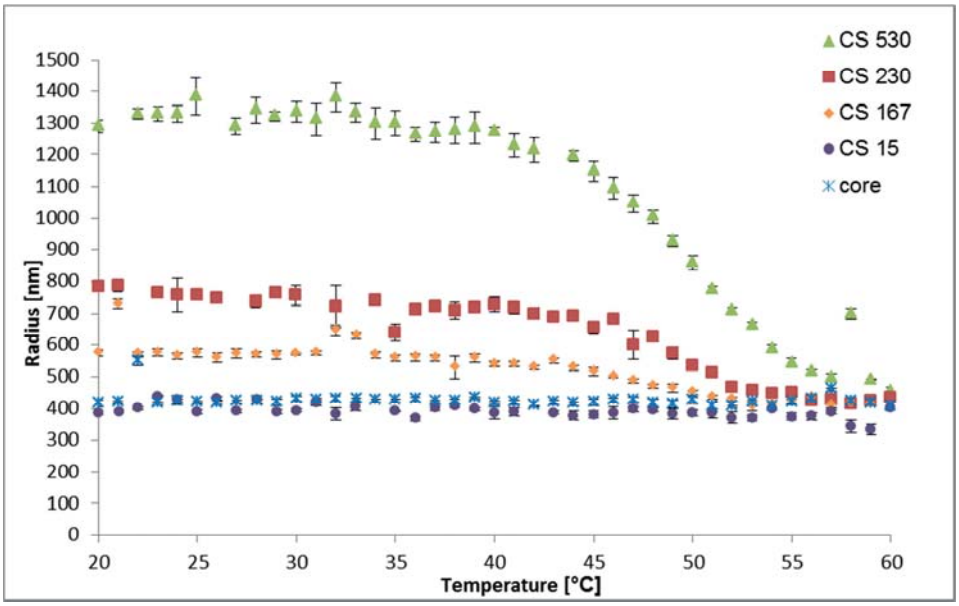


Fig. 1 Radius of core-shell particles (CS15, CS167, CS230, CS530) and core particles as function of temperature, size determination by dynamic light scattering, particles are dispersed in DI water in order to ensure colloidal stability at elevated temperatures (see text), particle sizes given here are accordingly larger than the dimension given in Tab. 1 which refers to the particle size at pH 6 and in the presence of 20 mM NaCl

### 3.3.2. Influence of electrolyte concentration on size and colloidal stability of core-shell particles

Next to their temperature response, the here synthesised core-shell particles change their size as a function of electrolyte concentration (see Fig.2). Addition of electrolyte leads to a pronounced particle size reduction. The large core-shell particles CS 530 reduce their radius from 1284 nm in DI water to 929 nm in the presence of 20 mM NaCl. The influence of electrolyte concentration on the particles size can be attributed to strong charge interaction between ionic co-monomers contained in the particle shell, these interaction are screened by the added electrolyte. As electrolyte is added, the range of electrostatic interaction is reduced, individual segments of the PNIPAM shell can come into closer contact, effectively the particle shell shrinks.

For most of the work done in the context of this thesis, we use 20 mM NaCl as background electrolyte. This background electrolyte concentration seems appropriate since the core-shell particles change their size substantially up to 20mM NaCl. Above this electrolyte concentration, size changes are less pronounced. Thus, changing the electrolyte concentration, e.g. through pH adjustment, will have no pronounced effect on the particle size.

Note that even at high electrolyte concentrations of 300 mM NaCl the measured hydrodynamic diameter of the core-shell particles CS 530 remains constant. The scattering intensity showed a linear decrease as function of electrolyte concentration. From this observation we conclude that core-shell particles do not undergo aggregation, they remain colloidal stable. This stability towards added electrolyte arises due to the fluffy PNIPAM shell with dangling chains on the particle surface. As PNIPAM is well water soluble, interpenetrating chains repel each other when particles are brought into contact. These repulsive forces provide good stability against aggregation of the core-shell particles.

The stability of the core-shell colloids towards electrolyte can be put into contrast to the marginal colloidal stability of the core particle dispersion in the presence of high electrolyte concentrations. Core particles are stabilized by electrostatic interaction only. For the core particles a radius of 400 nm is measured up to 75 mM NaCl (see Fig. 2). Above this concentration threshold the hydrodynamic radius of the core PS particles, as measured by DLS, is increasing. At an electrolyte concentration of 75 mM NaCl charge interaction seem to be screened to such an extent that solely electrostatic stabilization is insufficient to provide colloidal stability. Thus, particles tend to aggregate and the apparent particle radius as measured by DLS is increasing.

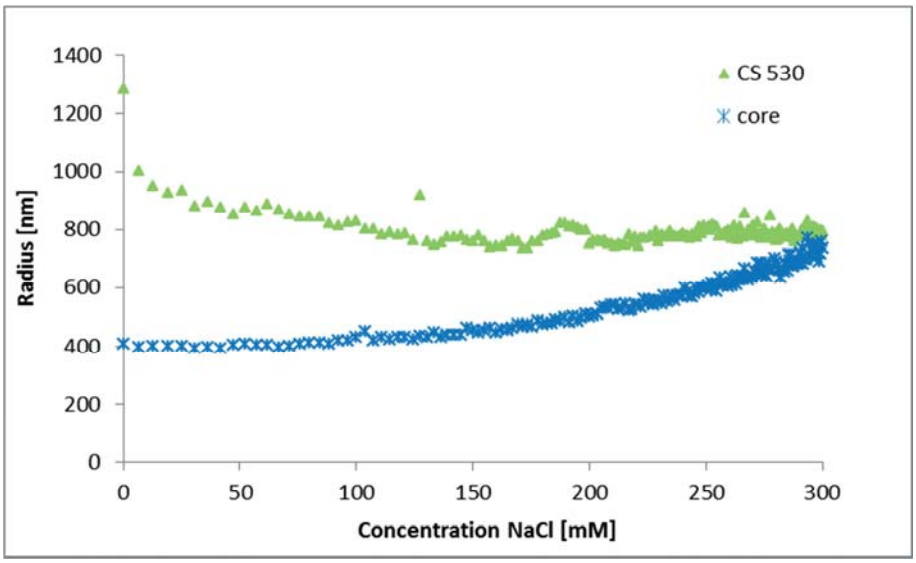


Fig. 2 Hydrodynamic radius of core-shell particles CS530 & core particles as function of NaCl concentration (other parameters: pH 6 and 20°C)

### 3.3.3. Influence of pH on core-shell particles

The ionic co-monomer contained in the particle shell makes the core-shell colloids synthesised here also responsive to changes of pH. The degree of swelling of the particle shell is a result of the equilibrium between the internal osmotic pressure within the shell and the entropic cost of stretching individual polymer chains. As a result, core-shell particles de-swell upon lowering the pH when the acrylic acid comonomer is protonated. Acrylic acid has a pKa of 4.25. This is also reflected in Fig. 3 which shows a strong decline in the hydrodynamic diameter of core-shell particles CS530 around pH 4. For PS core particles, a slight increase of the measured hydrodynamic diameter at low pH values can be ascertained. This is most likely the result of minor particle aggregation, owing to vanishing electrostatic stabilization at low pH.

A look at the particles electrophoretic motilities under electrophoresis allows to draw further conclusion on the bulk interparticle interaction as a function of pH: the measured electrophoretic mobility's are decreasing with decreasing pH. The low electrophoretic mobility at low pH let us conclude that the electrostatic contribution to the colloidal stability becomes vanishingly small. For core particles this causes the slight tendency to aggregate at low pH, whereas core-shell particles remain colloidal stable. Noticeable is also the different magnitude of electrophoretic motilities between core particles and core-shell particles. This may indicate that the PNIPAM layer inhibits the charging of surface functional groups on the PS core particle.

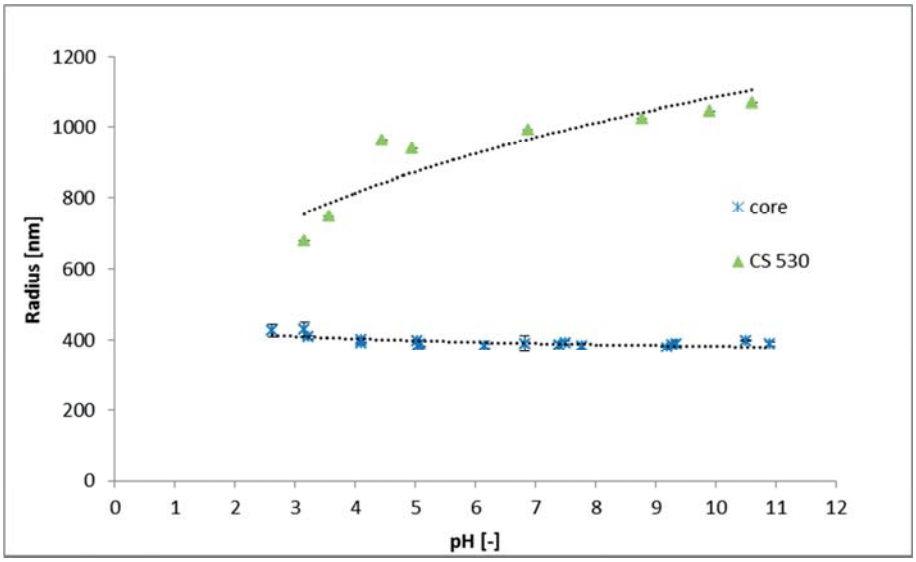


Fig. 3 Hydrodynamic radius of core-shell particles CS530 & core particles as a function of pH (other parameters: 20 °C and 20 mM NaCl as background electrolyte)

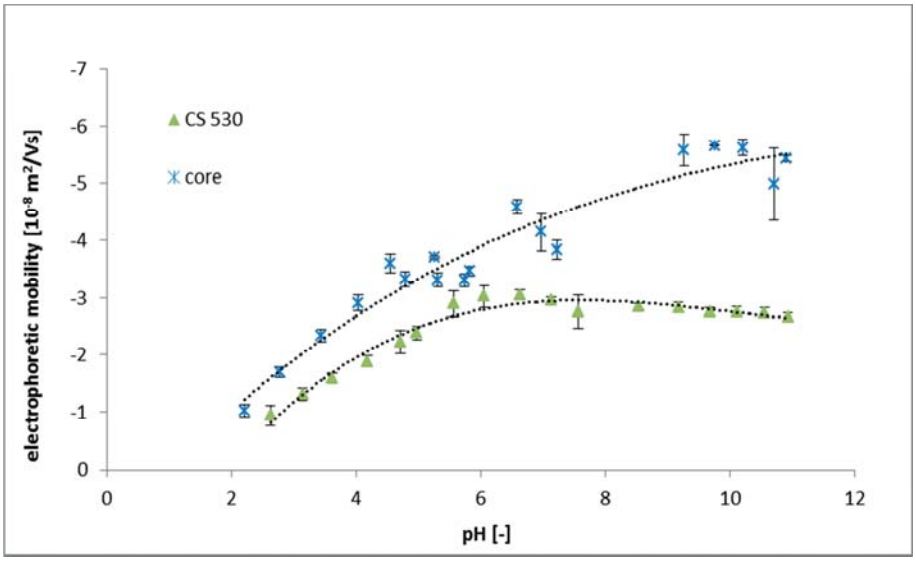


Fig. 4 Electrophoretic mobility $\mu_e$ of core-shell particles CS 530 & core particles as a function of pH (other parameters: 20°C and 20 mM NaCl as background electrolyte)

## 3.4. Conclusion

In the present work we prepared micron-sized core-shell particles consisting of a hard polystyrene (PS) core and a soft, poly-N-isopropylacrylamide (PNIPAM) shell functionalized with methacrylic-acid (MA). By varying the number of PS seed particles during the precipitation polymerization, the dimension of the PNIPAM shell could be varied from 15 nm up to 530 nm (at 20 °C, pH 6 and 20 mM NaCl present in the bulk phase). Despite the presence of the hard core, the core-shell particles exhibit responsiveness to external stimuli, such as temperature, pH and electrolyte concentration. This also verifies the successful assembly of the PNIPAM shell on top of the polystyrene core particles. The soft shell is highly swollen with water, as evident by the pronounced collapse of the shell upon increasing the temperature to 60°C.

### References


1. Hayes, R., et al., Core–shell particles: Preparation, fundamentals and applications in high performance liquid chromatography. Journal of Chromatography A, 2014. **1357**: p. 36-52.
2. Graf, C., et al., *A General Method To Coat Colloidal Particles with Silica.* Langmuir, 2003. **19**(17): p. 6693-6700.
3. Makino, K., et al., *Surface Structure of Latex Particles Covered with Temperature-Sensitive Hydrogel Layers.* Journal of Colloid and Interface Science, 1994. **166**(1): p. 251-258.
4. Dong, L.-c. and A.S. Hoffman, *A novel approach for preparation of pH-sensitive hydrogels for enteric drug delivery.* Journal of Controlled Release, 1991. **15**(2): p. 141-152.
5. Senff, H., et al., *Rheology of a Temperature Sensitive Core−Shell Latex.* Langmuir, 1999. **15**(1): p. 102-106.
6. Perro, A., et al., Design and Synthesis of Model Transparent Aqueous Colloids with Optimal Scattering Properties. Langmuir, 2009. **25**(19): p. 11295-11298.
7. Pelton, R. and T. Hoare, *Microgels and Their Synthesis: An Introduction*, in *Microgel Suspensions*. 2011, Wiley-VCH Verlag GmbH & Co. KGaA. p. 1-32.
8. Wang, J., et al., Monodisperse, Molecularly Imprinted Polymer Microspheres Prepared by Precipitation Polymerization for Affinity Separation Applications. Angewandte Chemie International Edition, 2003. **42**(43): p. 5336-5338.
9. Burmistrova, A., et al., The Effect of Co-Monomer Content on the Swelling/Shrinking and Mechanical Behaviour of Individually Adsorbed PNIPAM Microgel Particles. Polymers, 2011. **3**(4): p. 1575.
10. Snowden, M.J., et al., Colloidal copolymer microgels of N-isopropylacrylamide and acrylic acid: pH, ionic strength and temperature effects. Journal of the Chemical Society, Faraday Transactions, 1996. **92**(24): p. 5013-5016.

## Chapter 4

# Harnessing the advantages of hard and soft colloids by use of core-shell particles as interfacial stabilizers

The ability of colloidal particles to be inserted into fluid interfaces is a crucial factor in the preparation of particle stabilized disperse systems such as foams and emulsion. For hard micron-sized particles the insertion into fluid interfaces requires substantial energy input, but soft particles are known to adsorb spontaneously. Particle hardness, however, may also affect foam and emulsion stability. The high compliance of soft particles can compromise the ability to withstand lateral compression of the particle covered interface during disproportionation. Hence, particles which can spontaneously adsorb onto fluid interfaces, and yet depict low compliance may be ideal as interfacial stabilizers. In the present work, we prepared core-shell particles comprising a hard, polystyrene core and a soft poly(N-isopropylacrylamide) based shell. We found that such core-shell particles can spontaneously adsorb onto various fluid interfaces. The absence of a pronounced energy barrier for interfacial adsorption allowed for facile preparation of core-shell particle stabilized bubbles and emulsion droplets. The stability of the resulting bubbles was better than that of bubbles stabilized by entirely soft particles, but disproportionation was not stopped completely. This is in contrast to the emulsion droplets that showed excellent stability against coalescence and disproportionation. Lateral compression of core-shell particle due to disproportionation was clearly limited by the presence of the polystyrene core, and allowed for long-lasting emulsion stabilization and led to the occurrence of non-spherical emulsion droplets. Our results indicate that core-shell particles comprising a hard core and soft shell can combine the advantageous properties of hard and soft particles, namely spontaneous adsorption and limited compliance, and can therefore be superior materials for the preparation of particle-stabilized interfaces.

This Chapter is based on: C Buchcic, RH Tromp, MBJ Meinders and MA Cohen Stuart, Harnessing the advantages of hard and soft colloids by use of core-shell particles as interfacial stabilizers, Manuscript in preparation

## 4.1. Introduction

Colloidal particles are a prominent alternative to the application of small molecular weight surfactants (SMWS) and proteins for the stabilization of disperse systems such as foams and emulsions. As these particles are typically much larger than SMWS and proteins, they strongly anchor to the fluid interface and can impart greater stability compared to other interfacial stabilizers. Their superior stabilizing properties and the ability to respond to external stimuli lead to a recent surge of research carried out in the area of particle stabilized interfaces [1-9]. Particles which are used to stabilize dispersions can be differentiated into two classes by their softness and deformability: 'soft' particles have elastic moduli in the kPa range and can be substantially deformed by interfacial forces [9, 10], while 'hard' particles have high elastic moduli in the GPa range and, thus, do not easily deform by interfacial forces [11].

Since the early work of Ramsden and Pickering, hard particles, e.g. colloidal hydrophobized silica, are known as effective stabilizers of emulsions [12]. Accordingly, the term Pickering emulsion or Pickering stabilization is nowadays commonly adopted if one refers to a dispersion stabilized by solid particles. The particle's adsorption strength to fluid interfaces is largely determined by the ability of both fluids to wet the particle surface. The degree of wetting is characterized by the particle contact angle θ, with θ close to 0 degrees for hydrophilic, θ close to 180 degrees for hydrophobic and θ close to 90 degrees for particles which are equally wetted by both phases (intermediate wetting). Once particles larger than about a few nanometres and with a contact angle close to 90° are residing in the interfaces, they are practically irreversibly attached. This is because the energy of desorption for removing one particle from the interface into one of the two continuous phases is orders of magnitude larger than the thermal energy $k_BT$ [2].

The stability of a dispersion stabilized by hard particles arises due to a steric mechanism. Once the interface of a dispersion is covered by a sufficient amount of hard particles, coalescence of individual droplets or bubbles stops. Also, Ostwald ripening, the pressure-driven exchange of material between differently sized domains of the dispersed phase may initially proceed but will eventually stop once interfacial particles start to experience sufficiently large lateral repulsion due to increased surface coverage. At this point a so called 'colloidal armour' is formed. Ostwald ripening is arrested because the relative high elastic modulus of hard particles inhibits their deformation and particles of appropriate wettability possess a very high adsorption energy and, thus, are unlikely to desorb from the interface due to lateral repulsion [13].

An important property which qualitatively distinguishes hard particles from soft particles is their adsorption behaviour onto liquid interfaces. Hard particles, in particular when negatively charged, do not adsorb without mechanical energy input. The reasons for the difficulty to adsorb are not always clear, but generally electrostatic effects between particle and interface are held responsible [1]. The electrostatic repulsion between negatively charged hard particles and a negatively charged fluid interface causes an energy barrier for particle adsorption onto the interface. [14]. Promoting particle adsorption thus requires high energy input processing methods such as turbulent mixing or sonication [15]. In the context of applications, it is not always possible to modify the sign of the particle charge or use high energy processing methods. Therefore, an alternative should be welcome.

In contrast to the use of hard particles, the interest in soft particles (also known as microgel particles) as dispersion stabilizers arose more recently. Microgels are colloidal particles consisting of a cross-linked polymer network which is highly swollen by a good solvent. Such particles can be routinely made by the same methods as used for the preparation of hard particles, using cross-linker and polymers that are insoluble due to the increased temperature during the polymerization reaction, but dissolve on subsequent cooling. Poly(N-isopropylacrylamide) (PNIPAM) is a well-known material for soft, aqueous microgels. The polymer undergoes a structural transition from coil-to-globule upon increasing the temperature above the lower critical solution temperature (LCST) which leads to a volume reduction of the microgel particles. Incorporation of ionic co-monomers into the microgels can also impart responsiveness to ionic strength and pH. These structural changes in response to external stimuli make microgels very interesting materials for the particle stabilization of fluid interfaces, as the stability of the particles comprising dispersion can be altered by changing physico-chemical factors of the bulk solution [16].

Soft particles such as PNIPAM-based microgels are compliant and can be considerably deformed by capillary forces. Soft particles typically spread out radially at the interface. This spreading stops once the energy gain from covering the interface with polymer is balanced by the energy required for elastic deformation of the cross-linked polymer particles. Aside the particle deformation due to interfacial spreading, aqueous microgels are usually weakly hydrated in the non-polar phase which causes the particles to be substantially flattened at the non-polar side of the interface [17].

Soft particles are considered as good interfacial stabilizers for emulsion droplets [17, 18]. Due to their large size they irreversibly adsorb to liquid interfaces and provide a steric hindrance to coalescence [19]. In addition to the steric effect, the spreading of microgels onto a liquid interface can lead to the formation of a viscoelastic interfacial

layer which can provide certain kinetic stability against Ostwald ripening [20]. Very soft microgels which are highly swollen are most susceptible to form entangled contact zones leading to such a viscoelastic interface [21]. On the other hand the high compliance of microgels can also be a disadvantage for their ability to provide long-term stability against Ostwald ripening. Due to their high compliance, interfacial microgels may undergo radial compression and substantially deform during Oswald ripening. This viscous deformation might impair their ability to completely stop Ostwald ripening in the same way as hard particles do.

For soft particles interfacial adsorption occurs spontaneously and is, at least at low surface coverage, mainly governed by particle diffusion to the fluid-fluid interface [22, 23]. The absence of considerable energy barriers against interfacial adsorption of soft particles is desirable for preparation of a particle stabilized dispersion, as the energy input for processing is lower and the rate of particle adsorption can be simply controlled by the process parameter concentration.

From this introduction it should become clear that both kinds of particles markedly differ in their functional properties with regard to dispersion stabilization. Spontaneous adsorption as observed for soft particles is desirable, yet, the particles high compliance might impair the ability to establish a stress bearing network and stop Ostwald ripening. Hard particles in contrast, can be barely deformed and can effectively stop Oswald ripening, but are difficult to bring to the interface. We want to investigate, if core-shell particles, comprising a soft shell on top of a hard core may have characteristics of both particle types. The soft shell may enable spontaneous adsorption onto fluid interfaces, and the hard core may provide a well-defined end-point to the lateral compression of the particle-covered interface during disproportionation.

In order to test this hypothesis, we designed core-shell particles with a solid core and a soft shell. We investigated how particles with different shell dimension are taken up at liquid-gas and liquid-liquid interfaces, and what surface pressures they generate. We also studied the structure of particle covered interfaces, and the stability of bubbles and emulsion droplets stabilized by core-shell particles.

## 4.2. Material & Methods

### 4.2.1. Materials

Styrene, itaconic acid (IA), initiator 4,4′-azobis(4-cyanovaleric acid) (ACVA), N-isopropylacrylamide (NIPAM), N,N′-methylbisacrylamide (BIS), methacrylic acid (MA), potassium peroxodisulfate (KPS), Divinylbenzene (DVB) and sodium chloride (NaCl) were purchased from Sigma-Aldrich. Deionized (DI) water with a resistance of 18.2 MΩ.cm was used for all measurements.

### 4.2.2. Synthesis core particles

Polystyrene core particles were prepared by surfactant free emulsion polymerization. 20 g Styrene, 0.5 g itaconic acid and 180 g DI water were charged to a round-bottom flask sealed by a rubber septum. For cross-linked particles also 0.39 g DVB was added. The flask was placed in an oil bath and heated to 80°C under sparging with nitrogen gas for the duration of 20 minutes. 220 mg of the initiator 4,4′-azobis(4-cyanovaleric acid) dissolved in 5 ml of 0.2 M sodium hydroxide solution was added to the reaction mixture. The reaction proceeded for the duration of 18 hours at 80°C under stirring at 200rpm. After filtering through glass wool, the resulting particle dispersion was centrifuged at 2500g for 3h. The supernatant was removed and the precipitate was re-dispersed in DI water. The supernatant was removed and the precipitate was re-dispersed in DI water. This centrifugation-redispersion cycle was repeated until the surface tension of the supernatant measured by tensiometry was 72 mN $m^{-1}$.

### 4.2.3. Synthesis core-shell particles

Core-shell particles were prepared by precipitation polymerization. 90 g DI water, 0.5 g NIPAM, 20 mg BIS, 50 µl MA and varying amounts of core particle dispersion were charged to a round-bottom flask sealed by a rubber septum. The flask was placed in an oil bath and heated to 80°C under sparging with nitrogen gas for the duration of 20 minutes. 50 mg of the initiator potassium persulfate dissolved in 5 ml of DI water was added to the reaction mixture. The reaction proceeded for the duration of 2 hours at 80°C under stirring at 200rpm. At the end of the reaction the resulting product was filtered through glass wool and the resulting particle dispersion was centrifuged at 2500g and a temperature of 20°C for 2h. The supernatant was removed and the precipitate re-dispersed in DI water. Subsequent centrifugations steps were carried out at 5°C, 2500g for 16 hours. These centrifugation-redispersion cycles were typically repeated three times until the surface tension of the supernatant measured by tensiometry was 72 mN $m^{-1}$.

### 4.2.4. Dynamic Light Scattering

Dynamic light scattering (DLS) was performed on an instrument from ALV (Langen, Germany) equipped with a diode-pumped solid-state laser (Cobolt Samba 300 mW at 532 nm), ALV 50/100/200/400/600 µm pinhole system, a Thorn RFIB263KF photo multiplier detector, ALV7002 external correlator and a ALV-SP/86 goniometer. The scattering intensity of a diluted particle dispersion was measured at a scattering angle of 90°. Temperature was kept constant at 20 °C. Hydrodynamic diameter and polydispersity index (PDI) were obtained from a cumulant analysis. PDI is the square of standard deviation $\varphi$ divided by the mean diameter $d$:

$$PDI = \left(\frac{\varphi}{d}\right)^2 \quad (1)$$

### 4.2.5. Tensiometry

The surface tension of the particle dispersion was determined on a Drop Tensiometer, model TRACKER (Teclis, France). All measurements were performed in the pendant drop configuration. Prior to the measurement, the dispersion was diluted to the desired particle concentration and adjusted to pH 6.

### 4.2.6. Light microscopy

Light Microscopy was done on an upright Olympus BX 50 light microscope equipped with several long working distance objectives and a reflected light, vertical illuminator. For visualization of bulk aqueous dispersions, samples were filled into a home-made glass capillary of approximately 100 µm height. For visualisation of specimens located at a fluid interface, particle dispersion and the corresponding fluids were filled in a shallow quartz cuvette (3 cm x 2 cm x 0.5 cm).

### 4.2.7. Cryo-scanning electron microscopy

A stock of concentrated particle dispersion was diluted, yielding a volume number density $c_\infty$ (number of particles in a certain volume) of $9.25\times10^{-15}$ $m^{-3}$ with 20 mM NaCl as background electrolyte. 40 µl of this particle dispersion was transferred to a circular copper sample holder with 5 mm inner diameter and 1mm deep cavity. The particle dispersion was left to equilibrate for 20 minutes to enable particles to adsorb to the fluid interface. Freezing of the samples was done by plunging them in liquid nitrogene for two minutes. Subsequently, the specimens were partially freeze-dried at -93°C for 1 min to remove ice crystals, followed by tungsten coating up to 10 nm on a high vacuum coating system Leica EM MED 020. Sample transfer was done with a Leica EM VCT 100 vacuum cryo transfer system. Cryo-SEM imaging was performed on a ultra-high resolution field emission scanning electron microscope FEI Magellan 400. To ensure that only the top surface of the sample, on the order of nanometres, is imaged, we opted for a low accelerating voltage of the electron beam (2 kV). The low accelerating voltage also avoids charging of the samples and detection of secondary electrons; altogether it ensures a good image quality.

## 4.3. Results & Discussion

An overview of the synthesised particles together with their sizes is given in Tab. 1. Please note, that the particle size is a function of temperature $T$, salt concentration $c_s$ and $pH$. Particle sizes given in Tab. 1 are measured at 20 °C, pH 6 and in the presence of 20 mM NaCl as background electrolyte. The core sizes are all between 350 and 400 nm. The main source of variation in particle size is the variation in shell thickness.

Tab. 1 Overview of the synthesised particles and their sizes as measured by DLS at 20 °C, pH 6 and in the presence of 20 mM NaCl as background electrolyte, PDI= $(\varphi/d)^2$ (see equation 1)

| Sample code | Particle radius [nm] / PDI [-] | Shell thickness [nm] |
|---|---|---|
| core | 368 / 0.08 | 0 |
| CS15 | 383 / 0.07 | 15 |
| CS106 | 474 /0.05 | 106 |
| CS140 | 508 / 0.05 | 140 |
| CS167 | 567 / 0.07 | 167 |
| CS186* | 549 / 0.03 | 186 |
| CS230 | 630 / 0.07 | 230 |
| CS300 | 668 / 0.15 | 300 |
| CS530 | 930 / 0.09 | 530 |

*This particle type comprises cross-linked PS core particles

### 4.3.1. Interfacial tensiometry

The adsorption of particles to the air-water and oil-water interface was followed by pendant drop tensiometry. Clearly, all core-shell colloids, except the ones with the smallest shell dimension (CS15), readily develop considerable surface pressures while for the core particle dispersion the surface tension remained the same as for a clean interface (see Fig. 1). The same qualitative observation was made for decane-water (see Fig. 2), hexane-water and dodecane-water interfaces. We found that also hard polystyrene particles with cationic surface charge hardly adsorbed onto fluid interfaces, but could be made to adsorb at fluid interfaces by growth of a soft shell around them (data not shown). These observations highlight the generality of the method to promote interfacial adsorption of particles by means of a soft shell.

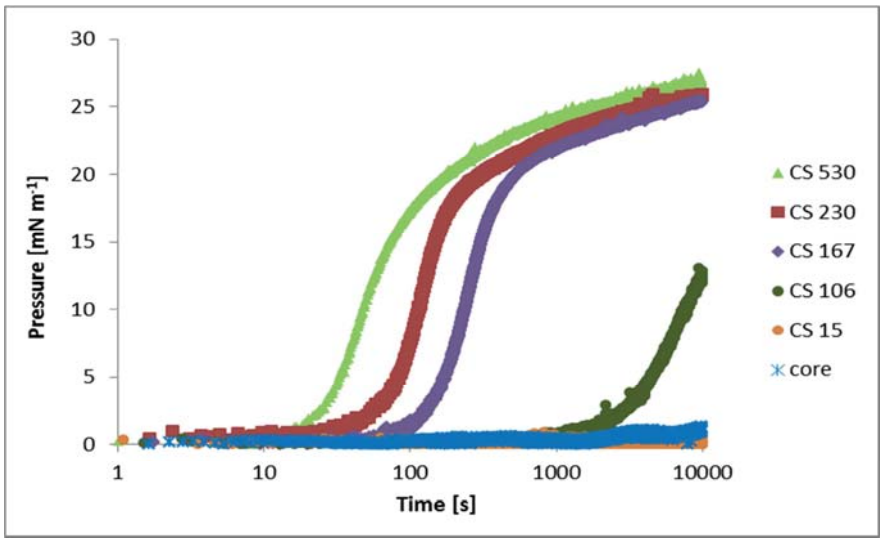


Fig. 1 Surface pressure development of core-shell vs core particle dispersion at the air-water interface, experimental condition: volume number density $c_\infty = 9.25\times10^{-15}$ m$^{-3}$, pH 6, 20 mM NaCl as background electrolyte

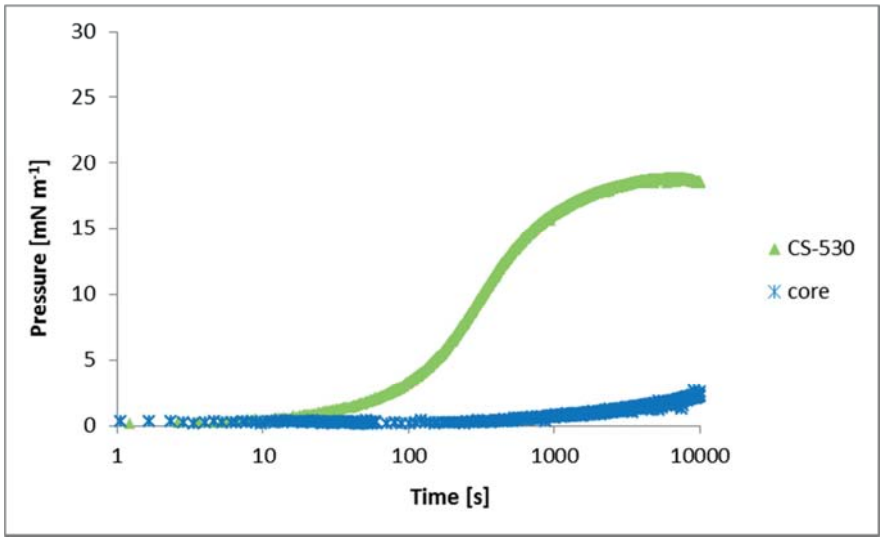


Fig. 2 Surface pressure development of core-shell vs core particle dispersion at the hexane-water interface, experimental condition: volume number density $c_\infty = 9.25\times10^{-15}$ m$^{-3}$, pH 6, 20 mM NaCl as background electrolyte

For quantitative interpretation of this data, one has to be aware that the equation of state for core-shell colloids is for the most part non-linear in the density, meaning that one cannot easily relate surface pressure to surface coverage [23].

For molecular species at low surface coverage, when molecules do not interact with each other, the surface pressure development is described by the ideal gas law:

$$\Pi = \bar{R}T\frac{n}{A} \quad (2)$$

where $\Pi$ is the surface pressure, $A$ is the area, $n$ is the number of particles in moles, $\bar{R}$ is the ideal gas constant and $T$ is the temperature of the system. Assuming full coverage of the interface by particles with a diameter of one micrometre, one arrives at a surface pressure on the order $10^{-6}$ mN m$^{-1}$ for a fully covered interface. The detection limit of the drop Tensiometer is on the order of $10^{-4}$ mN m$^{-1}$. Hence, the surface pressure we measure for micron-sized particles cannot be an 'ideal gas' pressure, rather, it must stem from the interaction between individual particles. One can safely say that any finite surface pressure measured must correspond to a situation where the surface coverage is significant and particles interact with each other via steric or electrostatic interaction.

To estimate a minimum timescale for a particle population to reach a certain surface coverage, the formula of Ward and Tordai can be used [24]. The formula is valid if there is no adsorption barrier and colloidal particles are irreversibly adsorbed to the interface.

$$\Gamma(t) \approx 2c_{\infty}\sqrt{\frac{Dt}{\pi}} \quad (3)$$

Where $\Gamma$ is the area number density (number of particles in a unit area), $c_{\infty}$ is the volume number density (number of particles in a unit volume), $t$ is time and $D$ is the particle diffusion coefficient.

For a rigorous determination of the timescale for development of a finite surface pressure according to equation 3, the equation of state would be necessary. For an order of magnitude estimate we can assume that core-shell particles start to interact once the interface reaches a certain $\Gamma^*$ which we choose for each different particle type in such a way to result in a surface coverage $\Gamma/\Gamma_{max}$ = 0.05. This value for the surface coverage we choose to yield a good fitting of our experimental data to the adsorption model. In Chapter 5 we confirm that core-shell particles can indeed yield a finite surface pressure at such a surface coverage. For the diffusion constant $D$ we use the values obtained by DLS. The volume number density $c_{\infty}$ was $9.25\times10^{-15}$ m$^{-3}$ for each particle type. According to equation 3 we calculate the corresponding time scales $t^*$ (the time it takes to reach $\Gamma/\Gamma_{max}=0.05$) and compare these to the measured $t^*$ from Fig. 1. The results are given in Tab. 2.

Tab. 2 Time for onset of finite surface pressure of 1 mN $m^{-1}$ $t^*_{measured}$ as obtained from Fig. 1 versus $t^*_{theoretical}$ calculated according to formula (3), also displayed are $\Gamma^*$ and D used to calculate $t^*_{theoretical}$

| Particle type | $\Gamma^*$ [$m^{-3}$] | D [$m^2$ $s^{-1}$] | t* measured [s] | t* theoretical [s] |
|---|---|---|---|---|
| CS 530 | 1.84E+10 | 2.20E-13 | 16 | 14 |
| CS 230 | 4.01E+10 | 3.42E-13 | 27 | 43 |
| CS 167 | 4.95E+10 | 3.79E-13 | 95 | 59 |
| CS 106 | 7.08E+10 | 3.79E-13 | 1900 | 122 |
| CS 15 | 1.09E+11 | 5.77E-13 | >10000 | 187 |
| core | 1.18E+11 | 5.96E-13 | - | 213 |

Clearly, for the core-shell particles with a thick shell, theoretical and measured time scales are on the same order of magnitude. For the core-shell particles CS106 and CS15 with a thin shell and for the core particles, however, $t^*_{measured} >> t^*_{theoretical}$. This picture is consistent with an energy barrier for interfacial adsorption. Such an energy barrier reduces the probability for particle attachment to the interface, thereby increasing the timescale for development of a certain surface pressure [1].

Our results suggest that the adsorption barrier, as existing for hard particles, seems to be substantially lowered, if not even absent, for the core-shell particles with a shell thickness above a given value. This value is larger than 100 nm. In contrast to hard particles, the core-shell particles seem to adsorb easily to the fluid interface once they reach the subsurface region.

### 4.3.2. Microscopic analysis of core-shell particles at the fluid interface

As the core-shell particles have a solid core with an index of refraction which differs markedly from the surrounding medium, they are well visible via light microscopy, in spite of their small size. This allowed us to conduct microscopic analysis to get an impression of the structure of particle layer on the fluid interface. For the core particles without soft shell, we could not detect any particles attaching to the fluid interface over a period of one day. In fact, we observed that particles are depleted from the subsurface region due to sedimentation. For all the core-shell samples, however, we found that particles can adsorb to the air-water (see Fig. 3) and oil-water interface (see Fig. 4). As we observed the samples under quiescent condition, this adsorption process seems to occur without energy input, solely by diffusion. These observations are in agreement with the results we obtained from tensiometry. Note that core-shell particles CS15 did not show any surface pressure development over the time-scale depicted in Fig. 1, but microscopy revealed a densely covered interface after an waiting time of one day.

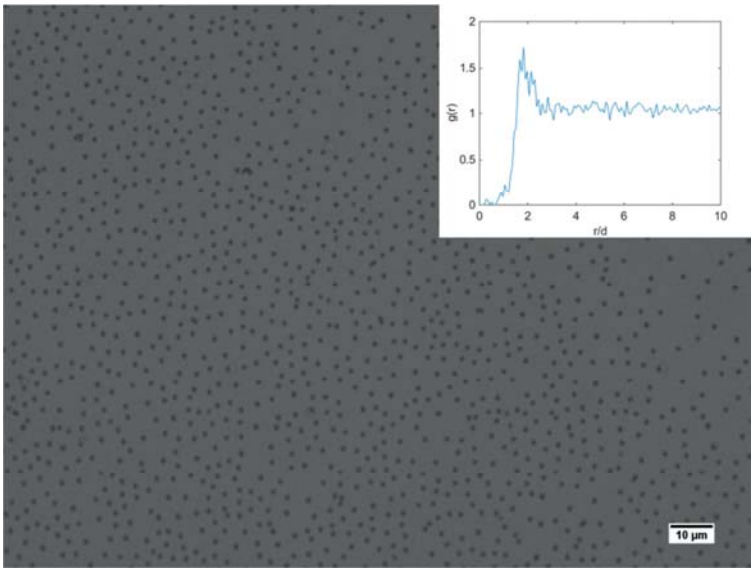


Fig. 3 Microscopic picture of an air-water interface onto which core-shell particles CS530 are adsorbed, Inset show the calculated particle pair-correlation function G(r) normalized by the particle diameter

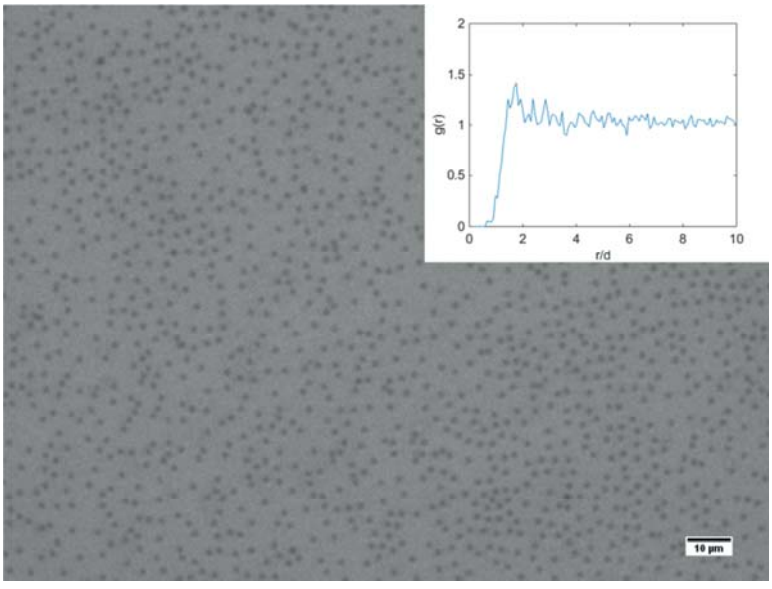


Fig. 4 Microscopic picture of a decane-water interface onto which core-shell particles CS530 are adsorbed, Inset show the calculated particle pair-correlation function G(r) normalized by the particle diameter

To obtain more detailed information about the morphology of core-shell particles adsorbed to the air-water interface we used cryo-SEM. The cryofixation procedure allows the samples to be frozen instantly, so that the structure of interfacially located core-shell particles can be studied in the hydrated state. Also with light microscopy only the core of the core-shell particles is visible, while with cryo-SEM also the structure of the soft shell can be ascertained.

From the SEM pictures it becomes evident that core-shell particles adopt a fried-egg like structure at the interface (see Fig. 5, Fig. 6). Due to the higher electron density of the core compared to the shell, both parts of the core-shell particle can be distinguished. The core seems to have a rough surface, while the outer shell is more smooth. The dimension of the inner part with the rough surface equals the measured hydrodynamic diameter of the core particles, which gives further support that this part is the actual core particle. The fact that the core is visible in the SEM picture implies that the core of the core-shell particles protrudes into the air. This is a striking feature, as the bare core particles without shell can not breach the interface.

Measurement of the overall particle dimensions in the SEM pictures reveals that the diameter of the core-shell particles at the interface is roughly equal to their hydrodynamic diameter as measured by DLS in the bulk. For the particles depicted in Fig. 5 we find a diameter of ~ 1.3 µm at the interface, and a hydrodynamic diameter of 1.3 µm. For another set of particles (see Fig. 6) we obtain ~ 1.9 µm particle cross-sectional diameter at the interface, and a hydrodynamic diameter of 1.9 µm by DLS in the bulk. This means that our core-shell particles do not undergo significant radial stretching at the interface, in contrast to what is frequently reported for microgels [17, 23]. Radial stretching of the soft shell seems to be suppressed by the solid core.

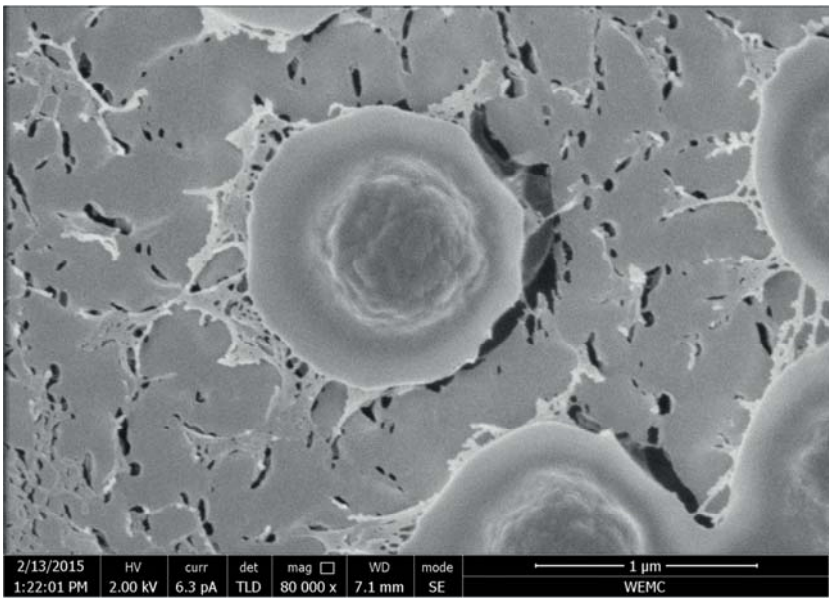


Fig. 5 Cryo-SEM picture from core-shell particles CS230 adsorbed onto an air-water interface

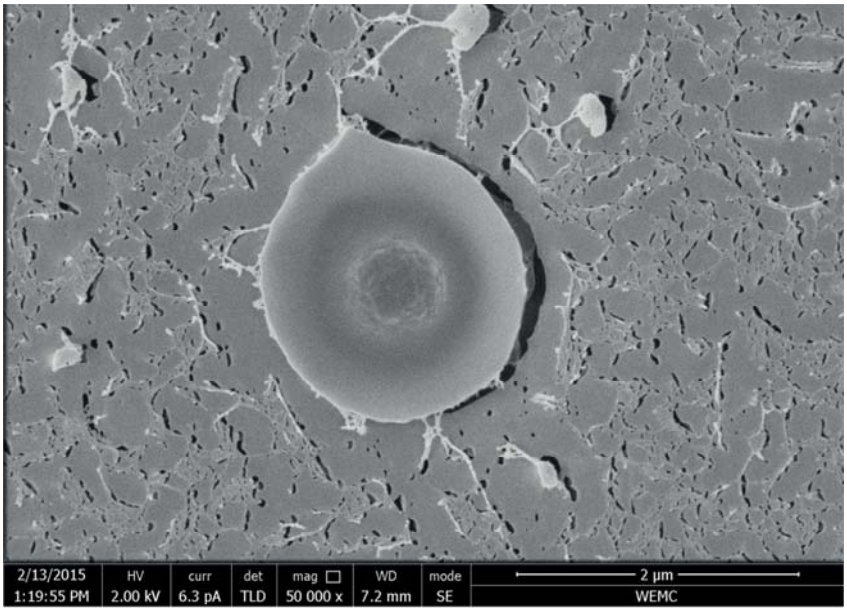


Fig. 6 Cryo-SEM picture from core-shell particle CS530 adsorbed onto an air-water interface

### 4.3.3. Stabilization of bubbles and emulsion droplets by core-shell particles

The facile adsorption of core-shell particles to fluid interfaces allowed for preparation of emulsions and air bubbles by low energy input methods, such as gentle hand-shaking. The typical size of bubbles and droplets obtained is 20 - 200 µm in diameter. Microscopic investigation reveals that the produced bubbles and droplets are stabilized by a monolayer of core-shell particles (see Fig. 7).

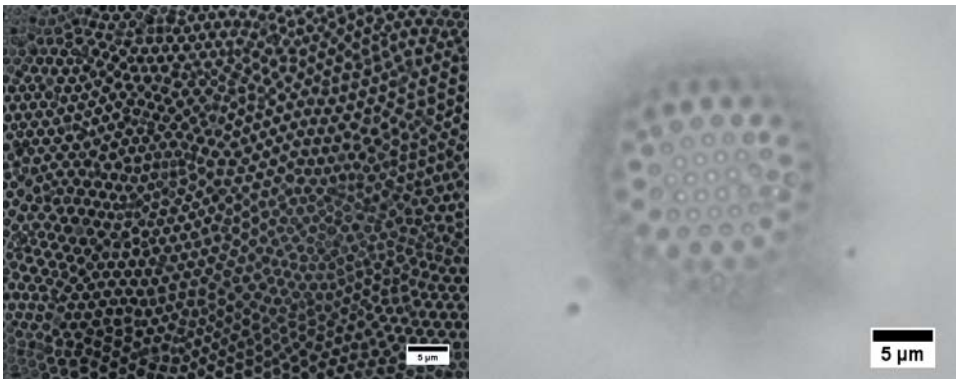


Fig. 7 Microscopic pictures showing the interfacial structure of air bubbles (a) and decane-in-water droplets (b) stabilized by core-shell particles CS 530

Apart from their facile adsorption to fluid interfaces, it is important for application purposes to check whether core-shell particles can effectively stabilize fluid interfaces against disproportionation and coalescence, and compare this with hard particles. For bubbles stabilized by core-shell particles we could still observe slow coarsening by disproportionation. The bubbles that we initially produced completely disappeared over a time frame of 2-3 days.

Oil-in-water emulsions of hexane, decane and toluene, showed much higher stability against coalescence and disproportionation. Decane-water emulsion did not show any signs of coarsening. Hexane and toluene emulsion droplets, comprising oils with rather high solubility in the aqueous phase, undergo an initial phase of coarsening, thereafter they are completely stable. This final stable state may be reached via the following sequence of events. Shrinking of small droplets leads to lateral compression of core-shell particles at the interface. The shrinkage of small droplets may stop when flat facets develop or when crumpling of the droplet interface leads to the occurrence of areas with convex and concave curvature, thus zero mean curvature, on the same droplet. The latter situation can arise after jamming and further lateral compression of the interfacial particles [25]. On the contrary, larger droplets grow in size. During the course of droplet growth, the particle surface

coverage is decreasing. Insufficient coverage with particles will promote coalescence of the larger droplets, thereby effectively decreasing the interfacial area [26, 27]. After a coalescence event, the effective surface coverage of the newly created droplet may exceed 100% which then leads to the adoption of non-spherical droplet shapes, crumpling of the droplet interface, occurrence of flat facets; similar to the situation described for shrinking droplets. The net result of these processes is that the surface coverage of the emulsion droplets is increasing and droplets stop coarsening [28-30]. Following the scenario described above, emulsion droplets may initially coarsen but then attain an interfacial monolayer of core-shell particles in which the soft shell is locally highly compressed, thereby enabling the establishment of a stress-bearing network at the interface which provides excellent stability against coarsening. This is indeed what we observe with hexane and toluene emulsion droplets covered by core-shell particles. As can be seen in Fig. 8, the structure of the core-shell particles at the liquid interfaces progresses from an uncompressed state (Fig. 8a) to strong lateral compression of the soft shell after 10 days of storage (see Fig. 8b). We also observed that initially spherical emulsion droplets attain pronounced non-spherical shapes (Fig. 9b), a property which is known for bubbles [15] and emulsion droplets [31] stabilized by hard particles. Thus, core-shell particles at the oil-water interface seem to combine two properties: the ability to spontaneously adsorb and the strong anchoring to the fluid interface. The question why core-shell particles can strongly anchor at the oil-water interface, but less so at the air-water interface cannot be answered yet.

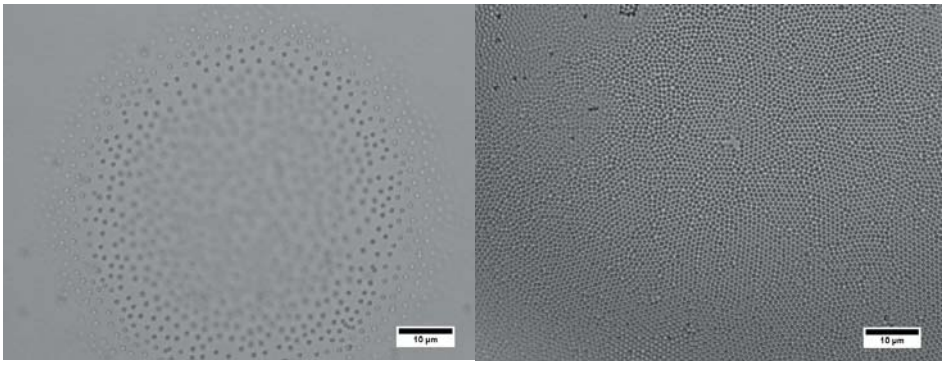


Fig. 8 Microscopic picture showing the interfacial structure of hexane-in-water emulsion droplets stabilized by core-shell particles CS230. Picture taken directly after emulsion preparation (a) and after 10 days of storage(b)

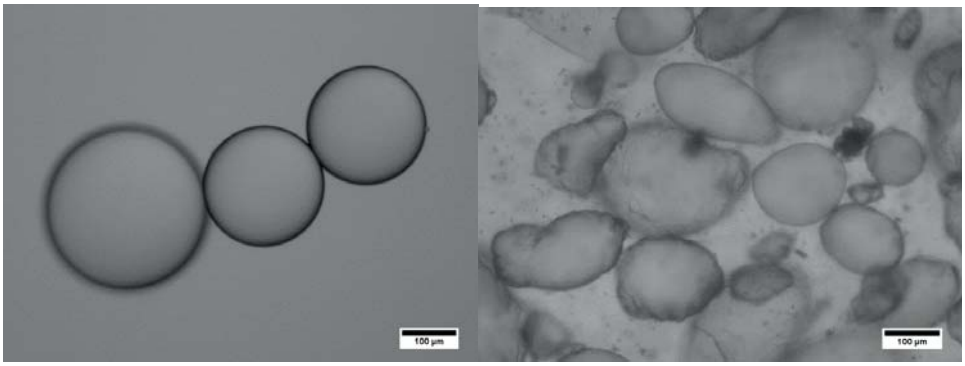


Fig. 9 Microscopic picture of hexane-in-water emulsion stabilized by poly-NIPAM microgels without PS core (radius 792 nm) (a) and core-shell particles CS140 (b)

Finally, we compare core-shell particles with conventional microgels without hard core. With them we were able to stabilize bubbles and emulsion droplets as reported elsewhere [21, 26, 32]. However, we find that microgel-covered air bubbles and hexane-in-water emulsion still undergo slow but continuous coarsening; during coarsening, bubbles and droplets remain spherical (see Fig. 9a), signalling a finite Laplace pressure. Hence, core-less soft particles are performing less well as stabilizers than core-shell particles. These observations seem to corroborate once more the conclusion that in order to stop coarsening and support non-spherical droplets, a colloidal amour of particles with low compliance is essential. Core-shell particles synthesized in this study seem to fulfil this requirement. Upon sufficient compression of their soft shell, they provide the necessary low compliance in order to allow the establishment of a solid-like interface which provides superior stability against Ostwald ripening of emulsion droplets.

## 4.4. Conclusion

In the present work we prepared micron-sized core-shell particles consisting of a hard polystyrene core plus a soft, poly-NIPAM based shell. By varying the number of seed particles during precipitation polymerization, the dimension of the NIPAM shell could be varied from 15 nm up to 530 nm. Interfacial adsorption of these core-shell particles was investigated by microscopy and tensiometry and provided evidence that the larger core-shell particles easily adsorb onto the air-water interface. For core-shell particles with shell dimension smaller than 100nm the adsorption rates where somehow reduced, which suggest that core-shell particles with a thin shell still possess a finite barrier for interfacial adsorption, nevertheless they could adsorb to

the air-water interface. Hard polystyrene core particles, in contrast, seem to experience such a pronounced energy barrier for interfacial adsorption that they did not adsorb at all.

The absence of a pronounced energy barrier for interfacial adsorption of core-shell particles allowed for facile, low energy-input production of bubbles and emulsion droplets stabilized by particles. Emulsions stabilized by core-shell particles showed good stability against coalescence and disproportionation. Bubbles stabilized by core-shell particles still underwent coarsening albeit slowly.

Remarkably, emulsion droplets stabilized by core-shell particles can adopt pronounced non-spherical shapes. This shows that core-shell particles strongly anchor to the fluid interface and that the hard core provides enough rigidity to the core-shell particles in order to allow the establishment of a stress bearing network which can sustain non-isotropic stresses present on non-spherical emulsion droplets. Consequently core-shell particles combine the advantageous properties of soft and hard particles: they can adsorb spontaneously to fluid interfaces, yet, anchor strongly at the interface and provide enough resistance against lateral compression due to disproportionation. Altogether our results show great promise for the application of core-shell particles to stabilize fluid interfaces as present in foams and emulsions.

## References


1. Tcholakova, S., N.D. Denkov, and A. Lips, *Comparison of solid particles, globular proteins and surfactants as emulsifiers.* Physical Chemistry Chemical Physics, 2008. **10**(12): p. 1608-1627.
2. Aveyard, R., B.P. Binks, and J.H. Clint, *Emulsions stabilised solely by colloidal particles.* Advances in Colloid and Interface Science, 2003. **100**: p. 503-546.
3. Binks, B.P., et al., *pH-responsive aqueous foams stabilized by ionizable latex particles.* Langmuir, 2007. **23**(17): p. 8691-4.
4. Du, Z., et al., *Outstanding Stability of Particle-Stabilized Bubbles.* Langmuir, 2003. **19**(8): p. 3106-3108.
5. Park, J.I., et al., *Titelbild: A Microfluidic Approach to Chemically Driven Assembly of Colloidal Particles at Gas–Liquid Interfaces (Angew. Chem. 29/2009).* Angewandte Chemie, 2009. **121**(29): p. 5321-5321.
6. Stocco, A., et al., *Particle-stabilised foams: an interfacial study.* Soft Matter, 2009. **5**(11): p. 2215-2222.
7. Ashby, N.P. and B.P. Binks, *Pickering emulsions stabilised by Laponite clay particles.* Physical Chemistry Chemical Physics, 2000. **2**(24): p. 5640-5646.
8. Kettlewell, S.L., et al., *Is Latex Surface Charge an Important Parameter for Foam Stabilization?* Langmuir, 2007. **23**(23): p. 11381-11386.

9. Style, R.W., L. Isa, and E.R. Dufresne, *Adsorption of soft particles at fluid interfaces.* Soft Matter, 2015. **11**(37): p. 7412-7419.
10. Abate, A.R., et al., *Measuring the elastic modulus of microgels using microdrops.* Soft Matter, 2012. **8**(39): p. 10032-10035.
11. Tan, S., R.L. Sherman, and W.T. Ford, *Nanoscale Compression of Polymer Microspheres by Atomic Force Microscopy.* Langmuir, 2004. **20**(17): p. 7015-7020.
12. Pickering, S.U., *CXCVI.-Emulsions.* Journal of the Chemical Society, Transactions, 1907. **91**(0): p. 2001-2021.
13. Subramaniam, A.B., M. Abkarian, and H.A. Stone, *Controlled assembly of jammed colloidal shells on fluid droplets.* Nat Mater, 2005. **4**(7): p. 553-556.
14. Nguyen, A.V., P. George, and G.J. Jameson, *Demonstration of a minimum in the recovery of nanoparticles by flotation: Theory and experiment.* Chemical Engineering Science, 2006. **61**(8): p. 2494-2509.
15. Buchcic, C., et al., *Assembly of jammed colloidal shells onto micron-sized bubbles by ultrasound.* Soft Matter, 2015. **11**(7): p. 1326-34.
16. Pelton, R., *Temperature-sensitive aqueous microgels.* Advances in Colloid and Interface Science, 2000. **85**(1): p. 1-33.
17. Geisel, K., L. Isa, and W. Richtering, *Unraveling the 3D Localization and Deformation of Responsive Microgels at Oil/Water Interfaces: A Step Forward in Understanding Soft Emulsion Stabilizers.* Langmuir, 2012. **28**(45): p. 15770-15776.
18. Richtering, W., *Responsive Emulsions Stabilized by Stimuli-Sensitive Microgels: Emulsions with Special Non-Pickering Properties.* Langmuir, 2012. **28**(50): p. 17218-17229.
19. Liu, T., et al., *Non-coalescence of oppositely charged droplets in pH-sensitive emulsions.* Proceedings of the National Academy of Sciences, 2012. **109**(2): p. 384-389.
20. Brugger, B., J. Vermant, and W. Richtering, *Interfacial layers of stimuli-responsive poly-(N-isopropylacrylamide-co-methacrylicacid) (PNIPAM-co-MAA) microgels characterized by interfacial rheology and compression isotherms.* Phys Chem Chem Phys, 2010. **12**(43): p. 14573-8.
21. Destribats, M., et al., *Soft microgels as Pickering emulsion stabilisers: role of particle deformability.* Soft Matter, 2011. **7**(17): p. 7689-7698.
22. Zhang, J. and R. Pelton, *Poly(N-isopropylacrylamide) Microgels at the Air−Water Interface.* Langmuir, 1999. **15**(23): p. 8032-8036.
23. Deshmukh, O.S., et al., *Equation of state and adsorption dynamics of soft microgel particles at an air-water interface.* Soft Matter, 2014. **10**(36): p. 7045-7050.
24. Ward, A.F.H. and L. Tordai, *Time-Dependence of Boundary Tensions of Solutions I. The Role of Diffusion in Time-Effects.* The Journal of Chemical Physics, 1946. **14**(7): p. 453-461.

25. Abkarian, M., et al., *Dissolution arrest and stability of particle-covered bubbles.* Phys Rev Lett, 2007. **99**(18): p. 188301.
26. Destribats, M., et al., *Water-in-Oil Emulsions Stabilized by Water-Dispersible Poly(N-isopropylacrylamide) Microgels: Understanding Anti-Finkle Behavior.* Langmuir, 2011. **27**(23): p. 14096-14107.
27. Leal-Calderon, F. and V. Schmitt, *Solid-stabilized emulsions.* Current Opinion in Colloid & Interface Science, 2008. **13**(4): p. 217-227.
28. Wiley, R.M., *Limited coalescence of oil droplets in coarse oil-in-water emulsions.* Journal of Colloid Science, 1954. **9**(5): p. 427-437.
29. Arditty, S., et al., *Some general features of limited coalescence in solid-stabilized emulsions.* The European Physical Journal E, 2003. **11**(3): p. 273-281.
30. Madivala, B., et al., *Exploiting particle shape in solid stabilized emulsions.* Soft Matter, 2009. **5**(8): p. 1717-1727.
31. Bon, S.A.F., et al., *Route to stable non-spherical emulsion droplets.* European Polymer Journal, 2007. **43**(11): p. 4839-4842.
32. Destribats, M., et al., *Pickering Emulsions Stabilized by Soft Microgels: Influence of the Emulsification Process on Particle Interfacial Organization and Emulsion Properties.* Langmuir, 2013. **29**(40): p. 12367-12374.

## Chapter 5

# Equation of state of core-shell particles adsorbed at the air-water interface

Core-shell particle comprising a hard core and a soft, deformable shell can be an interesting alternative to rigid particles for the stabilization of foams and emulsions. We experimentally determined the 2D equation of state for various core-shell particles adsorbed at the air-water interface. The different particles investigated in this study vary in the particle shell thickness and thereby the particle size. The largest core-shell particles can develop a finite surface pressure at a surface coverage as low as 0.05, far from the close-packing limit. From this we infer that interaction among these particles is long-ranged. After on-set of a finite pressure, the surface pressure diverges and then levels-off, indicating relaxation of the system. The collapse pressure of the interfacial layer was found to be a function of the particle's shell thickness. Particles with a thin shell could withstand larger surface pressures than particle with a thick shell. We propose that these differences arise due to variations in the lateral interaction potential between the different particle types. This study gives a first insight into the structure and interaction of core-shell particles at a fluid interface upon compression.

This Chapter is based on: C Buchcic, RH Tromp, MBJ Meinders and MA Cohen Stuart, Equation of state of core-shell particles adsorbed at the air-water interface , Manuscript in preparation

## 5.1. Introduction

Since the discovery that colloidal particles adsorbed at the fluid interface can impart long-term stability to emulsion droplets, numerous studies have harnessed particles for the preparation of foams and emulsions [1-5]. As a general conclusion of these studies one can assert that colloidal particles can effectively stop coarsening of emulsion droplets and bubbles. Hard particles, such as silica or polystyrene particles, but also soft, cross-linked polymeric particles have been successfully used as stabilizers for fluid-fluid dispersions [2, 6]. Recently, also another interesting particle variety, namely core-shell particles, comprising a solid polystyrene (PS) core and a soft poly-N-isopropylacrylamide (PNIPAM) shell were used for the stabilization of emulsion droplets and bubbles. Particles seemed to adsorb stronger at the oil-water interface, were they could stop coarsening, compared to the air-water interface were they slowed down coarsening but could not stop the process. It was also found that core-shell particles undergo substantial radial compression at the oil-water interface before coarsening stops (Chapter 4).

The behaviour of colloidal particles situated at an fluid interface upon compression can be studied in a Langmuir-trough. Particles are first spread onto a flat fluid-fluid interface which is confined by mobile teflon barriers. Thereafter the interfacial area available for the particles is reduced by movement of the mobile barriers. The surface pressure is monitored simultaneously. The interfacial area available for the particles is a function of the initial amount of particles and the compression ratio. If the amount of particles which is spread at the interface is known and particles do not desorb during compression, the compression isotherm can thus be recorded. Compression of the interface leads to a smaller interparticle distance which typically causes enhanced lateral interaction between interfacial particles and a rise of the surface pressure. The surface pressure detected in such an experiment can be ascribed to electrostatic or steric interaction between particles situated at the fluid-fluid interfaces. The compression of interfacial particles in a Langmuir-trough can thus emulate the behaviour of particles at the interface of a shrinking bubble or droplet and yield quantitative information on the interaction strength between particles as a function of the interparticle distance.

For hard particles interparticle-interaction typically arises due to electrostatic interaction. These electrostatic interaction can be long-ranged and induce particle repulsion over distances as large as several particle diameters [7-10]. A strongly soaring surface pressure can be detected once interfacial particles are sufficiently close to each other. If the affinity of these hard particles for the fluid interface is strong enough, particles can remain attached to the interfaces up to the point where the start to touch each other (steric interaction). At this point further compression can

lead to a buckling instability, a corrugation of the particle stabilized interfacial layer can be observed when the net-area available for each particle is smaller than the particles cross-sectional area [11, 12].

Soft particles, such as polymeric microgels which are highly swollen in a good solvent have different properties. Microgels are thought to interact mainly via steric interaction [13]. Once the interfacial coverage of microgels is sufficiently high and excluded volume effects come into play, a rise in surface pressure can be observed. The surface pressure typically rises slowly, the compression isotherm is much more shallow than for particles interacting via electrostatic interaction [14]. A further characteristic of soft particle is that they can strongly deform upon adsorption to the interface [15]. Surface tension can cause particles to adopt a stretched configuration. This fact was also used to explain why soft, polymeric microgels developed a significant surface pressure at relatively low surface coverage where it was not expected that particles experience steric interaction. It has been postulated that because of the particles stretched configuration at the interface, the actual surface coverage is higher than the coverage calculated based on the particles hydrodynamic diameter in the bulk aqueous phase [16].

The shape of the compression isotherm (point of onset pressure, slope, maximum surface pressure) for colloidal particles adsorbed at a fluid interface is determined by several factors. For hard particles interacting via electrostatic interaction, the minimum interparticle distance prior to the onset of a finite surface pressure is determined by the particles penetration depth into the non-polar phase and the total particles surface charge [7]. For soft particles interacting via steric interaction, the extend of stretching may determine when particles yield a finite surface pressure [17]. As already mentioned, the slope of the compression isotherm is dictated by the type of interparticle interaction. Hard particles interacting by electrostatic interaction typically yield a strong slope, while soft particles typically give rise to a more gradual surface pressure development [13]. Dilational surface elasticities for hard particles can be on the order of several hundred mN $m^{-1}$ [18, 19]. In contrast, dilational surface elasticities for fluid interfaces covered by soft particles are reported to be a few mN $m^{-1}$ only [14, 20]. The maximum surface pressure before the compression isotherm levels off is another important quantity. It is a measure for the mechanical stability of the interfacial layer. This value can also serve as a measure for the particles adsorption strength to the fluid interface. This argument has been used to estimate the adsorption energy for soft particles at an oil-water interface [21]. Similar arguments also lead to an set of equation which can be used to estimate adsorption energy and particle contact angle of solid particles at a fluid interface [22].

The purpose of the current work was to characterize the behaviour of micron-sized core-shell particles adsorbed onto the air-water interface upon compression of the

interfacial layer. The core-shell particles comprise a hard PS core and a soft PNIPAM shell. Interparticle interaction of such core-shell particles particle may arise due to a combination of steric and electrostatic interaction. Which type of interaction prevails may depend from the length scale of electrostatic interaction as well as the dimension of the particles soft shell. In order to compare different core-shell particles in which either the one or the other kind of interaction prevails, we synthesized core-shell particles with the same PS core but different PNIPAM shell dimension. We recorded the compression isotherm of the respective core-shell particles upon spreading a known amount of particle dispersion onto the air-water interface. The structure of the particle laden interface upon spreading and compression was monitored via optical microscopy throughout the whole compression cycle.

## 5.2. Material & Methods

### 5.2.1. Materials

Styrene, itaconic acid (IA), initiator 4,4′-azobis(4-cyanovaleric acid) (ACVA), N-isopropylacrylamide (NIPAM), N,N′-methylbisacrylamide (BIS), methacrylic acid (MA), potassium peroxodisulfate (KPS) sodium chloride (NaCl), acetone and Iso-propanol (IPA) were purchased from Sigma-Aldrich. Deionized (DI) water with a resistance of 18.2 MΩ.cm was supplied by a MilliQ water purification system.

### 5.2.2. Synthesis core-shell particles

Core particles of polystyrene were prepared by surfactant free emulsion polymerization. 20 g Styrene, 0.5 g itaconic acid and 180 g DI water were loaded to a round-bottom flask sealed by a rubber septum. The flask was placed in an oil bath and heated to 80°C while flushing with nitrogen gas for the duration of 20 minutes to remove dissolved oxygen. 220 mg of the initiator 4,4′-azobis(4-cyanovaleric acid) dissolved in 5 ml of 0.2 M sodium hydroxide solution was added to initiate the polymerization reaction. Polymerization proceeded for the duration of 18 hours at 80°C under stirring at 200rpm and was stopped by admission of ambient air to the round-bottom flask. The resulting particle dispersion was filtered through glass wool and centrifuged at 2500g for 3h. The supernatant was discarded by decanting and the remaining precipitate was re-dispersed in DI water under stirring. This centrifugation-redispersion cycle was repeated three times until the surface tension of the supernatant measured by tensiometry was 72 mN $m^{-1}$.

Preparation of core-shell particles was done by precipitation polymerization with the core particles prepared beforehand. 90 g DI water, 0.5 g NIPAM, 20 mg BIS, 50 µl MA and varying amounts of core particle dispersion were loaded to a round-bottom flask sealed by a rubber septum. The flask was placed in an oil bath and heated to

80°C under sparging with nitrogen gas. 50 mg of the initiator potassium persulfate dissolved in 5 ml of DI water was added to start the polymerization. The reaction proceeded for the duration of 2 hours at 80°C under stirring at 200rpm. The product of the polymerization reaction was filtered through glass wool and centrifuged at 2500g, at a temperature of 20°C for 2h. The supernatant was removed and the precipitate re-dispersed in DI water. Subsequent centrifugation steps were carried out at 5°C, 2500g for 16 hours. Three centrifugation-redispersion cycles were carried out. The resulting particle dispersion was further purified by dialysis against DI water in a ready-to-use dialysis device with a molecular weight cut-off of 1000 kD (Spectrumlabs, USA). The surface tension of the aqueous dialysate solution as measured by tensiometry was 72 mN $m^{-1}$, verifying the absences of small molecular weight surface-active contaminants.

### 5.2.3. Size determination by dynamic light scattering

Dynamic light scattering (DLS) was carried-out on an instrument from ALV (Langen, Germany) equipped with a diode-pumped solid-state laser (Cobolt Samba 300 mW at 532 nm), ALV 50/100/200/400/600 µm Pinhole system, a Thorn RFIB263KF Photo Multiplier Detector, ALV7002 external correlator and a ALV-SP/86 goniometer. The scattering intensity of a diluted particle dispersion was measured at a scattering angle of 90°. The particle dispersion was allowed to equilibrate for 30 minutes after adjustment of the NaCl concentration to 20 mM, while the temperature was kept constant at 20 °C. Hydrodynamic diameter and polydispersity index (PDI) of core-shell particles were obtained from a cumulant analysis.

### 5.2.4. Langmuir trough measurement of compression isotherm

The pressure-area isotherm for core-shell particles at an air-water interface was measured on a Microtrough-X (Kibron Inc.,Finland) with inner dimension of 59 x 393 mm and equipped with a wire probe for surface pressure measurement. The base plate contains a glass window which allows for observation of the interface via microscopy. For observation of the interfacial structure the Langmuir trough was placed on an upright Olympus BX 50 light microscope equipped with several long working distance objectives.

Prior to the measurement the trough was carefully cleaned with large amounts of DI water and acetone. The subphase consisted of 70 ml DI water containing 20 mM NaCl and was pipetted onto the trough. IPA was added to the particle dispersion to facilitate spreading of the particles at the interface. The IPA containing particle dispersion (25 vol. % IPA) was transferred onto the interface with a microsyringe. The system was left to equilibrate for a duration of 30 min prior to the start of compression. Compression of the interfacial layer was conducted at a speed of 10 mm $min^{-1}$. Three subsequent compression cycles were carried out; in between each

compression cycle the interface was expanded at a speed of 30 mm $min^{-1}$. For each particle type at least two different experiments with a new subphase and newly spread particles were performed. The compression isotherms displayed are the average of these experiments, each experiment comprising three subsequent compression cycles.

## 5.3. Results and Discussion

An overview of the core-shell particles investigated in this study together with their sizes is given in Tab. 1. We first synthesized polystyrene particles, demarked as core particles in Tab. 1, and used these as seed particles for the synthesis of the core-shell particles. By varying the amount of seed particles present during the precipitation polymerization of NIPAM, we were able to vary the amount of PNIPAM deposited on the PS cores and thereby modify the dimension of the soft shell from 167 nm up to 530 nm. Particle sizes given in Tab. 1 are measured at 20 °C, pH 6 and in the presence of 20 mM NaCl as background electrolyte. These are the same experimental condition applied during subsequent determination of the pressure-area isotherm. The electrolyte concentration was chosen by purpose, because at 20 mM NaCl, small changes in electrolyte concentration did have only minor effect on the particle size.

Tab. 1 Overview of particles investigated in this study, size measured by DLS at 20 °C, pH 6 and in the presence of 20 mM NaCl as background electrolyte

| Sample code | Particle radius [nm] / PDI [-] | Shell thickness [nm] |
|---|---|---|
| core | 368 / 0.08 | 0 |
| CS167 | 567 / 0.07 | 167 |
| CS230 | 630 / 0.07 | 230 |
| CS530 | 930 / 0.09 | 530 |

### 5.3.1. Surface pressure-area isotherms

We started by recording surface pressure - area isotherms for the PS core particles. The isotherm depicted starts off with a finite surface pressure of around 5 mN $m^{-1}$. By reducing the amount of particles spread onto the air-water interface by 90 %, this surface pressure at time $t_0$ could be decreased to zero. Under this condition, however, the surface pressure only slightly increased even after full compression of the interfacial layer down to 12 % of the initial available interfacial area. We can thus conclude that the initial part of the pressure-area isotherm proceeds markedly shallow.

The isotherm for core particles depicted in Fig. 1 shows a strongly soaring surface pressure starting from an area per particle of 1E-12 $m^2$. This value corresponds to a circular area with a radius of 564 nm available for each individual particle, whereas the hydrodynamic radius of the particles is only 368 nm. This suggests that the PS particles at the air-water interface start to interact with each other when the surfaces of the PS particles are on average a few hundred nm apart from each other. For hard particles dispersed in aqueous solution such values would be nonsensical, whereas for particles protruding a fluid interface into the low dielectric constant medium, long ranged repulsive interaction was indeed observed [10, 23, 24].

Starting from an area per particle of 1E-12 $m^2$, compression of the interfacial particle layer down to 40 % of the initially available area causes the surface pressure to diverge up to ~ 53 mN $m^{-1}$. The dashed line in Fig. 1 demarks the point where PS particles are assuming a closed-packed configuration at the interface. Maximum pressure development nearly coincides with this close-packed limit. Beyond this point the surface pressure levels off. This indicates that the increasing stress present in the interfacial layer is mediated by buckling of the particle layer or expulsion of particles from the air-water interface [25]. Overall the pressure-area isotherm recorded by us seem to be well in agreement with the pressure isotherm as reported by other authors. Also Aveyard et al. and Lenis et al. reported that PS particles at the oil-water and air-water interface yield maximal pressure development and a subsequent plateau of the isotherm after compression to 50 % of the initially available interfacial area (starting from the point where the surface pressure starts to kick-off) [9, 26].

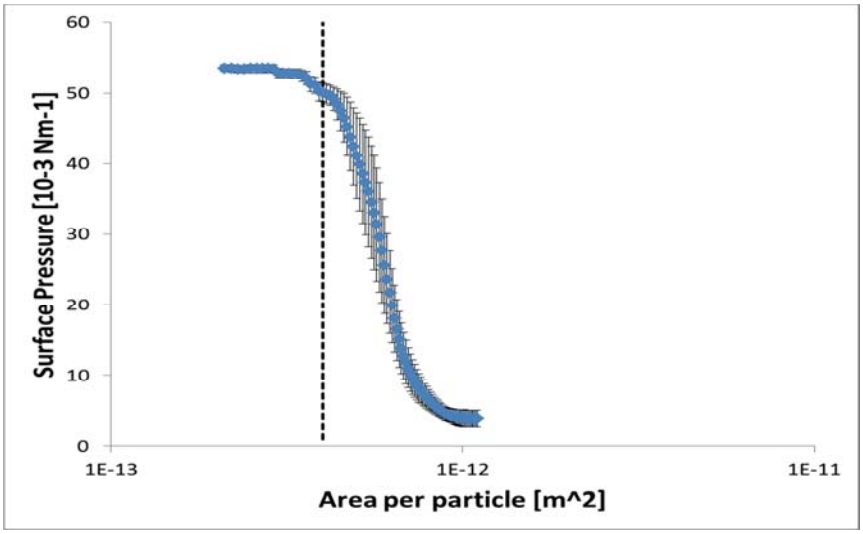


Fig. 1 Pressure-area isotherm for PS particles 'core' with radius of 368 nm, error bars correspond to one standard deviation, depicted values are the average of two experiments with three subsequent compression cycles (see materials & methods section)

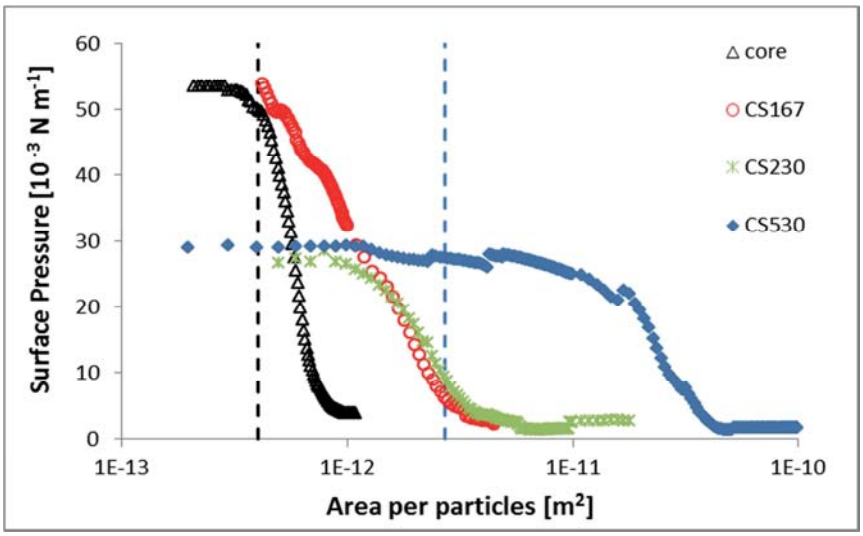


Fig. 2 Surface pressure – area isotherm for core particles 'core' vs. core-shell particles 'CS' (with the number indicating the shell thickness)

The surface pressure–area isotherms for the various core-shell particles synthesized in this study are shown in Fig. 2. The largest core-shell particles CS530 show a steep increase in surface pressure from an area per particle of ~ 4E-11 $m^2$. This value corresponds to a circular area with a radius of 3.57 µm available for each individual particle, meaning CS530 particles start to interact at a centre-to-centre distance of roughly two particle diameters. Such long-ranged interaction are not uncommon. They are usually attributed to electrostatic or dipolar repulsion between interfacial particles [10]. Alvarez et al. found significant surface pressure development after adsorption of polymer-grafted nanoparticles to the air-water interface at area fractions as low as 0.02 and linked it to long-range electrostatic interaction [27]. At this point we cannot proof the presence of electrostatic interaction, but such interaction forces between charge bearing core-shell colloids seem plausible. Alternatively, the long-range interaction may also arise due to overlap of loosely cross-linked PNIPAM chains which spread out radially at the interface.

In Fig. 2 also the closed-packed limit for the core-shell particles CS530 is indicated as blue dashed line. Maximum pressure development seems to occur before a closed-packed configuration is reached. The interval from the point where the surface pressure kick's-off to the point of maximum pressure development equals one order of magnitude. The isotherm of CS530 particles is thus slightly more shallow than the one recorded for the bare PS particles. Another very important difference between PS particles and CS530 particles is the maximal pressure reached: while PS particles can withstand pressures as high as 53 mN $m^{-1}$, the isotherm CS 530 levels of around

29 mN $m^{-1}$. This value is comparable to the maximum pressure pure PNIPAM particles and PNIPAM homopolymers develop after sufficient compression at the air-water interface [16]. With respect to the maximum surface pressure, the large CS530 particles thus behave similar to the constituting polymer of the soft shell.

The smaller core-shell particles CS230 and CS167 both start to develop a significant surface pressure at an area per particle of 4E-12 $m^2$, a value which is one order of magnitude smaller than the one reported for CS530 particles. This value corresponds to a circular area with radius 1.13 µm available for each particle and an average center-to-center distance roughly twice the particle size. Although these values are definitely smaller than the one's for CS530 particles, it still highlights that surface pressure development starts at a surface coverage which is far from the close-packing limit.

Besides their comparable origin, the isotherms for CS230 and CS167 particles are dissimilar. CS230 particles develop their maximal surface pressure after roughly 80 % area reduction (starting from the point where the surface pressure starts to kick-off) and develop a pressure of 28 mN $m^{-1}$, again a value which compares to the pressure reached for PNIPAM particles and PNIPAM polymers at the air-water interface [16, 28].

While the pressure for CS230 particles levels-off at an area per particle of 1E-12 $m^2$, the surface pressure-area isotherm for CS 167 particles, keeps ascending upon further compression. The surface pressure increases up to 53 mN $m^{-1}$ upon compression to an effective area per particle of 4E-13 $m^2$. After compression to such a small area fraction, the soft shell of the CS167 particles shall be actually completely compressed as the theoretical value for hexagonal close-packing of the core particles is reached. At his point we also observe that the surface pressure-area isotherms for core PS particles and core-shell particles CS167 nearly coincide. From these results it appears that the smallest core-shell particles CS167 are stronger adsorbed to the air-water interface than the larger core-shell particles CS230 and CS530. This is counterintuitive as particle adsorption energy should scale with the square of the particle radius, thus, yielding stronger adsorption for the larger particles. Yet, the smallest core-shell particles are the only one's which can sustain equally high pressures as the core particles. Finally we want to stress that we observed a similar dependence of collapse pressure on shell dimension for other core-shell particles with different surface functionalities. The above described behaviour seems generic for core-shell colloids.

Eventually it is also interesting to point out what the above results mean for particle laden air-water interfaces covered by particles. The purpose of using particles for stabilization of fluid interfaces is to attain a long-term stability with regard to Ostwald-ripening. Herefore, particles must strongly anchor to the fluid interface and be able to

sustain surface pressures comparably high as the surface tension of the bare fluid interface. In this way particle stabilized dispersion can attain near-zero Laplace pressures, the driving force for Ostwald ripening can vanish [29]. None of the above described particles can withstand pressures as high as 72 mN $m^{-1}$, the surface tension of a clean air-water interface. It is therefore to be expected that none of the particles used in this study can completely stop Ostwald ripening. Nevertheless, the adsorption of core-shell particles at the interface will lead to the formation of a thick particle layer which may slow-down mass transport across the interface and may also yield a certain surface elasticity. Both phenomena are expected to slow down Ostwald ripening [29].

For core-shell particles CS 167 we here found that they can develop equally high surface pressures as the PS core particles, but spontaneously adsorb to the air-water interface (see Chapter 4). This confirms that is possible to design core-shell particles which can sustain very high surface pressures, yet, being able to spontaneously adsorb to the fluid interface. A different core particle with a small dimension of the soft shell, comparable to the thickness of CS 167 particles investigated here, may yield core-shell particles which can develop surface pressures of 72 mN $m^{-1}$ and be able to stop Ostwald ripening.

### 5.3.2. Microscopic analysis of interfacial structure

To get a qualitative impression of the structure PS particles are assuming at the air-water interface, we monitored the particle layer throughout the whole compression cycle by light microscopy. The images displayed in Fig. 3 reveal that PS 'core' particles are aggregating and form clusters at the interface. This is in contrast to the phase behaviour in the bulk aqueous phase were a low polydispersity index over prolonged periods of time indicated a good colloidal stability and no aggregation of the particles. Differences in colloidal stability between bulk and interface and aggregation of colloidal particles at fluid interfaces is a common observation reported in literature. Particles aggregation at the fluid interface is frequently attributed to capillary interaction between individual particles [30-32]. Capillary interactions at fluid interfaces are thought to arise due to particle surface roughness. This can lead to undulation of the contact line around individual particles, which in turn promotes particle aggregation as overlapping menisci lower the total interfacial energy.

From Fig. 3 one can deduct that increasing surface coverage with particles leads to higher surface pressures. At a surface pressure of 1 mN $m^{-1}$ the surface coverage is rather low, whereas a nearly fully packed interface correspond to a pressure ~53 mN $m^{-1}$ (see Fig. 3 a - d). An interesting observation can be made in Fig. 3b, where circular particle clusters are visible. Circular aggregates may in principle arise due to multipole interaction, that means undulation of the interface around a particle with

hexagonal or higher symmetry. A more simple explanation may be the formation of such circular particle clusters due to rapid evaporation of the spreading solvent that was used to deposit particles at the interface.

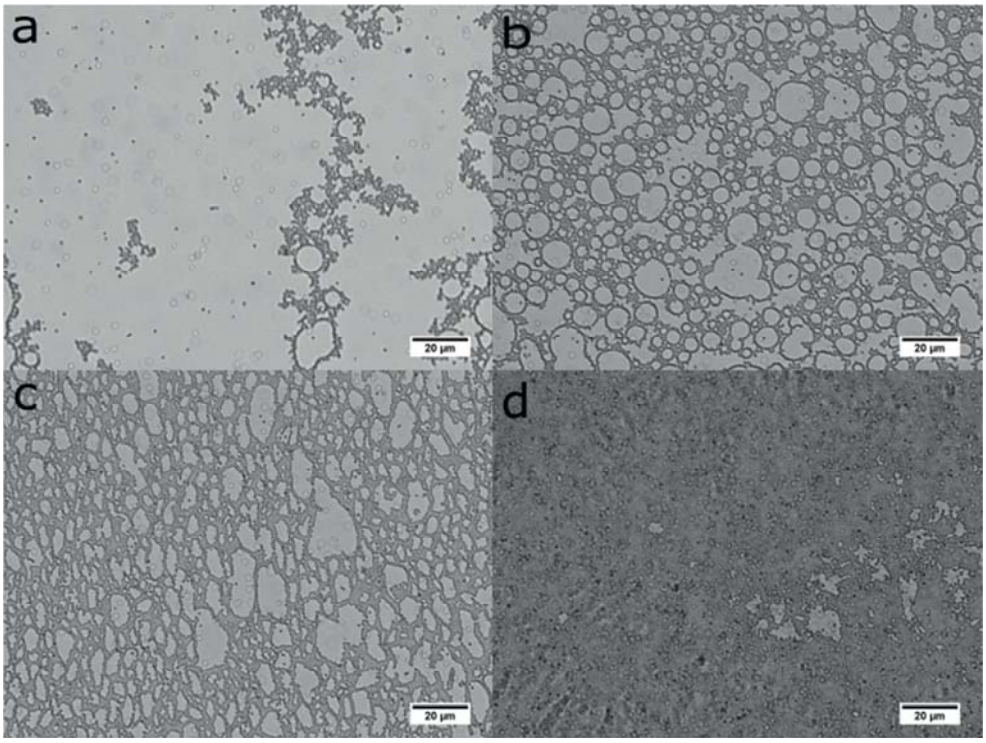


Fig. 3 Microscopic picture of air-water interface onto which PS particles 'core' are adsorbed (magnification 50x, scale bars = 20µm). Different pictures represent interfacial structure at different surface pressures (a) 1 mN $m^{-1}$ (b) 5 mN $m^{-1}$ (c) 35 mN $m^{-1}$ (d) 53 mN $m^{-1}$

Further we observed the structures core-shell particles are forming at the interface. The micrographs displayed in Fig. 4 show the structure adopted by core-shell colloids 'CS167' at the air-water interface. Also here one can ascertain particle aggregation. PS 'core' particles and the smaller core-shell particles 'CS167' seem to display similar phase behaviour at the interface. The clusters formed by CS167 particles seem to be a bit larger and more dense than the clusters formed by PS 'core' particles. Further, one can observe that higher surface coverage correspond to higher surface pressures. At a pressure of 52 mN $m^{-1}$ the interface is nearly covered with a dense layer of particles. In Fig. 4d one can observe a small gap in the densely packed particle layer. From this gap particles appear to be desorbed into the bulk aqueous phase. This indicates that particles start to desorb at this point. This would fit to the corresponding surface pressure- area isotherm. According to the isotherm

'CS167' depicted in Fig. 2, the soft particle shell should be completely compressed at a surface pressure ~ 52 mN $m^{-1}$. Further compression must inevitably lead to relaxation of the particle layer. A movie taken at the corresponding surface pressure indicated that relaxation occurs through desorption of particles into the bulk phase. This was evident since particle attain a higher diffusivity and disappear from the focal place.

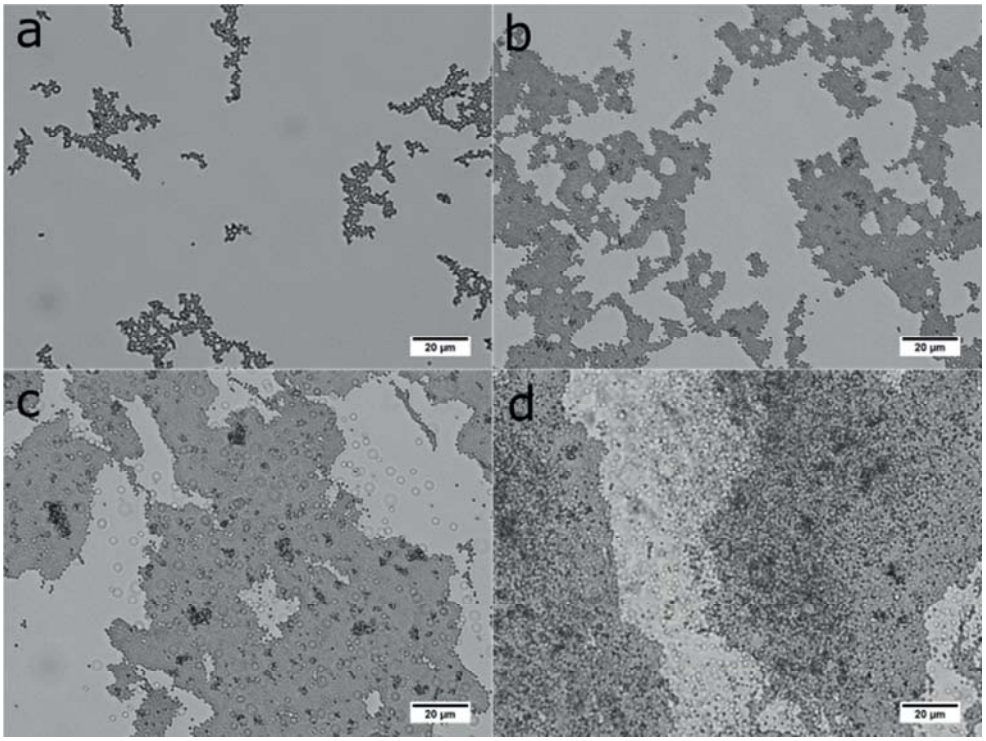


Fig. 4 Microscopic picture of air-water interface onto which core-shell particles 'CS167' are adsorbed (magnification 50x, scale bars = 20µm). Different pictures represent interfacial structure at different surface pressures (a) 7 mN $m^{-1}$ (b) 25 mN $m^{-1}$ (c) 30 mN $m^{-1}$ (d) 52 mN $m^{-1}$

Next we observe the structures formed by 'CS230' core-shell particles at the air-water interface (see Fig. 5). Also this type of core-shell particle mostly forms aggregates at the fluid interface, a few individual particles are visible only. The aggregates observed display a different structure from the one's discussed before: the cores of the core-shell particles, the part of the core-shell particle which we can actually observe by light microscopy, appear to be well separated from each other. Further, also here higher surface coverage corresponds to a higher surface pressure. At a surface pressure of 28 mN $m^{-1}$, which is also the maximum surface pressure for

this particle type (see Fig. 2), the air-water interface is covered with a densely packed particle layer with a few voids (see Fig. 5d).

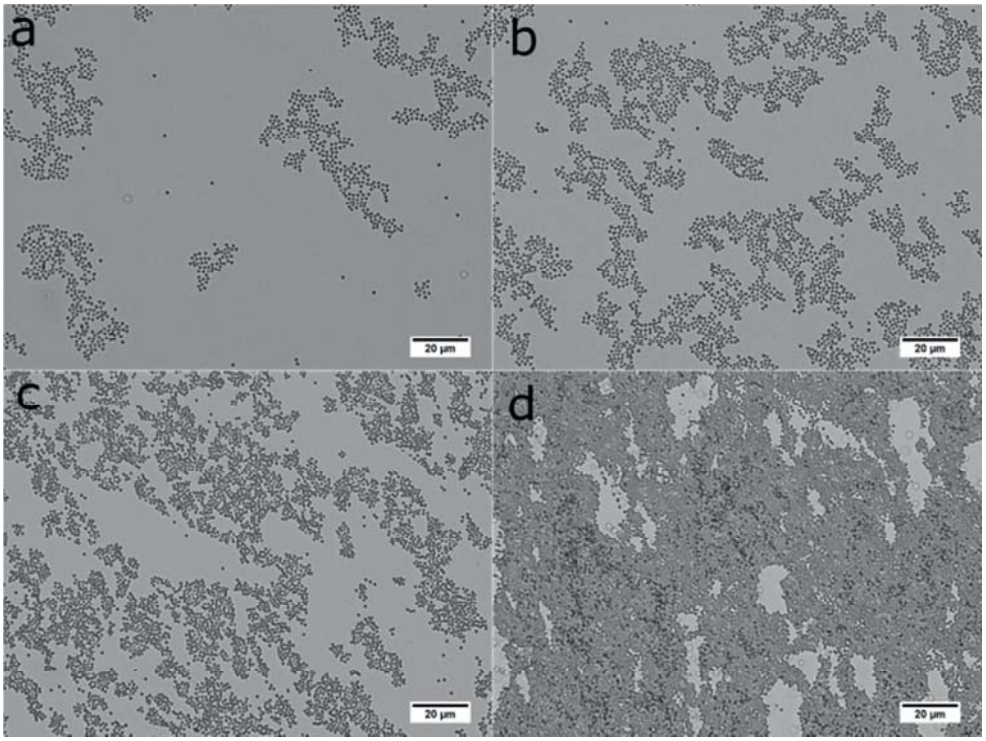


Fig. 5 Microscopic picture of air-water interface onto which core-shell particles 'CS230' are adsorbed (magnification 50x, scale bars = 20µm). Different pictures represent interfacial structure at different surface pressures (a) 2 mN $m^{-1}$ (b) 6 mN $m^{-1}$ (c) 21 mN $m^{-1}$ (d) 28 mN $m^{-1}$

Ultimately, we look at the structured formed by the largest core-shell colloids CS530 at the air-water interface. Concerning the interfacial structure one can ascertain that at least at higher surface pressures, particles are equally distributed over the whole fluid interface. Further, at a surface coverage as low as 0.05, a surface pressure of 1 mN $m^{-1}$ develops already (see Fig. 6a). A finite surface pressure at such low surface coverage indicates that particles interact with each other through long-range interaction. Long-range interaction were also found by Alvarez et al. for polymer-grafted nanoparticles at the air-water interface [27]. Increasing the surface coverage to 0.1 gives a surface pressure of 11 mN $m^{-1}$ (see Fig. 6b), an even higher coverage of 0.22 yields a surface pressure of 25 mN $m^{-1}$. Further compression yields a close-packed interfacial layer of particles which is characterized by 2D crystalline arrangement of particles. The formation of a 2D crystal indicates that particles repel each other strongly at such short distances.

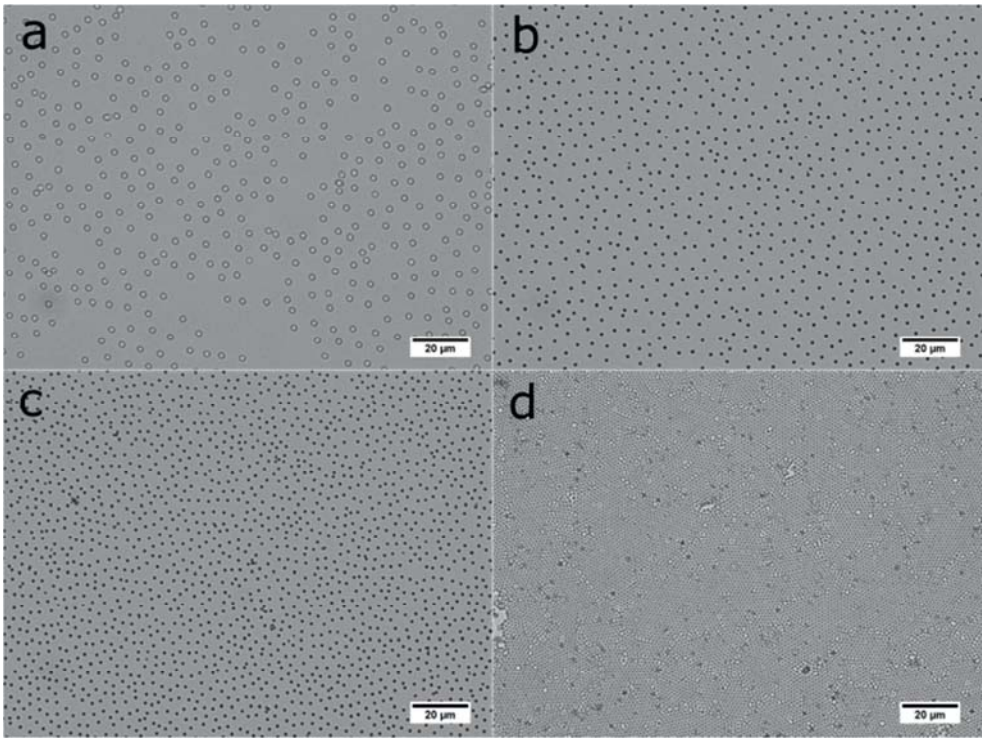


Fig. 6 Microscopic picture of air-water interface onto which core-shell particles 'CS530' are adsorbed (magnification 50x, scale bars = 20µm). Different pictures represent interfacial structure at different surface pressures (a) 1 mN $m^{-1}$ (b) 11 mN $m^{-1}$ (c) 25 mN $m^{-1}$ (d) 29 mN $m^{-1}$

Through visual inspection of Fig. 3 - Fig. 6 we found that the interfacial structures formed by the different particle types varies greatly. In order to quantify the interfacial structure of the different particle types, we used digital image processing and determined the separation distance between the particles and calculated the respective pair correlation functions (see Fig. 7). The pair correlation function measures the probability of finding a particle at a distance r from any other particles at the interface. A peak in the pair correlation function indicates the preferred centre-to-centre distance between particles, a measure which we use as the main parameter for further comparison. For all particle types, calculation of the pair correlation function was performed for microscopic pictures which corresponded to a surface pressure of a few mN $m^{-1}$.

As visible by the first peak in Fig. 7 a & b, PS 'core' particles and the smallest core-shell particles 'CS167' adopt a separation distance which equals one particle diameter. From this result together with the microscopic observations from Fig. 3 & Fig. 4, one can deduct that these particles are attractive and form aggregates in which particles are in direct contact with each other. In contrast, the first peak visible

in Fig. 7c is situated at a distance around 1.2 – 1.3 particle diameters. This means that core-shell particles ‘CS230’ adopt a centre-to-centre interparticle distance which is larger than the actual particle diameter. Analysis of the interfacial structure of ‘CS530’ particles reveal that the largest core-shell particles even adopt a larger interparticle distance than ‘CS230’ core-shell particles. The first peak in the pair correlation function appears at a distance of two particle diameters. This means that the mean particle centre-to-centre distance is two particle diameters.

We propose that the measured interfacial particle distance is an equilibrium distance which results from an interplay between repulsive and attraction interaction. Repulsive interaction may arise due to electrostatic interaction between particles. Attractive interaction can arise due to undulation of the particle contact line which induces capillary interaction between particles. The presence of long-range attractive capillary interaction in interplay with a repulsive interaction can yield an interaction potential that gives rise to particle aggregates with a measurable equilibrium distance between individual particles. In this case capillary forces favour the aggregate formation while the equilibrium interparticles distance is a result of strong electrostatic interaction at shorter distances.

This leaves us with the question why core-shell particles ‘CS230’ adopt a smaller interparticle distance than core-shell particles ‘CS530’. This question can also be explained by the interplay between attractive and repulsive interaction. We suggest that a larger particle shell will alter the menisci profile around individual particle, thereby modifying the attractive capillary interaction among individual particles. A larger shell may reduce the magnitude of attractive capillary forces, thus, the electrostatic interaction becomes more dominant, as a consequence of which particles adopt a larger equilibrium distance. This argumentation would also hold for explanation of the phase behaviour of PS particles and ‘CS167’ core-shell particles.

Although we do not deliver experimental proof of the here sketched interaction potential, the two mentioned interaction forces are known to play a vital role in the lateral interaction profile of colloidal particles at liquid interface. Further, the aggregates observed for PS ‘core’ particle and the smaller core-shell particle types ‘CS167’ and ‘CS230’ give a hint that attractive interaction forces play a dominant role in their lateral interaction at the air-water interface. Note, that also the interfacial structure of ‘CS530’ core-shell particles displayed in Fig. 6 a may be interpreted as aggregates with a large interparticle distance. After further compression to smaller interparticle distances only the repulsive interaction become apparent (see Fig. 6 b & 6 c).

The observed differences between the interaction of core-shell particles with different shell dimension may also give a hint how to alter capillary interaction among non-spherical particles at liquid interfaces. Grafting of a soft polymer shell may be a

suitable way to tailor capillary interaction and effectively engineer the desired particle interaction profile. In combination with a thermo- or pH-responsive polymer, one might even be able to alter capillary interaction in response to environmental condition. This could lead to the design of truly novel, advanced interfacial materials.

It is also worth mentioning that the here reported particle aggregation as well as the finite interparticle distance between individual particles has also been observed for microgel covered fluid interfaces. Cohin et al. found that microgels aggregate at the air-water interface [20]. A recent article by Huang et al. which addresses the interfacial structure of microgel covered interfaces finds that microgels form clusters at the fluid interface, but adopt a measureable distance between particle pairs [34]. This shows that our findings are not specific for the core-shell particles investigated in this study, but are equally applicable to a wider-range of soft particles systems at fluid interfaces.

Eventually it is interesting to link the results we obtained from the interfacial structure characterization to the differences in the surface pressure – area isotherms of the different particle types. The PS 'core' particles as well as the smaller core-shell particles 'CS167' both develop an equally high surface pressure of 53 mN $m^{-1}$ after compression. Both particle types are also observed to form dense aggregates in which individual particles are in close contact to each other. This points to a strong attractive interaction force among individual particles. In contrast, the larger core-shell particles 'CS230' and 'CS530' both yield a maximal surface pressure of 28 – 29 mN $m^{-1}$ after sufficient compression. We assume that for these particle types a repulsive forces dominates a short particle distances. From these results it appears that the smaller particles can withstand higher surface pressures than the larger particles. Based on the particle adsorption energies which should scale with the square of the particle size, we would have expected the opposite behaviour. Taking into account the observations onto the interfacial structure, we hypothesise that a pronounced attractive interaction force among particles impedes particle expulsion from the interface. The effective particle adsorption energy may be higher because of the cohesive interaction between interfacial particles. Similar conclusion can be drawn from the results of Poulichet and Garbin. They found that ultrasound can facilitate particle desorption from bubble interfaces by breakup of particle aggregates at the interface [35]. Similarly, Razavi et al. found that attractive interparticle interaction can prevent particle desorption from the fluid interface into the bulk phase. They also found that for certain particle types with pronounced attractive interaction, the collapse of the particle monolayer upon compression in a Langmuir trough takes place at higher surface pressures [25]. The mentioned literature references thereby corroborate the findings of the current study.

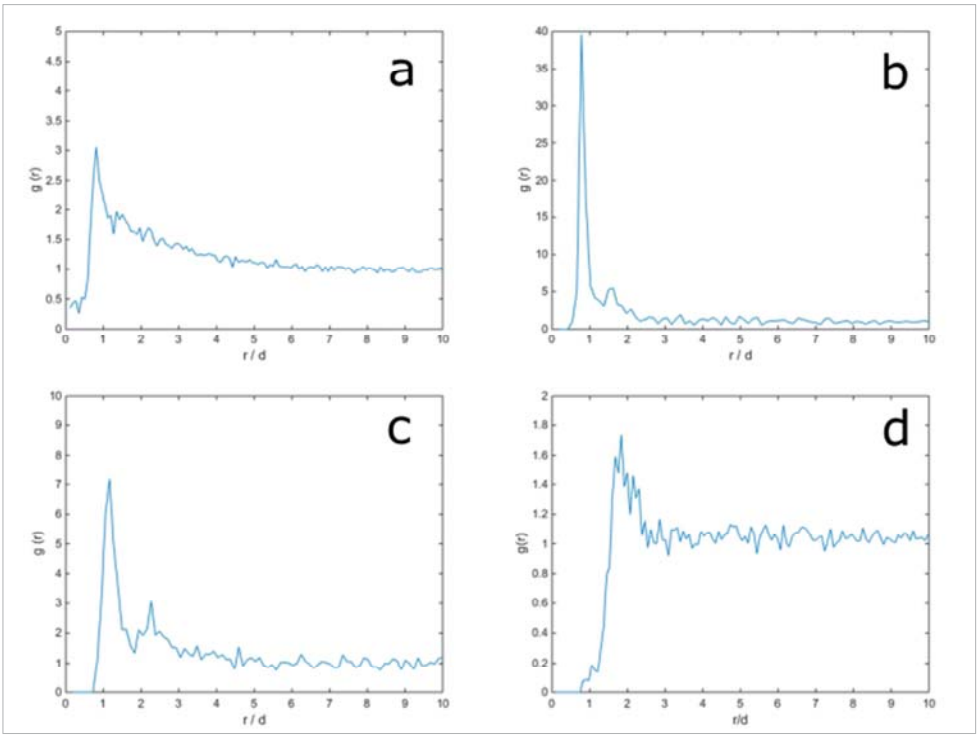


Fig. 7 Pair correlation function G(r) characterizing the monolayer-structure adopted by different particle types at the air-water interface. (a) 'core' particles and (b) CS167 (c) CS230 (d) CS530 core-shell particles

## 5.4. Conclusion

We experimentally determined the surface pressure – area isotherms for monolayers of differently sized core-shell particles adsorbed at the air-water interface. We find that the onset of surface pressure development occurs far from the close-packing limit, which suggests that the interaction between interfacial core-shell particles is long-ranged. The measured surface pressure must arise from lateral interparticle interaction, as the ideal gas law would not yield a measurable surface pressure for micron-sized particles.

After the onset of a finite pressure, the surface pressure –area isotherm diverges and levels-off upon compression to a certain surface pressure. PS spheres, which constitute the core of all the core-shell particles, as well as the smallest core-shell particles can endure the same high surface pressure of 53 mN $m^{-1}$. For larger core-shell particles with thick shell, the maximum surface pressure does not exceed 29 mN $m^{-1}$. We link the capability to attain higher surface pressure to different lateral interaction forces among interfacial particles. PS spheres and the smallest core-shell

particles are characterized by a pronounced attractive interaction. The resulting cohesive particle monolayer is able to stand a higher surface pressure than an individual particle. In contrast, for the larger core-shell particles repulsive forces are more pronounced, the interface is more fluid like and hence only endures lower surface pressures of 29 mN $m^{-1}$. The measured collapse pressure of 29 mN $m^{-1}$ is equal to the collapse pressure of an interface covered with PNIPAM homopolymer. It appears that the polymeric shell determines the maximum surface pressure of the particles and the maximum surface pressure is not linked to the particle size. This suggests that the larger core-shell particles may not desorb as a whole entity, but rather in a polymer like fashion through sequential desorption of polymer segments.
None of the particles studied is observed to leave the interface before surface pressures of 25 mN $m^{-1}$ are reached. The part of the surface pressure-area isotherm up to 25 mN $m^{-1}$ may thus be interpreted as a 2D equation of state.

## References


1. Aveyard, R., B.P. Binks, and J.H. Clint, *Emulsions stabilised solely by colloidal particles.* Advances in Colloid and Interface Science, 2003. **100**: p. 503-546.
2. Binks, B.P., *Particles as surfactants - similarities and differences.* Current Opinion in Colloid & Interface Science, 2002. **7**(1-2): p. 21-41.
3. Binks, B.P., et al., *pH-responsive aqueous foams stabilized by ionizable latex particles.* Langmuir, 2007. **23**(17): p. 8691-4.
4. Park, J.I., et al., *Titelbild: A Microfluidic Approach to Chemically Driven Assembly of Colloidal Particles at Gas–Liquid Interfaces (Angew. Chem. 29/2009).* Angewandte Chemie, 2009. **121**(29): p. 5321-5321.
5. Stocco, A., et al., *Particle-stabilised foams: an interfacial study.* Soft Matter, 2009. **5**(11): p. 2215-2222.
6. Richtering, W., *Responsive Emulsions Stabilized by Stimuli-Sensitive Microgels: Emulsions with Special Non-Pickering Properties.* Langmuir, 2012. **28**(50): p. 17218-17229.
7. Danov, K.D., et al., *Particle-interface interaction across a nonpolar medium in relation to the production of particle-stabilized emulsions.* Langmuir, 2006. **22**(1): p. 106-115.
8. Chen, W., et al., *Measured long-ranged attractive interaction between charged polystyrene latex spheres at a water-air interface.* Physical Review E, 2006. **74**(2): p. 021406.

9. Aveyard, R., et al., *Compression and Structure of Monolayers of Charged Latex Particles at Air/Water and Octane/Water Interfaces.* Langmuir, 1999. **16**(4): p. 1969-1979.
10. Pieranski, P., *TWO-DIMENSIONAL INTERFACIAL COLLOIDAL CRYSTALS.* Physical Review Letters, 1980. **45**(7): p. 569-572.
11. Monteux, C., et al., *Determining the mechanical response of particle-laden fluid interfaces using surface pressure isotherms and bulk pressure measurements of droplets.* Physical Chemistry Chemical Physics, 2007. **9**(48): p. 6344-6350.
12. Kassuga, T.D. and J.P. Rothstein, *Buckling of particle-laden interfaces.* Journal of Colloid and Interface Science, 2015. **448**: p. 287-296.
13. Deshmukh, O.S., et al., *Hard and soft colloids at fluid interfaces: Adsorption, interactions, assembly & rheology.* Advances in Colloid and Interface Science, 2015. **222**: p. 215-227.
14. Brugger, B., J. Vermant, and W. Richtering, *Interfacial layers of stimuli-responsive poly-(N-isopropylacrylamide-co-methacrylicacid) (PNIPAM-co-MAA) microgels characterized by interfacial rheology and compression isotherms.* Phys Chem Chem Phys, 2010. **12**(43): p. 14573-8.
15. Geisel, K., L. Isa, and W. Richtering, *Unraveling the 3D Localization and Deformation of Responsive Microgels at Oil/Water Interfaces: A Step Forward in Understanding Soft Emulsion Stabilizers.* Langmuir, 2012. **28**(45): p. 15770-15776.
16. Deshmukh, O.S., et al., *Equation of state and adsorption dynamics of soft microgel particles at an air-water interface.* Soft Matter, 2014. **10**(36): p. 7045-7050.
17. Style, R.W., L. Isa, and E.R. Dufresne, *Adsorption of soft particles at fluid interfaces.* Soft Matter, 2015. **11**(37): p. 7412-7419.
18. Bykov, A.G., et al., *Dilational surface elasticity of spread monolayers of polystyrene microparticles* Soft Matter, 2014. **10**: p. 6499.
19. Liggieri, L., et al., *Wide-frequency dilational rheology investigation of mixed silica nanoparticle-CTAB interfacial layers.* Soft Matter, 2011. **7**(17): p. 7699-7709.
20. Cohin, Y., et al., *Tracking the interfacial dynamics of PNiPAM soft microgels particles adsorbed at the air–water interface and in thin liquid films.* Rheologica Acta, 2013. **52**(5): p. 445-454.
21. Monteillet, H., et al., *Ultrastrong Anchoring Yet Barrier-Free Adsorption of Composite Microgels at Liquid Interfaces.* Advanced Materials Interfaces, 2014. **1**(7): p. n/a-n/a.
22. Clint, J.H. and S.E. Taylor, *Particle size and interparticle forces of overbased detergents: A Langmuir trough study.* Colloids and Surfaces, 1992. **65**(1): p. 61-67.
23. Aveyard, R., et al., *Measurement of long-range repulsive forces between charged particles at an oil-water interface.* Physical Review Letters, 2002. **88**(24): p. 246102.

24. Stancik, E.J., M. Kouhkan, and G.G. Fuller, *Coalescence of Particle-Laden Fluid Interfaces.* Langmuir, 2004. **20**(1): p. 90-94.
25. Razavi, S., et al., *Collapse of Particle-Laden Interfaces under Compression: Buckling vs Particle Expulsion.* Langmuir, 2015. **31**(28): p. 7764-7775.
26. Lenis, J., et al., *Mechanical Stability of Polystyrene and Janus Particle Monolayers at the Air/Water Interface.* Journal of the American Chemical Society, 2015. **137**(49): p. 15370-15373.
27. Alvarez, N.J., et al., *Interfacial Dynamics and Rheology of Polymer-Grafted Nanoparticles at Air–Water and Xylene–Water Interfaces.* Langmuir, 2012. **28**(21): p. 8052-8063.
28. Okumura, Y. and M. Kawaguchi, *Surface pressure–area isotherms and surface dilational moduli of poly (N-isopropyl acrylamide) monolayers spread at air–water interface.* Colloids and Surfaces A: Physicochemical and Engineering Aspects, 2014. **441**: p. 275-280.
29. Meinders, M.B.J. and T. van Vliet, *The role of interfacial rheological properties on Ostwald ripening in emulsions.* Advances in Colloid and Interface Science, 2004. **108–109**(0): p. 119-126.
30. Williams, D.F. and J.C. Berg, *The aggregation of colloidal particles at the air—water interface.* Journal of Colloid and Interface Science, 1992. **152**(1): p. 218-229.
31. Danov, K.D., et al., *Interactions between particles with an undulated contact line at a fluid interface: Capillary multipoles of arbitrary order.* Journal of Colloid and Interface Science, 2005. **287**(1): p. 121-134.
32. Reynaert, S., P. Moldenaers, and J. Vermant, *Control over Colloidal Aggregation in Monolayers of Latex Particles at the Oil−Water Interface.* Langmuir, 2006. **22**(11): p. 4936-4945.
33. Petkov, P.V., K.D. Danov, and P.A. Kralchevsky, *Monolayers of charged particles in a Langmuir trough: Could particle aggregation increase the surface pressure?* Journal of Colloid and Interface Science, 2016. **462**: p. 223-234.
34. Huang, S., et al., *Microgels at the Water/Oil Interface: In Situ Observation of Structural Aging and Two-Dimensional Magnetic Bead Microrheology.* Langmuir, 2016. **32**(3): p. 712-722.
35. Poulichet, V. and V. Garbin, *Ultrafast desorption of colloidal particles from fluid interfaces.* Proceedings of the National Academy of Sciences, 2015. **112**(19): p. 5932-5937.

## Chapter 6

# Adsorption behaviour of core-shell particles at the air-water interface

We analysed the adsorption behaviour of micron-sized core-shell particles consisting of a solid polystyrene (PS) core and soft Poly(N-isopropylacrylamide)-based shell. For short and long timescales we observed different adsorption dynamics. At short timescales adsorption data could be well described by the Ward and Tordai model, signifying that particle adsorption to the air-water interface is diffusion limited. At long timescales adsorption to the air-water interface becomes hindered by an energy barrier due to crowding of particles at the interface. These results prove that the presence of a soft, polymeric shell can completely alter the particle adsorption dynamics, from a kinetically controlled process for solid PS core particles, to a diffusion limited process for core-shell particles with a soft shell. Despite the spontaneous adsorption to the air-water interface, particle adsorption was found to be irreversible; no dynamic equilibrium between interfacial and bulk particles exists. Further, we found by microscopic analysis that core-shell particles with a thick shell can adsorb in two different states at the fluid interface. We speculate that this is an elastocapillary phenomenon: there may be two equally favourable states that maximize the spreading of the soft shell at the fluid interface while minimizing the elastic energy required for particle deformation. Our results show that markedly different interfacial behaviour may arise due to the presence of a soft shell around a solid core particle.

This Chapter is based on: C Buchcic, RH Tromp, MBJ Meinders and MA Cohen Stuart, Adsorption dynamics and interfacial structure of core-shell particles at the air-water interface, Manuscript in preparation

## 6.1. Introduction

Colloidal particles are becoming an prominent alternative for the stabilization of fluid interfaces in foams and emulsions. This is because they typically adsorb strongly to the interface and can form highly elastic interfacial layers which are able to completely arrest the processes of coalescence and Ostwald ripening [1]. However, due to their size, adsorption of particles to fluid interfaces is slow. In addition, adsorption to the interface is often hindered by an energy barrier which manifests itself by a low probability for particles to stick to the interface [2]. A solution for the latter problem could be the application of core-shell particles with a solid core and a soft, polymeric shell. Such particles were shown to easily assemble onto fluid interfaces without being repelled by a pronounced energy barrier. We previously came to the preliminary conclusion that adsorption of such particles to the air-water interface is most likely limited by diffusional transport from the bulk phase to the subsurface region (Chapter 4). However, the 2D equation of state must be known in order to derive adsorption rates from tensiometric measurements and fit an adsorption model. This has not been done up to now.

Colloidal particles, especially soft ones, show some peculiar properties at fluid interfaces. Experiment and simulation showed that colloidal particles at liquid interfaces undergo a variety of time dependent relaxation processes. Upon adsorption to the liquid interface, particles have been found to slowly change their height with respect to the interface before they reach an equilibrium position [3]. Additionally, surface tension may deform soft colloids and induce spreading of particles at the fluid interface [4]. The extend of spreading is governed by the interplay between particle elasticity and surface tension [5]. Due to the relaxation processes mentioned, the evolution of surface pressure development may not only be related to the surface coverage, but also to the interfacial configuration of particles may play a role [6]. This makes it interesting to study interfacial configurations in the context of particle adsorption dynamics.

The purpose of the current paper is to investigate the behavior of core-shell particles with an overall radius of 930 nm, consisting of a solid polystyrene (PS) core and a soft Poly(N-isopropylacrylamide) (PNIPAM) shell, with respect to their adsorption dynamics at the air-water interface. We measure the evolution of surface pressure as core-shell particles of varying number concentrations adsorb from the aqueous bulk to the interface of a newly created droplet. With the help of a previously established surface pressure – area relationship (Chapter 5) we obtain adsorption rates from the tensiometric data and fit an appropriate adsorption model. Further, we also apply various microscopic analysis techniques in order to obtain information about the position of the particles with respect to the fluid interface.

## 6.2. Materials & Methods

### 6.2.1. Materials

Styrene, itaconic acid (IA), initiator 4,4′-azobis(4-cyanovaleric acid) (ACVA), N-isopropylacrylamide (NIPAM), N,N′-methylbisacrylamide (BIS), methacrylic acid (MA), potassium peroxodisulfate (KPS) sodium chloride (NaCl), acetone and Iso-propanol (IPA) were purchased from Sigma-Aldrich. Deionized (DI) water with a resistance of 18.2 MΩ.cm was supplied by a MilliQ water purification system.

### 6.2.2. Synthesis core-shell particles

Core-shell particles were prepared via a two-step procedure. Charge-stabilized PS particles were synthesized by surfactant free emulsion polymerization. PS particles were used as seed particles for the subsequent precipitation polymerization of NIPAM with MA co-monomer. Details on the preparation procedure can be found in Chapter 3 and Chapter 4 of this thesis.
In this chapter only kind of core-shell particle with a radius of 930nm, comprising a shell with a thickness of 530 nm and a PS core with a radius of 400nm was used (as measured by dynamic light scattering at 20°C, pH6 and with 20 mM NaCl present in the bulk). As in other parts of this thesis we use the sample code CS530 for this particle type.

### 6.2.3. Measurement of surface tension

A dilution series was made to obtain particle dispersions of appropriate concentration. The dynamic surface tension of the particle dispersions was measured on a Drop Tensiometer, model TRACKER (Teclis, France). All measurements were performed in the pendant drop configuration at 20°C.

### 6.2.4. Drop-exchange experiment

We used a PAT-1 drop shape tensiometer (Sinterface, Germany) equipped with a coaxial double capillary for droplet exchange experiments. The surface tension of a core-shell particle dispersion with a particle volume number density of $9.25\times10^{-15}$ $m^{-3}$ and 20 mM NaCl as background electrolyte was measured by analysis of the shape of a liquid drop. After the surface tension was constant ($\pm$ 0.2 mN $m^{-1}$), we started to exchange the liquid inside the droplet with 20 mM NaCl solution. Liquid exchange was done at a rate of 0.07 $mm^3$ $s^{-1}$. The total amount of exchanged liquid amounts to the tenfold droplet volume. The surface tension was measured at all times and monitored up to 10 hours after the liquid exchange was completed.

### 6.2.5. Cryo-scanning electron microscopy

A stock of concentrated particle dispersion was diluted with NaCl solution, yielding a particle volume number density of $9.25\times10^{-15}$ $m^{-3}$ with 20 mM NaCl as background electrolyte. 40 µl of this particle dispersion was transferred to a circular copper sample holder with 5 mm inner diameter and 1mm deep cavity. The particle dispersion was left to equilibrate for 20 minutes inside a glass petri dish filled with a shallow water layer at the bottom, to ensure a water saturated atmosphere and avoid sample evaporation. Freezing of the sample was done by plunging it in liquid nitrogene for two minutes. Subsequently, the specimen was partially freeze-dried at -93°C for 1 min to remove ice crystals, followed by tungsten coating up to 10 nm on a high vacuum coating system Leica EM MED 020. A first tungsten layer of 5nm was applied by tilting the sample homogenously at all angles between 0° and 180 °. A second tungsten layer up to 5 nm was applied by sputtering under an angle of 45°. Sample transfer was done with a Leica EM VCT 100 vacuum cryo transfer system. Cryo-SEM imaging was performed on a ultra-high resolution field emission scanning electron microscope FEI Magellan 400. Imaging was done at an accelerating voltage of 2 kV.

### 6.2.6. Dark field light microscopy

Dark field light microscopy was performed on an upright Olympus BX 50 light microscope equipped with several long working distance objectives, a vertical illuminator and a dark field mirror block. The particle dispersion was filled in a shallow quartz cuvette (3 cm x 2 cm x 0.5 cm). The air-water interface was observed in reflected light mode to focus on the interface. After focusing, the dark field mirror block was placed into the light path and micrographs were taken with a digital camera (Olympus DP 70).

## 6.3. Results & Discussion

### 6.3.1. Assessment of particle adsorption dynamics by tensiometry

As found earlier, the polymeric nature of the soft shell eliminates any pronounced adsorption barrier as usually exists between hard particles and a fluid interface (Chapter 4). Therefore, the rate of core-shell particle adsorption to the interface may be governed by particle diffusion in the bulk. Due to the micron-sized diameter of our particles we can also expect that they do not desorb from the interface spontaneously [1]. Irreversible anchoring and diffusion limited transport to the interface are also the assumptions of the Ward and Tordai equation [7]:

$$\Gamma = 2\, c_\infty \sqrt{\frac{D\, t}{\pi}} \qquad (1)$$

where $\Gamma$ is the area number density (number of particles in a unit area), $c_\infty$ is the volume number density (number of particles in a unit volume), $D$ is the particle diffusion coefficient in the bulk and $t$ is the time. In what follows we want to investigate to what extend this model can describe the adsorption behavior of our core-shell particles.

We first measured, for a range of particle concentrations, the surface pressure development due to adsorption of core-shell particles to the air-water interface of a newly created droplet. As can be seen in Fig. 1 the change in particle bulk concentration $c_\infty$ leads to pronounced differences in the evolution of surface pressure. The curves differ with respect to the lag time $t^*$ where a finite pressure can first be measured, as well as with respect to the rate of surface pressure development and the maximum pressure reached after a time period of $10^4$ seconds. In all cases, one observes that the surface pressure development first occurs rather fast and then slows down at higher surface pressures around 20 mN $m^{-1}$.

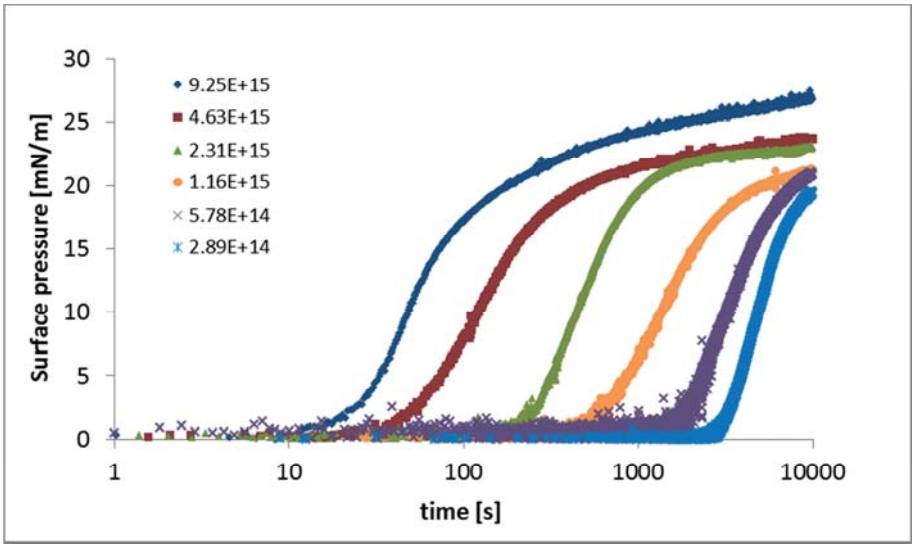


Fig. 1: Evolution of surface pressure vs time for core-shell particles CS530, the inset indicates the volume number density $c_\infty$ of the respective curve

The most straightforward measure for differentiation of the different curves in Fig. 1 appears the lag time $t^*$ were a finite surface pressure can be observed. According the Ward and Tordai equation [7], this time point $t^*$ of each curve must correspond to a certain interfacial particle concentration $\Gamma^*$ with:

$$t^* = \frac{\Gamma^{*2}\,\pi}{4\,D\,{c_\infty}^2} \qquad (2)$$

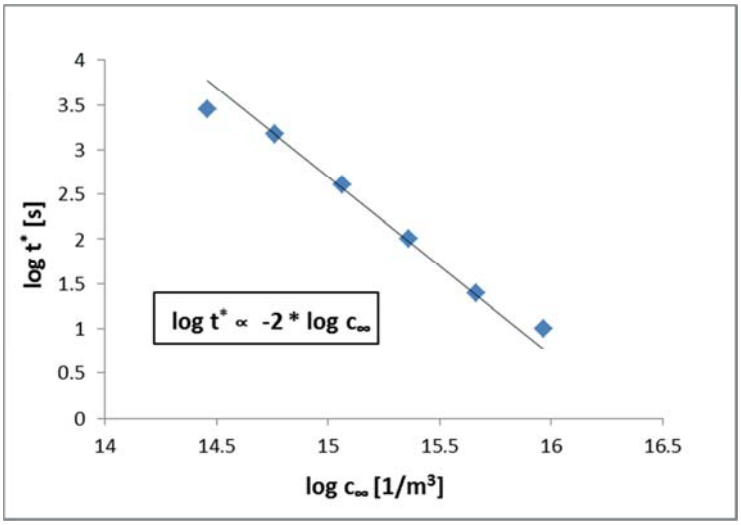


Fig. 2 log-log plot displaying lag time log $t^*$ vs. number of particle in bulk log $c_\infty$

We plotted log $t^*$ vs. log $c_\infty$ and found that the curve fits a straight line with a slope of -2. This means the relation between $t^*$ and $c_\infty$ can be best described by a power law dependence of the following form:

$$t^* \propto \frac{1}{{c_\infty}^2} \qquad (3)$$

This is in line with diffusion controlled adsorption.

To get a more detailed picture, we must determine the area number density $\Gamma$ as a function of time $t$. For that we need to convert surface pressure vs time curves into area number density $\Gamma$ vs time curves. For this conversion, we must obtain a 2D equation of state which expresses the surface pressure as a function of the number of adsorbed particles at the interface. We determined such a 2D equation of state previously (Chapter 5); using these data, we plot the number of adsorbed particles vs surface pressure in Fig. 3. As we discussed the results previously, we only want to draw attention to the most important results in the context of this study. It becomes clear from Fig. 3 that for an area number density $\Gamma$ between $2.5^{10}$ and $5^{10}$ particles

per $m^2$, the equation of state is linear, whereas for higher area number densities $\Gamma$ and a surface pressure higher than 23 mN $m^{-1}$ the slope of the curves changes. Further compression of the interfacial layer to even higher surface coverage leads only to marginal increases of the surface pressure. The maximum surface pressure reached by lateral compression is around 28.5 mN $m^{-1}$. Interestingly, this surface pressure is only 1 – 2 mN $m^{-1}$ higher than the maximum pressure measured after spontaneous adsorption of core-shell particles onto the air-water interface (see Fig. 1). Note that all surface pressure curves displayed in Fig. 1 still exhibit a positive slope at $10^4$ seconds, meaning that surface coverage and surface pressure may increase further due to adsorption and interfacial re-organization of particles.

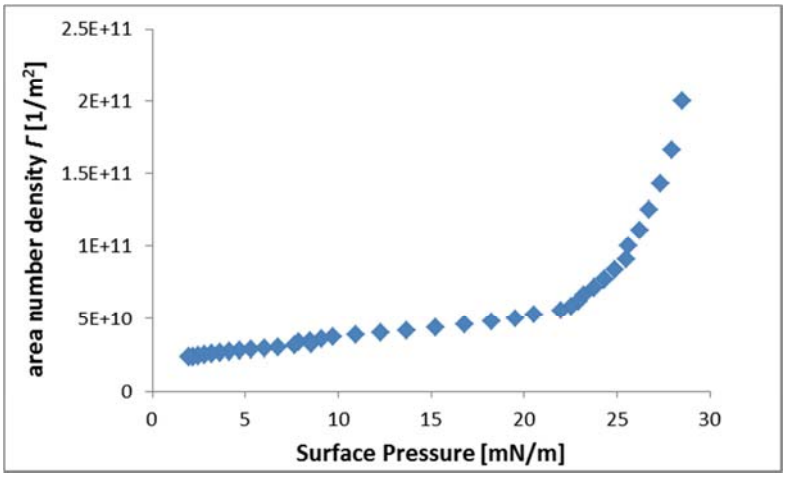


Fig. 3: Amount of adsorbed core-shell particles CS530 vs. surface pressure on an air-water interface, data are obtained by first spreading particles onto an air-water interface and subsequent measurement of the surface pressure upon compression of the interfacial area, data shown are the average of three experiments with a newly prepared particle layer - each consisting of three compression cycles

Knowledge of the 2D equation of state (see Fig. 3) provides us with the means to convert the surface pressure curves obtained by tensiometry into area number density $\Gamma$ vs time. The minimum surface pressure in Fig. 3 is around 2 mN $m^{-1}$. At this onset pressure there are already many particles at the interface. Only increasing the area number density $\Gamma$ above $2.5^{10}$ particles per $m^2$ results in a measurable surface pressure above the onset pressure. Thus, the curves displayed in Fig. 4, which give area number density $\Gamma$ as a function of $t^{0.5}$, start at an ordinate intercept of $2.5^{10}$ particles per $m^2$.

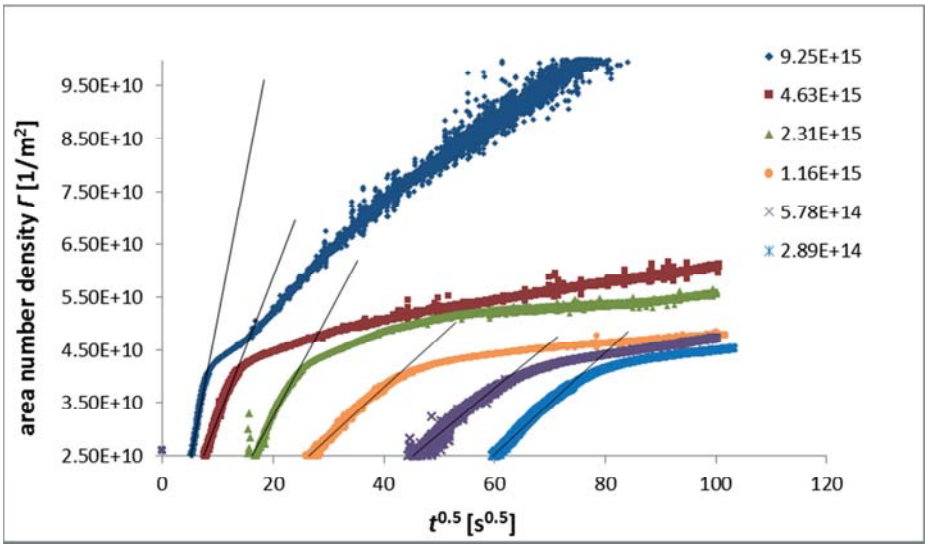


Fig. 4 area number density $\Gamma$ vs. square root of time $t^{0.5}$ for varying bulk concentration of core-shell particles CS530, the inset indicates the volume number density $c_\infty$ of the respective curve

As can be seen in Fig. 4, the first part of the curves in the range from $2.5^{10}$ to $4^{10}$ particles per $m^2$ can be fitted by a straight line. From this we can conclude that the initial increase in surface coverage is proportional to $t^{1/2}$, which is again in agreement with the Ward and Tordai model [7]. The slope of the fitted line corresponds to a rate constant which measures how fast particles at the respective bulk concentration $c_\infty$ adsorb at the air-water interface. The slopes of the lines fitted to the curves in Fig. 4 can be found in Tab. 1.

Tab. 1 volume number density $c_\infty$ vs. rate constants determined by fitting a linear equation to the curves in Fig. 4

| volume number density $c_\infty$ [ $1/m^3$ ] | rate constant $k_1$[ $1/(m^2 s^{0.5})$ ] |
|---|---|
| 9.25E+15 | 5.40E+09 |
| 4.63E+15 | 2.70E+09 |
| 2.31E+15 | 1.93E+09 |
| 1.16E+15 | 9.50E+08 |
| 5.78E+14 | 8.66E+08 |
| 2.89E+14 | 9.62E+08 |

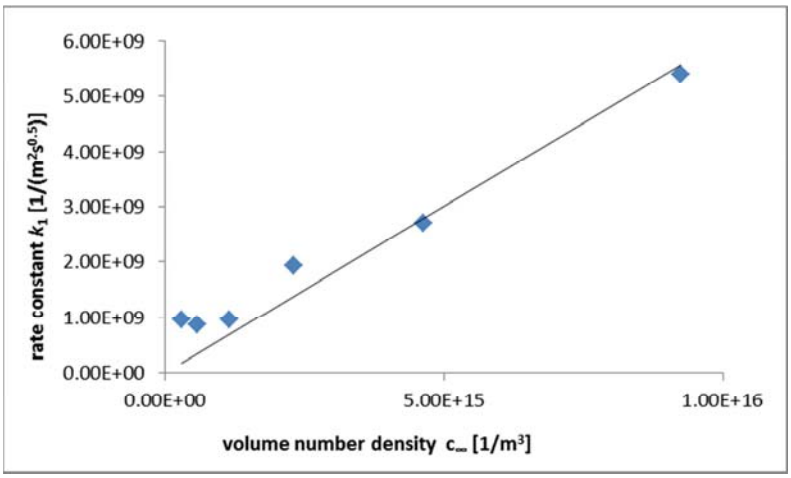


Fig. 5 Rate constant $k_1$ vs. volume number density $c_\infty$, data are taken from Tab.1 and plotted here for visualization and determination of a proportionality constant *m*

We also plot rate constants from Tab.1 as a function of $c_\infty$ and fit a linear curve (see Fig. 5). Although the fit is not very good, one may still assume a linear interdependence and fit a straight line with originates at the cross-over of abscissa and ordinate. From the slope *m* of this straight line the diffusion constant *D* which goes into equation 1 can be calculated. According to Ward and Tordai [7] the diffusion constant *D* is obtained as:

$$D = \left(\frac{m}{2}\right)^2 \pi \qquad (4)$$

With a slope m = 5.7E-07 µm/s$^{1/2}$ one obtains a diffusion coefficient D= 2.5E-13 µm$^2$/s. This is in line with the diffusion coefficient we obtained by dynamic light scattering $D_{DLS}$= 2.3E-13 µm$^2$/s. The above results suggest that the first stages of particle adsorption to the interface can be well described by the Ward and Tordai model.

In contrast, starting from $\Gamma \geq 4^{10}$ particles per m$^2$, equivalent to a surface coverage of 12 percent, particle adsorption to the air-water interface slows down markedly. The slowdown of the adsorption dynamics is probably attributed to the crowding of particles at the interface [9]. Insertion of new particles into the interface requires diffusion and interfacial reorganization of already adsorbed particles. In this stage insertion of new particles into the interface becomes hindered by an adsorption barrier [10, 11]. Under this condition particle adsorption to the already populated interface may be best described by first order kinetics, leading to equation 5:

$$\Gamma = \Gamma_{max}\,(1 - e^{-k_2 t}) \qquad (5)$$

Where $\Gamma_{max}$ corresponds to a fully covered interface and $k_2$ is a rate constant which characterizes the slow-down in the adsorption dynamics upon increasing the surface coverage. The inverse $1/k_2$ is the relaxation time of the system. $1/k_2$ can be thought of as the time it takes for reorganization of the particle covered interface before new particle from the bulk phase can be inserted.

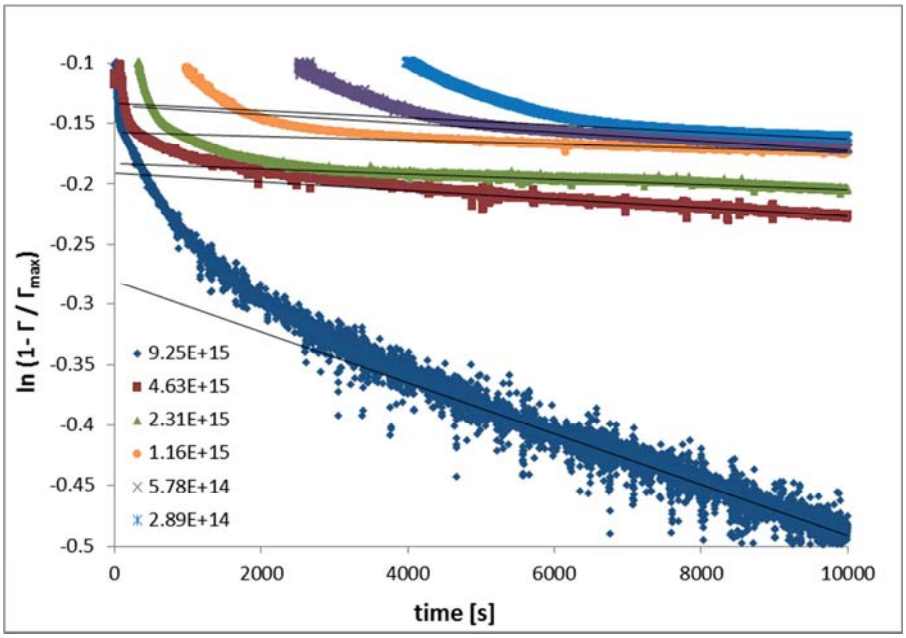


Fig. 6 Plot of $ln(1 - \Gamma/\Gamma_{max})$ vs. $t$ for varying bulk concentration of core-shell particles CS530, the inset indicates the volume number density $c_\infty$ of the respective curve, the solid straight line is the best linear fit at long adsorption times

Tab. 2 volume number density $c_\infty$ vs. rate constants $k_2$ determined by fitting linear equation to the curves in Fig. 6

| volume number density $c_\infty$ [ $1/m^3$ ] | rate constant $k_2$ [1/s] |
|---|---|
| 9.25E+15 | 2.00E-05 |
| 4.63E+15 | 4.00E-06 |
| 2.31E+15 | 2.00E-06 |
| 1.16E+15 | 2.00E-06 |
| 5.78E+14 | 4.00E-06 |
| 2.89E+14 | 3.00E-06 |

Plotting the adsorption data as $ln(1 - \Gamma/\Gamma_{max})$ vs. $t$ results into the curves displayed in Fig. 6. Long adsorption times can be fitted well to a straight line. We can conclude that at long adsorption times equation 5 can describe the experimental data very well. The slopes of the curves in Fig. 6 were determined and are given in Tab. 2 as rate constant $k_2$. For the highest bulk concentration $k_2$ is around one order of magnitude higher than for the other curves. The reason why this is so, is not clear. The $k_2$ values of the remaining curves in Fig. 6 differ only marginally. This behaviour was expected since $k_2$ depends on how fast the relaxation of the particle covered interface occurs. The speed of this relaxation process may be driven by the 2D interfacial diffusion as a main determinant, resulting in similar timescales for relaxation of the system, regardless of the bulk concentration $c_\infty$. This statement is valid only, if the surface coverages of the various systems are comparable. If not, the slope $k_2$ may decrease with increasing surface coverage due to crowding of particles which hinders self-diffusion [12]. For all the data in Fig. 6, except for the highest bulk concentration $c_\infty$, the surface pressure and surface coverage, at the point where a slowdown of the adsorption process is observed, are similar.

### 6.3.2. Assessment of particle desorption by droplet profile analysis tensiometry

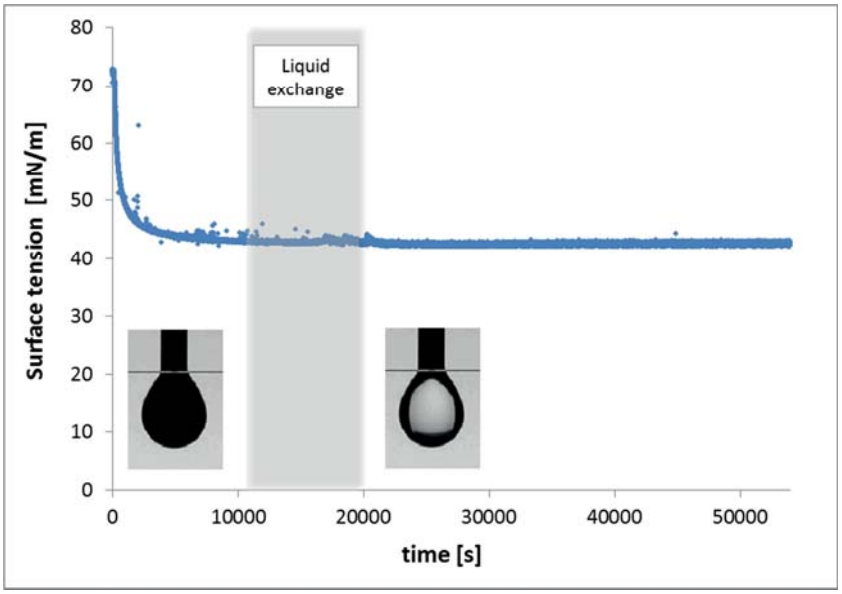


Fig. 7 Plot shows the evolution of surface tension $\sigma$ *vs. time t;* in the timeframe indicated by the grey box exchange of the bulk phase against salt solution takes place, insets show the appearance of the aqueous droplet before and after exchange of the bulk phase: before strong scattering can be observed while after the droplet appears transparent

In addition to determining particle adsorption rates, one may also investigate if particles desorb from the interface, and if so, at which rates they leave the interface. Particles are often supposed not to leave the interface spontaneously, but only experimental assessment can validate this assumption. In Fig. 7 we plot the evolution of surface tension $\sigma$ as measured by profile analysis tensiometry on a droplet containing core-shell particles. The surface tension $\sigma$ first decreases and then remains largely unchanged. At this point we exchange the bulk phase of the droplet by particle-free electrolyte solution, while following the surface tension $\sigma$. We observe that surface tension $\sigma$ remains unchanged. Hence, there is no sign of a dynamic equilibrium between particles in bulk solution and at the interface. Once adsorbed to the interface, particles remain there even if the bulk phase is depleted of particles. This is because due to their size, the particles possess a very high adsorption energy so that thermal energy cannot induce desorption from the interface [1]. Irreversible adsorption was also one of the requirements for application of the Ward and Tordai model [7]. We thus corroborate that the model is rightfully applied in the analysis of particle adsorption onto the air-water interface.

### 6.3.3. Determination of the interfacial structure of core-shell particles by scanning electron microscopy (SEM) and epi-illumination dark field microscopy

In the context of investigating the adsorption dynamics of core-shell particles onto the air-water interface one might wonder in which state core-shell particles adsorb to the air-water interface. Particles might adsorb in a polymeric fashion with polymer segments of the particle's shell attached to the fluid interface only. Alternatively, the whole core-shell particle may breach the interface leading to a state where a significant protrusion of the solid core into the non-polar phase can be ascertained. Alternative scenarios are possible too.

Given that the maximum surface pressure developed by the core-shell particles is 28 - 29 mN $m^{-1}$ (see Fig. 1) and this surface pressure is similar to the pressure developed by populations of PNIPAM based polymers [13] and PNIPAM based microgels at the air-water interface [14, 15], one might speculate that the interfacial behavior is dominated by the crosslinked PNIPAM shell and that core-shell particles adsorb in a polymer-like fashion at the air-water interface. However, we recently found by cryo-SEM shadow casting that core-shell particles are able to straddle the air-water interface and adopt a 'fried egg' like structure (Chapter 4). In order to confirm earlier results, we performed more cryo-SEM measurements. During these measurements we repeatedly find pictures like displayed in Fig. 8 where parts of the

interface are populated with core-shell particles breaching the interface, but the rest of the interface is covered with structures resembling polymer strands.

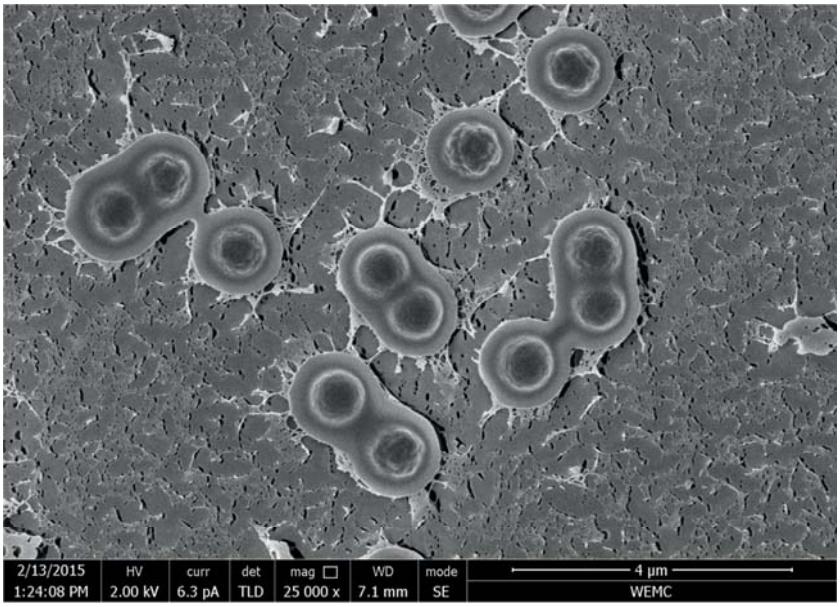


Fig. 8 SEM micrograph of core-shell particle at the air-water interface as obtained by cryo-SEM shadow casting technique, a sputter coating was applied under an angle of 45°, a visible shadow in the particles vicinity reveals that the particles protrude the air-water interface

In order to shed light on this issue we performed epi-illumination dark field microscopy. With this technique the signal produced is due to surface scattering of light rays which reach the interface under an oblique angle [16]. In Fig. 9 we can indeed observe two populations of signals, one of higher intensity and one of low intensity. The difference in intensity must mean that the two populations scatter different amounts of light. As the amount of scattered light is proportional to the specific scattering coefficient of the particles and the concentration of particles just at or above the interface, we reason that the two populations of different intensity correspond to two populations of particles with different interfacial configuration. Interestingly, also the g(r) of the populations differs from each other, with the bright, high intensity signals typically at larger distances from each other than the dark, low intensity signals (see Fig. 10). One might speculate that the high intensity signals correspond to core-shell particles where the solid core predominantly resides in the non-polar phase and which therefore experience a long-ranged electrostatic repulsion through the non-polar phase leading to larger interparticle distances. The other population, visible as low intensity signals in Fig. 9, may correspond to core-

shell particles where only parts of the particles PNIPAM shell are adsorbed to the air-water interface and the solid core predominantly resides in the aqueous phase.

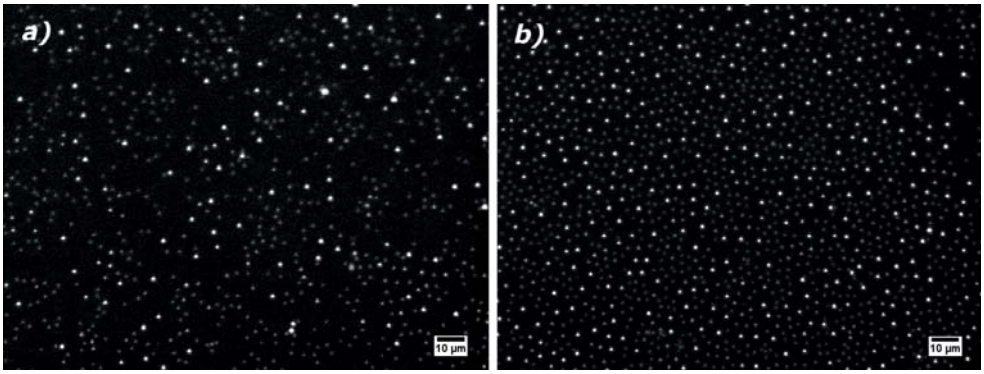


Fig. 9 Micrograph of core-shell particles at the air-water interface as obtained by epi-illumination dark field microscopy at different times (a) after 600s and (b) after 3600s

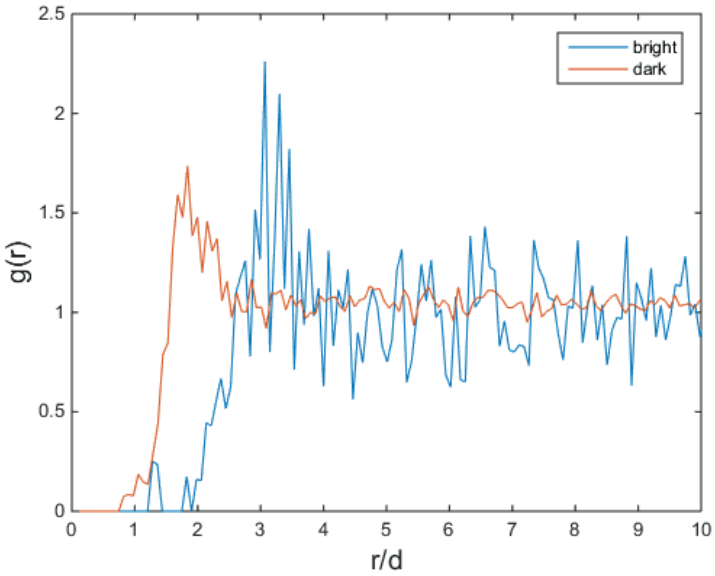


Fig. 10 Pair correlation function g(r) of the core-shell particles displayed in micrograph Fig. 9 (b), the g(r) of the two different populations of signals visible in Fig. 9 (b) is calculated separately and denoted as g(r) bright particles and g(r) dark particles

The question which arises is why two such populations of particles would exist, while for solid particles a rather well-defined contact angle and similar interfacial configuration of all particles is found [17, 18]. The reason might be the soft nature of the particle's shell. Capillary forces tend to deform the soft particles in order to maximize interfacial coverage. This spreading process stops once the energy gain

from covering additional interfacial area is counterbalanced by the energy needed for elastic deformation of the particle. As a net-result of these processes the interfacial free energy is lowered [5, 19].

As mentioned before, different interfacial configuration of core-shell particles can be envisioned. In the most favorable situation maximization of particle deformation must go along with minimization of the energy needed for elastic deformation of the material. Modelling of these processes is not straightforward, but one might envision that it is most favourable if the solid core resides mostly in either of the two phases adjacent to the interface and the soft polymeric shell occupies most of the air-water interface (see Fig. 11). Both situations may be equally favourable in terms of elastocapillary forces and can explain our experimental findings on the interfacial configuration of the core-shell particles.

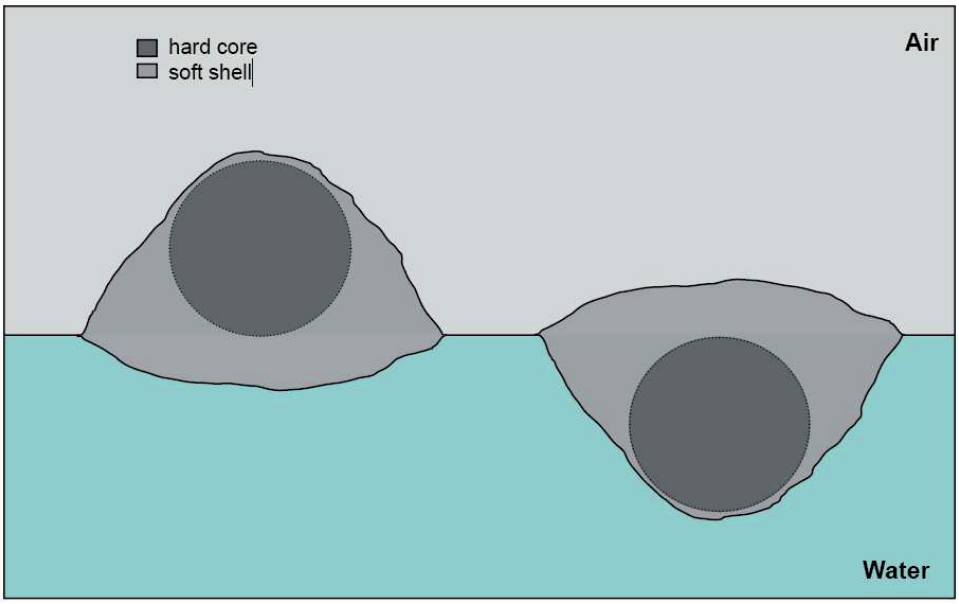


Fig. 11 Sketch showing two possible interfacial configurations of core-shell particles at the air-water interface

## 6.4. Conclusion

We analysed the adsorption dynamics of core-shell particles consisting of a solid polystyrene core and a soft PNIPAM shell. Previously we found that solely the PS core with a radius of 400 nm does not adsorb to the air-water interface. In this study we found that covering the PS core with a soft shell resulted in core-shell particles with an overall radius of 930nm and which are adsorbing much more readily at the

air-water interface. For short and long timescales we observed different behaviour. At short timescales we found that $\Gamma$ is proportional to $t^{1/2}$ and the rate of particle adsorption onto the interface is proportional to the particle bulk concentration $c_\infty$. Our experimental data were best described by the Ward and Tordai model. These results suggests that the first stages of particle adsorption to the air-water interface are indeed diffusion limited. At longer timescales the rate of interfacial adsorption slows down because part of the interface is already covered with particles which hinders insertion of new particles into the interface. The adsorption dynamics at long time scales are best described by an exponential decrease of the particle adsorption rates as the surface coverages increases.

Complete removal of all particles from the bulk phase does not cause desorption of particles from the interface, signifying that there is no dynamic equilibrium between particles in the bulk and particles adsorbed at the interface. This means that despite the spontaneous, barrier free adsorption of core-shell particles at the air-water interface, core-shell particle are irreversibly adsorbed there. Irreversible adsorption of particles is also one of the assumptions underlying the Ward and Tordai model, giving extra credibility to the application of this model for description of the particle adsorption dynamics at the air-water interface.

Microscopic analysis of the interfacial configuration of core-shell particles at the air-water interface reveals some peculiar insights. Two different populations of core-shell particles which apparently adopt different positions with respect to the air-water interface can be identified. We propose that the solid core can either residue below or above the interface, while the soft PNIPAM shell covers most of the air-water interface. Both situations may be equally favourable in terms of the elastocapillary forces involved, while minimizing the interfacial free energy.

## References


1. Binks, B.P., *Particles as surfactants - similarities and differences.* Current Opinion in Colloid & Interface Science, 2002. **7**(1-2): p. 21-41.
2. Tcholakova, S., N.D. Denkov, and A. Lips, *Comparison of solid particles, globular proteins and surfactants as emulsifiers.* Physical Chemistry Chemical Physics, 2008. **10**(12): p. 1608-1627.
3. Kaz, D.M., et al., Physical ageing of the contact line on colloidal particles at liquid interfaces. Nature Materials, 2012. **11**(2): p. 138-142.
4. Richtering, W., Responsive Emulsions Stabilized by Stimuli-Sensitive Microgels: Emulsions with Special Non-Pickering Properties. Langmuir, 2012. **28**(50): p. 17218-17229.

5. Style, R.W., L. Isa, and E.R. Dufresne, *Adsorption of soft particles at fluid interfaces.* Soft Matter, 2015. **11**(37): p. 7412-7419.
6. Maestro, A., et al., Particle and Particle-Surfactant Mixtures at Fluid Interfaces: Assembly, Morphology, and Rheological Description. Advances in Condensed Matter Physics, 2015. **2015**: p. 17.
7. Ward, A.F.H. and L. Tordai, Time-Dependence of Boundary Tensions of Solutions I. The Role of Diffusion in Time-Effects. The Journal of Chemical Physics, 1946. **14**(7): p. 453-461.
8. Li, Z., et al., Poly(N-isopropylacrylamide) microgels at the oil-water interface: adsorption kinetics. Soft Matter, 2013. **9**(41): p. 9939-9946.
9. Yong, X., Modeling the Assembly of Polymer-Grafted Nanoparticles at Oil–Water Interfaces. Langmuir, 2015. **31**(42): p. 11458-11469.
10. Isa, L., et al., Adsorption of core-shell nanoparticles at liquid-liquid interfaces. Soft Matter, 2011. **7**(17): p. 7663-7675.
11. Schwenke, K., L. Isa, and E. Del Gado, *Assembly of Nanoparticles at Liquid Interfaces: Crowding and Ordering.* Langmuir, 2014. **30**(11): p. 3069-3074.
12. Peng, Y., et al., Short-time self-diffusion of nearly hard spheres at an oil-water interface. Journal of Fluid Mechanics, 2009. **618**: p. 243-261.
13. Lee, L.T., B. Jean, and A. Menelle, Effect of Temperature on the Adsorption of Poly(N-isopropylacrylamide) at the Air–Solution Interface. Langmuir, 1999. **15**(9): p. 3267-3272.
14. Zhang, J. and R. Pelton, *Poly(N-isopropylacrylamide) Microgels at the Air−Water Interface.* Langmuir, 1999. **15**(23): p. 8032-8036.
15. Cohin, Y., et al., Tracking the interfacial dynamics of PNiPAM soft microgels particles adsorbed at the air–water interface and in thin liquid films. Rheologica Acta, 2013. **52**(5): p. 445-454.
16. Piller, H., *Microscope photometry*. 1977, Berlin [etc.]: Springer.
17. Paunov, V.N., Novel Method for Determining the Three-Phase Contact Angle of Colloid Particles Adsorbed at Air–Water and Oil–Water Interfaces. Langmuir, 2003. **19**(19): p. 7970-7976.
18. Horozov, T.S., et al., Novel Film-Calliper Method of Measuring the Contact Angle of Colloidal Particles at Liquid Interfaces. Langmuir, 2007. **24**(5): p. 1678-1681.
19. Mehrabian, H., J. Harting, and J.H. Snoeijer, *Soft particles at a fluid interface.* Soft Matter, 2016. **12**(4): p. 1062-1073.

# Chapter 7
# General Discussion

## 7.1. Performance of hard particles as interfacial stabilizers

Here we first discuss the results we obtained on hard particles as sole stabilizers for fluid interfaces. This part focusses on the application of hard particles for the stabilization of air bubbles. Yet, in some parts of this text we also refer to emulsion droplets, especially when the underlying concepts by which particles are stabilizing fluid interfaces are discussed.

### 7.1.1. Sonication for assembly of particle stabilized bubbles

The work described in this thesis started off with the primary aim to evaluate techniques for the production of particle-stabilized air bubbles. From there we had several options regarding the type of colloidal particle to be used and the technique applied for bubble creation. In an initial attempt to produce particle-stabilized dispersion, we decided to test an existing ultrasound set-up for the creation of particle-stabilized air bubbles (Chapter 2). Ultrasound offers the advantage that very small, submicron gas nuclei can be created through cavitation [1]. These submicron bubbles are expected to grow until enough surface active particles are adsorbed at the interface in order to grant stability against coalescence and Ostwald ripening. The typical size of the bubble dispersions produced in this way is expected to be much smaller than dispersions produced by conventional methods based on entrainment of air (via shaking or turbulent mixing) [2].

By applying ultrasound via a needle probe to a dispersion of micron-sized PS particles, we were indeed able to produce an appreciable amount of bubbles. The typical size of these bubbles was in the range of 10 – 100 µm (Chapter 2). In contrast, the same sonication set-up did yield protein-stabilized microbubbles below 1 µm in diameter [3]. Also, reference [2] reports on particle-stabilized bubbles ≤ 10 µm in diameter produced by a cavitation-based-method. The typical bubble size we obtained, thus, appears rather large.

In order to rationalize this result, one might ask if there is a minimum ratio between the radius of the disperse phase R and the particle radius r, and indeed there is. For bubbles, as well as droplets, stabilized by particles we can expect that the ratio between the radius of the dispersed phase *R* and the particle radius *r* is:

$$\frac{R}{r} \geq 10 \qquad (1)$$

In other words, the size of the particles must be significantly smaller than the size of the bubbles/droplets. This is because in the limit where the size of the disperse phase is close to the particle size, the particle adsorption energy declines strongly.

To illustrate why this is so, imagine a solid particle with a well-defined contact angle at an initially flat interface. Progressively increasing the radius of curvature of the interface around the particles will increase the interfacial area, the energy penalty to be paid for that reduces the particle adsorption energy [4, 5]. Given the fact that the minimum bubble size we obtained by our sonication approach is just one order of magnitude larger than the size of the colloidal particles we use for stabilization, we can conclude that with regards to the minimum bubble size the process parameters are not the limiting factor. It appears that the particle size limits the stabilization of even smaller bubbles. Future research shall aim to use smaller particles, perhaps nanoparticles, which may then enable the production of true microbubbles ($\leq$ 1 µm) via the needle probe sonication set-up we used.

The application of ultrasound to a particle dispersion can also lead to desorption of particles from a fluid interface, as recently shown by Poulichet et al. [6]. However, that happens only under a specific set of conditions; the effect is particularly pronounced when the bubbles are spatially confined and experience regular pressure variation. To a certain extent particle desorption from the interface might also occur with our experimental set-up. However, the fact that we are able to produce an appreciable amount of bubbles, means that interfacial assembly of particles prevails over particle desorption.

A seemingly more important factor which came into our attention was the efficiency of particle adsorption onto the fluid interface. We used particle dispersions with a dry matter content around 5 % w/w to produce bubbles by sonication. However, we noted that with our sonication approach the majority of PS particles remained in the bulk phase instead of adsorbing onto the fluid interface. From literature it is known that relatively high concentrations of particles are necessary to produce a particle-stabilized dispersion. This observation is often attributed to an energy barrier for interfacial adsorption of particles which manifests itself by a low probability for particles to stick to the fluid interface, so that a high concentration of particles is needed to successfully stabilize bubbles and droplets [7-9]. An alternative reason for the low adsorption probability to the air-water interface might be the transient contact between particle and fluid interface. Drainage of the liquid film between particle and interface might take more time (in comparison with the particles residence time near the interface) than available for forming a three phase contact line. The improved ability of higher concentrated particle dispersions (5% w/w) to stabilize fluid interfaces may be related to the increased viscosity of the liquid phase which leads to a longer contact time between particle and interface. Modification of bulk viscosity by addition on non-adsorbing polymers to the particle dispersion may therefore improve the efficiency of particle adsorption onto the air-water interface. Unfortunately, the effect of bulk phase viscosity on the amount of bubbles which can be created under an

otherwise specified set of condition has not been investigated here, but might be worth looking at.

### 7.1.2. Effect of electrolyte on the ability of hard particles to adsorb onto the fluid interface

Qualitatively we observed that electrolyte addition to the particle dispersion has a pronounced effect on the probability for particles to stick to the air-water interface. By sonication of a particle dispersion with added electrolyte in the bulk phase, a higher overrun, that is the percentage of incorporated air with respect to the liquid volume, was obtained than without electrolyte present. A similar trend was also observed if bubble creation was done via vigorous hand-shaking. We took this result as a confirmation that added electrolyte and/or also pH induced protonation of charged groups can promote particle attachment by screening repulsive electrostatic interaction between particle and interface [6, 7, 10].

Negative side effects of the increased electrolyte concentration are that it also impairs the colloidal stability of particles in the bulk phase, and that it weakens the electrostatic repulsion between individual particle-stabilized bubbles/droplets. In a situation where the aggregation stability of the particle stabilized bubbles/droplets is of interest, measures must be taken in order to grant stability despite the lack of electrostatic repulsion. Salari et al. found that addition of block-co-polymers which bind to the outer surface of particle stabilized emulsion droplets can prevent their aggregation [11]. It would be interesting, to investigate the effect of adsorbed polymer on the stability of particle stabilized dispersion against Ostwald ripening. While polymer addition can inhibit aggregation of the dispersed bubbles/droplets, it will certainly also alter the capillary interaction by which particles are held at the fluid interface. This in turn may alter their stability against phase separation.

Another unexpected observation we made is on the amount of electrolyte which is necessary to promote particle adsorption onto the fluid interface. The electrolyte concentration $c_{el}$ necessary to promote interfacial adsorption differed from particle type to particle type. More interestingly, in many case we found that $c_{el}$ should be well above 100mM NaCl. In some cases we found improved particle adsorption by increasing the electrolyte concentration to values above 400 to 500 mM NaCl. This discovery surprised us, because already at 100 mM NaCl a rather short electrostatic interaction range was expected. The typical length scale for electrostatic effects in electrolyte solution is given by the Debye length $\kappa^{-1}$.

$$\kappa^{-1} = \frac{\varepsilon_r \varepsilon_0 k_B T}{2 N_A e^2 I} \qquad (2)$$

where $I$ is the ionic strength of the electrolyte in mol $m^{-3}$, $\varepsilon_0$ is the dielectric permittivity of free space, $\varepsilon_r$ is the relative dielectric constant, $k_B$ is the Boltzmann constant, $T$ is the temperature, $N_A$ is the Avogadro number and $e$ is the elementary charge.

Based on equation 2 one obtains, for an electrolyte concentration $c_{el}$ of 0.1 mol $l^{-1}$ and a monovalent salt, a screening length around 1nm. Any electrostatic effects should be confined to this small length scale. In contrast, some of the interaction between an air-bubble and a colloidal particle are attractive, stemming from van der Waals forces or hydrophobic forces [12-14], and can be long-ranged [14]. We thus expected that the through addition of 0.1 mol $l^{-1}$ NaCl the electrostatic effects diminish and any remaining energy barrier in the particle-bubble interaction potential is sufficiently small to be easily overcome by the hydrodynamic forces occurring during bubble preparation. This hypothesis was proven to be wrong, since we often frequently found that electrolyte concentration well above 100 mM NaCl are necessary to facilitate particle adsorption onto the fluid interface. Similar observations were also made by other authors who found that up to 500 mM NaCl are necessary to promote particle assembly at the oil-water interface and prepare stable emulsion [6, 11, 15, 16]. The reason why these high concentration of electrolyte are necessary to promote particle adsorption to the fluid interface is unknown.

At this point it seems interesting to mention that also the 2D phase behaviour of interfacial particles can be altered by addition of electrolyte. In Fig. 1 one can observe that the 2D structure adopted by PS particles at the air-water interface gradually changes by increasing the electrolyte concentration in the subphase. With 1mM NaCl in the subphase particles are repelling each other. With 10 mM NaCl in the subphase particle interaction seems characterized by a long-range attraction with a short range repulsive component. At 1 M NaCl particles are completed attractive and clusters are visible. The important note is that 2D particle-particle interaction are sensitive to the electrolyte concentration in the bulk. As to why this electrolyte sensitivity arise is not completely clear either, but a coupling between the charges in the water immersed part of the particle and the resulting dipol-dipol interaction is likely.

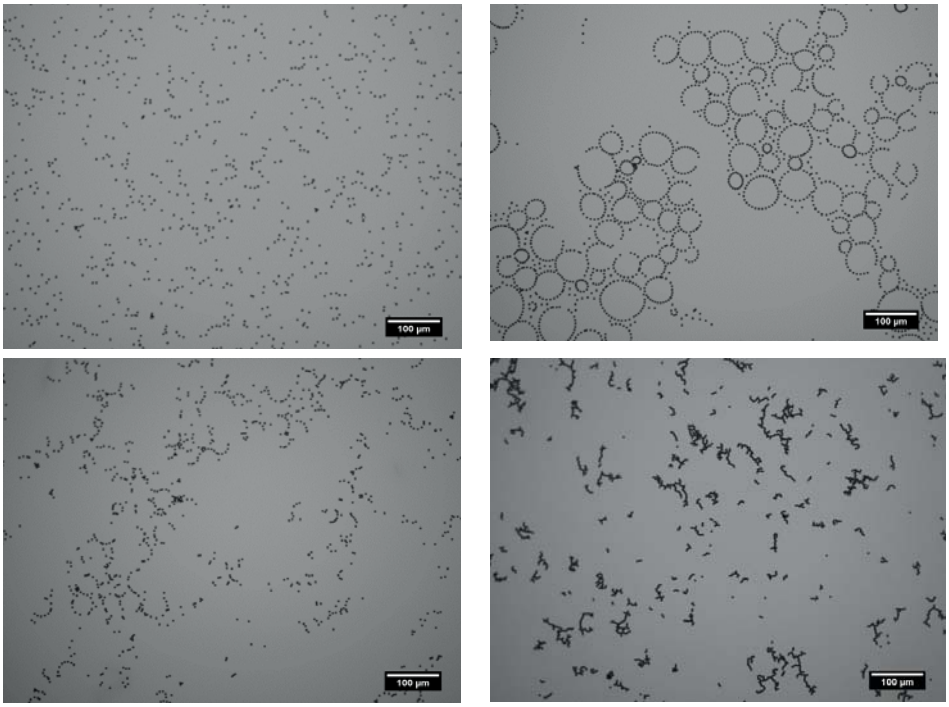


Fig. 1 Two-dimensional structure adopted by PS-sulfonate particles (4 µm diameter) at the air-water interface in the presence of varying amounts of electrolyte in the subphase, upper left: 1mM NaCl, upper right: 10 mM NaCl, lower left: 100mM NaCl, lower right: 1000 mM NaCl, scale bars of all images correspond to 100µm

### 7.1.3. Influence of particle wettability on the adsorption of hard particles onto fluid interfaces

Another factor which had a strong effect on the ability to produce particle-stabilized bubbles, by ultrasound as well as by hand-shaking, was the type of particle. We tested a variety of colloidal particles, from PS to silica particles, with diameters ranging from nm to µm. Particles also carried different surface functional groups. What is intriguing, is that no particle-stabilized bubbles could be produced with silica, while all the PS particles gave an at least satisfying performance as interfacial stabilizers for air bubbles. This observation signifies that particle wettability is of utmost importance for the ability of hard particles to strongly adhere to fluid interfaces. Only particles with intermediate wettability for both phases adhere strongly to the interface [8]. Silica particles are hydrophilic and reside mostly in the aqueous phase [17], while PS particles are more hydrophobic and adopt contact angles around 90°C at the air-water as well as oil-water interface [18]. Therefore PS particle are well suited to stabilize foams and emulsions [19-21]. It was also shown that silica particles can be hydrophobically modified through in-situ surfactant adsorption, as

well as by chemical modification, to increase their affinity for the fluid interface and to impart the ability to stabilize foams [22-24]. Surface wettability may not only affect adsorption energy at the fluid interface, it may even have an impact on the adsorption behaviour of particles to fluid interfaces, as we will outlay in the next paragraph:
The adsorption energy of particles at the fluid interface is given as:

$$\Delta E = \pi r^2 \sigma (1 \pm \cos\theta)^2 \quad (3)$$

where *n* is the number of adsorbed particles on the area *A,* $\sigma$ is the interfacial tension of the bare interface, *r* the particle radius and $\theta$ is the particle contact angle. For particles with a radius of a few nm, the particle adsorption energy at common fluid interfaces may be a few $k_BT$ only. With such a low adsorption energy, thermal energy can induce a displacement of the respective particles from the fluid interface. Presuming that the bulk is filled by two populations of equally-sized nanoparticles, interfacial adsorption is diffusion limited and the adsorption energy is in the range of several $k_BT$, a preferential segregation of the more hydrophobic particles with higher adsorption energy onto the fluid interface can be expected. This has been also confirmed by experiments with nanoparticles [25] and is based on altering the dynamic equilibrium between particle ad- and desorption. For larger, micron-sized particles such an effect is not expected as particles are assumed to adsorb irreversibly. Nevertheless, one could imagine that particle wettability can influence the magnitude and length scale of the hydrophobic or van der Waals interaction between particles and bubble/droplet. This in turn may impact the energy barrier for interfacial adsorption of particles and thereby lead to a different probability for certain particles to adsorb to the fluid interface. Similar discussion on the topic are also found in literature. Englert et al. showed by a combination of surface force measurements and theoretical modelling of the measured force curves that surface properties can modify the length scale of the hydrophobic forces and thereby alter the height of the energy barrier for interfacial adsorption [26]. HJ Butt measured a repulsive force between a hydrophilic silica particle and a bubble, whereas attractive forces could be measured between hydrophobic silica particles and a bubble. In the latter study the impact of surface modification on the electrostatic interaction is not clear, though [27]. Fielden et al. reported that the interaction between hydrophilic silica and an air bubble is monotonically repulsive, an attractive component at short distances could be induced by hydrophobic modification of the particle [28]. Based on the mentioned AFM measurements it appears that the surface properties of the particle can indeed impact the particle-bubble interaction potential and thereby influence the ability of a particle to adsorb to the fluid interface.

### 7.1.4. Surface pressure development due to particles adsorption at the fluid interface

With the aim to establish an elegant technique for testing if particles can spontaneously adsorb at a certain fluid interface, we decided to use drop shape tensiometry. The technique determines the surface tension by analysis of the bubble/droplet shape and is a standard technique to determine the surface activity of surfactants and polymers. For low molecular weight compounds the magnitude of the surface pressure initially follows a linear relation with respect to the amount of adsorbed material per unit area.

$$\Pi = \bar{R}T\frac{n}{A} \qquad (4)$$

where Π is the surface pressure, A is the area, n is the number of particles in moles, $\bar{R}$ is the ideal gas constant and T is the temperature of the system. For micron-sized particles equation 4 would predict surface pressures on the order of $10^{-6}$ mN $m^{-1}$, a value which is three to four orders magnitude lower than the surface pressures reported for compressed particle layers at the air-water or oil-water interface [29-33]. Equation 4 thus cannot represent the surface pressure development for micron-sized colloidal particles at the fluid interface. Aveyard et al. consequentially ascribes the surface pressure development of colloidal PS particles at the fluid interface to lateral interaction between adsorbed particles [31].

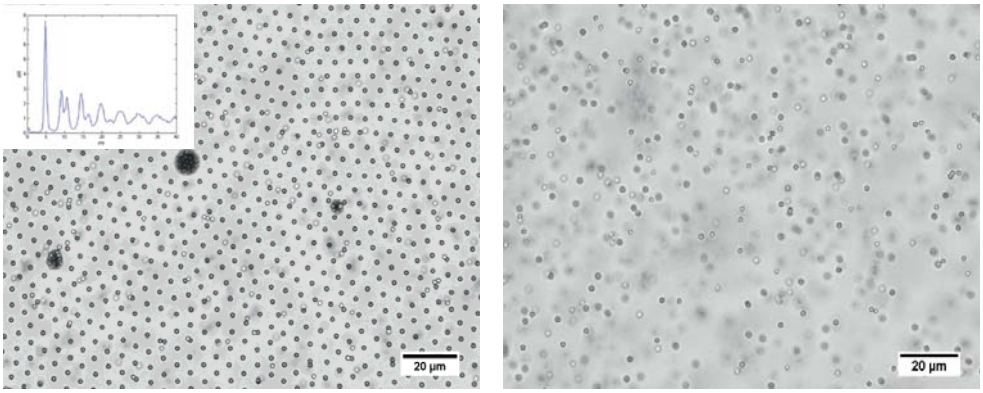


Fig. 2 Microscopic picture of colloidal PS particles at the air-water interface on a subphase of DI water (a) and the same particles dispersed in DI water (b)

An impression over the length scale of these interaction gives Fig. 2, which shows the structure of a particle monolayer at the air-water interface. The fact that the particles form a crystalline structure at the air-water interface serves as evidence that they repel each other strongly. The particles displayed in Fig. 2 experience lateral

repulsion at interparticle distances as large as five particle diameter. The general notion is that these pronounced long-ranged interaction arise due to electrostatic and dipol-dipol interaction [31, 34, 35]. Such a long-range interaction is not possible in water; even for particles being dispersed in deionized water and bearing high surface charges, the maximum range of electrostatic interaction is on the order of 100nm.

Given the relatively high surface pressures which can be developed by micron-sized colloidal assemblies at the fluid interface [29-33], it seemed certainly possible to detect particle adsorption at the fluid interface through tensiometry. We thus measured the surface pressure development of a range of different particle dispersion by drop shape analysis of a water droplet containing dispersed particles. We tested silica, PS and PMMA particles, all of which had diameters in the range from 800nm up to a few micrometres. Interestingly, we could not identify any particles which gave rise to a measureable surface pressure due to spontaneous adsorption at the air-water interface (see Chapter4 for PS particles). We tested also the influence of added electrolyte, up to 500 mM NaCl, on the particle's ability to cause spontaneous surface pressure development. Finally, we also tested uncharged particles with regards to spontaneous adsorption at the air-water interface. In none of the cases we measured a finite surface pressure.

One could now argue that particles were not hydrophobic enough to adsorb to the fluid interface and yield a finite pressure. We can give evidence that this is not the case though. PS particles which fulfil the partial wetting criteria at the air-water interface, which give a measurable pressure after lateral compression in a Langmuir through and which can stabilize air bubbles, do not yield a surface pressure when they are initially dispersed in the aqueous phase (see Fig. 3).

One could further argue that particles maybe adsorb to the fluid interface, but not yield a finite surface pressure, as this would require a high surface coverage, so that the particles experience lateral repulsion. Such a state may not be reached by spontaneous adsorption from the bulk. We also investigated this possibility by observing the air-water interface above a relatively concentrated particle dispersion, using reflected-light microscopy. We observed a few individual particles adsorbing to the air-water interface. However, the majority of diffusion driven particle approaches to the air-water interface did not led to particle adsorption. This could be concluded since particles came into focus when they reached the subsurface region, but then disappeared again. On timescales of 1-2 days we observed depletion of the subsurface region with particles, due to gravity induced sedimentation, but the particle surface coverage did not surmount 1%. Based on these results, we ascertain that hard particles cannot easily adsorb to a fluid interface. Breaching of the fluid interface seems characterized by a pronounced energy barrier, even for uncharged

(sterically stabilized) colloidal particles. We conclude that hard particle must be imparted with sufficient kinetic energy (e.g. by stirring) to breach the fluid interface.

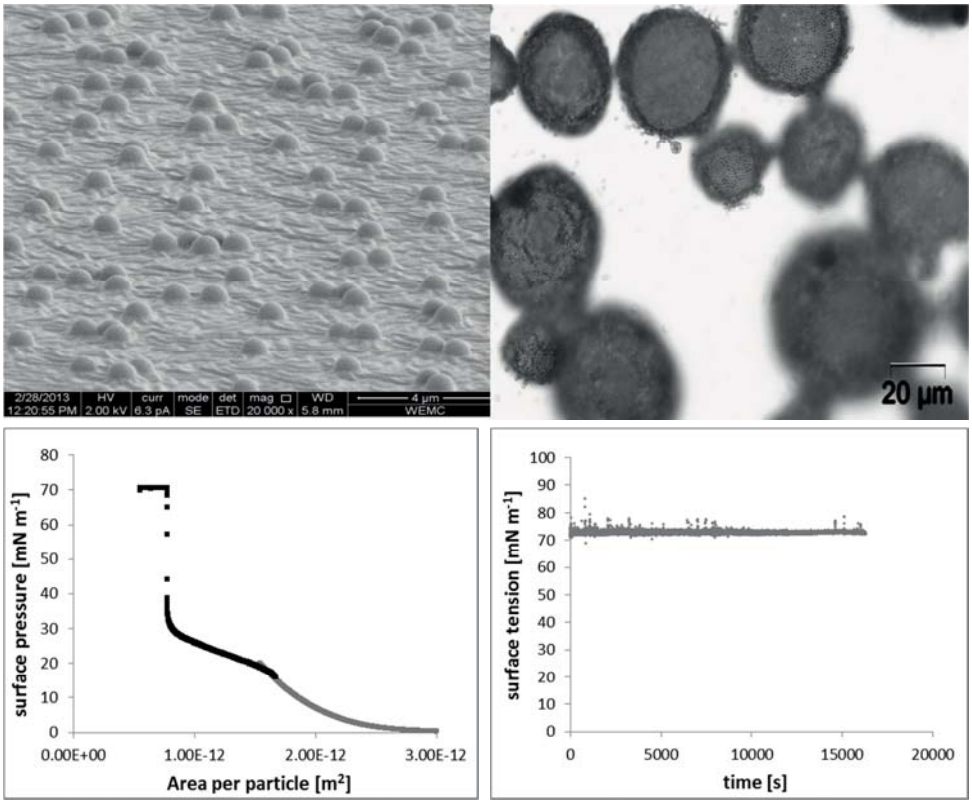


Fig. 3 Properties of cationic PS particles with radius of r=508nm at the air-water interface : immobilization via the gel trapping technique (upper left) provides evidence that particles show partial wettability for both phases, bubbles stabilized by the same particles (upper right), surface pressure evolution after spreading and subsequent compression of the particles in a Langmuir trough (lower left), surface tension of a particle dispersion with a concentration of 2.5 g $l^{-1}$ measured with drop-shape tensiometry (lower right)

### 7.1.5. Structure of bubbles/droplets stabilized by hard particles

During research for this thesis we exhaustively investigated the structure of particle stabilized bubbles by microscopy. In all cases we could ascertain that the bubble interface is covered by a closed-packed interfacial layer of particles, irrespective of particle size, charge and shape. This is in agreement with an earlier observation on particle stabilized bubbles prepared by microfluidics [36]. The formation of a colloidal amour on the bubble interface can thus be seen as a requirement for the efficient stabilization of gas bubbles against phase separation by Ostwald ripening and coalescence. In many cases the polydispersity of the particles was very low, as a result of which crystalline domains on the bubble interface emerged (Chapter 2).

The colloidal amour formed is thought to be solely held together by capillary interaction. Once particles are adsorbed at the air-water interface, a three-phase contact line is formed. Subsequent removal of the particle from the interface is energetically unfavourable as the interface must be substantially deformed before the particle can be pulled off. Even pronounced lateral interaction due to surface compression may not cause desorption of particles if their adsorption energy is very high [13, 37]. Desorption can be induced by surfactant addition, as the strong capillary forces are substantially lowered and the stresses on the bubble are relieved through particle release in the bulk, followed by bubble dissolution (Chapter 2).
As to how the colloidal amour is formed, we observed that during sonication or hand-shaking a partially covered bubble is formed. In the course of Ostwald-ripening and due to coalescences, bubbles attain a closed-packed interfacial layer which provides an excellent stability to air-bubbles and can stabilize them for years (as we observed with some samples which we kept on the bench for this long).

## 7.2. Performance of core-shell particles as interfacial stabilizers

Many of the aspects we discussed above on particle stabilized bubbles equally apply for disperse systems stabilized by core-shell particles comprising a hard PS core and a soft PNIPAM shell. We will confine the following discussion to aspects and properties of core-shell particles which are fundamentally different from the behaviour of homogenous hard particles. This discussion should lead to an understanding of the superior performance of this type of particles as interfacial stabilizers.

### 7.2.1. Adsorption of core-shell particles at fluid interfaces

Comparison of the adsorption behaviour of core-shell particles with PS “core only” particles, revealed pronounced differences between the two classes. While PS particles hardly adsorbed to any of the investigated fluid interfaces, the core-shell particles readily populated the air-water interface as well as the oil-water interface, regardless whether polar or apolar oils were used (Chapter 4). In this respect core-shell particles behave identically to pure PNIPAM particles which were also shown to adsorb at different fluid interfaces [38-40]. Our results show that for hard particles a pronounced energy barrier for interfacial adsorption exists, which is substantially lowered by the presence of the soft PNIPAM shell.
By investigating the adsorption kinetics of our core-shell particles in detail, we found that particle adsorption to the air-water interface is diffusion-limited. The rate

determining step for particle adsorption to the air-water interface is the diffusive transport of particles from the bulk to the interface. No barrier for interfacial adsorption exists, as long as the surface coverage is low. If the surface is already covered with a high amount of particles, a surface coverage dependent barrier for interfacial adsorption arises, as the presence of other particles make the insertion of an additional particle into the interface less likely (Chapter 6).

A question which arose in the context of this research was on the influence of the size of the PNIPAM shell on the ability of core-shell particles to spontaneously adsorb onto fluid interfaces. We presumed that there must be a critical shell dimension, above which particles spontaneously adsorb and below which particles do not adsorb to the fluid interface. By designing a variety of core-shell particles with shell dimensions in the range from 15nm to 530 nm, and analysing their adsorption at the air-water interface, we found a critical shell dimension around 167 nm (Chapter 4). As to why this critical dimension exists, we can speculate that it has to do with the softness of the PNIPAM shell. A small shell on top of a hard core might be less flexible than a large shell. A core-shell particle with small shell may therefore adsorb less easily to the fluid interface than a particle with large shell. Determination of the core-shell particles elastic modulus as function of radial distance to the core via AFM might confirm this hypothesis.

Another interesting, experimental approach might be to systematically alter the softness of the particle shell, by introducing different amounts of cross-links, while keeping the shell thickness constant. From such an experiment a critical elastic modulus of the shell, in other words, a critical softness, may be found which can ensure facile adsorption of particles onto the fluid interface.

The fact that particles could adsorb at all fluid interfaces, irrespective of the nature of the oil, appears to be in sharp contrast to the behaviour of hard particles (Chapter 4). For hard particles the general notion is that the surface properties determine whether a particle can adsorb at the fluid interface [22]. For the here investigated core-shell particles, however, the nature of the water-fluid interface does not play a dominant role for the particle adsorption at the fluid interface; in any case, particles adsorb.

### 7.2.2. Elastic properties of interfacial layers covered by core-shell particles

#### 7.2.2.1. Air-water interface

By determination of the maximum surface pressure developed after spontaneous adsorption of core-shell particles at the air-water interface, we found that all core-shell particles gave a similar surface pressure around 26 mN $m^{-1}$ (Chapter 4). This surface pressure is very close to the surface pressure developed by PNIPAM

polymers at the air-water interface under good solvent condition [41, 42]. This suggests that the surface pressure arises due to overlap of the peripheral PNIPAM segments on the core-shell particles. This hypothesis was further supported by cryo-SEM pictures which showed that at the air-water interface, next to the actual core-shell particles, a continuous, polymer-like structure is visible (Chapter 6). These polymer like strands are most likely polymer chains which are emerging from the surface of individual core-shell particles and form an interface spanning network, giving rise to a surface pressure. Similar findings on the origin of the surface pressure development of PNIPAM microgels were reported by Destribats et al. [43]. In conclusion, it appears that the surface pressure development of microgels and of our core-shell particles is based on the same physical origin, on the steric interaction between the particle's peripheral PNIPAM chains.

Analysing the compression isotherm of the core-shell particles given in Chapter 5 gave further evidence that the behaviour of core-shell particles at the air-water interface is dominated by the PNIPAM shell. For compressional strains up to 40 % (starting from the point where the surface pressure diverges), we determined a low-frequency dilational modulus of at most 27 mN $m^{-1}$ for all core-shell particles. This value is close to the maximum dilatational elastic modulus we estimated from the data of Deshmukh et al. for PNIPAM microgels at the air-water interface [38].

The compressional modulus of the interface is presumably linked to the mechanical properties of the adsorbed material [44]. In the limit of large compressional strains (>> 40% starting from the point where the surface pressure starts to diverge) we thus expected the hard core to influence the response of the core-shell particles. However, we did not find evidence for that. For larger core-shell particles the elastic modulus declined strongly upon application of large strains, indicating collapse of the 2D particle layer. Core-shell particles with a shell dimension of 167 nm, behaved somewhat differently. Even by application of large strains, the compressional elastic modulus remained constantly high until a surface pressure of around 53 mN $m^{-1}$ was reached. Note, the dilational elastic modulus of the these core-shell particles did not exceed 27 mN $m^{-1}$, while hard core particles yield values of ~ 100 mN $m^{-1}$ (Chapter 5).

It can be concluded that the core-shell particles with appropriate shell thickness (here the sample with shell thickness of 167nm) can indeed combine spontaneous adsorption with the ability to withstand high surface pressures. The compressional response of core-shell particles seems dominated by the PNIPAM shell, though. We did not find evidence that the core contributes to the mechanical response to interfacial compression. The fact that core-shell particles of intermediate size (with a shell dimension of 167 nm) can built up higher surface pressures than the larger ones (with a shell dimension of 230 nm and 530nm), may be related to the more cohesive

structure of the 2D particle layers of medium sized core-shell particles, in comparison with the open structure adopted by larger core-shell particles (Chapter 5).

#### 7.2.2.2. Oil-water interface

As we did not have a Langmuir trough available which is suitable for the study of oil-water interfaces, we attempted to investigated the behaviour of core-shell particles at the oil-water interface with a tensiometer based on drop shape analysis. By adsorption of core-shell particles on the interface of a hanging oil-in-water droplet and subsequent size reduction of the oil droplet by sucking oil out of it, we could observe that a non-spherical droplet shape arises. Further, we found that upon interfacial adsorption of core-shell particles and subsequent application of large compressional strains, the surface tension can become as low as 5 mN $m^{-1}$. For large strains, right before a non-spherical droplet arises, we estimate a dilational modulus of 100 mN $m^{-1}$ based on the tensiometric data (data not shown). All these observations show that the dilational response of core-shell particles at the oil-water interface is similar to the typical interfacial behaviour of hard (polystyrene) particles.

### 7.2.3. Tuning the dilational response of particle-laden fluid interfaces

The microgels investigated in this study contained functional groups which can be protonated and deprotonated in response to the pH. By protonating the anionic functional groups, the PNIPAM shell swells, and vice versa. This shall alter the softness, *i.e.* the bulk elastic modulus, of the particles PNIPAM shell. The bulk elastic modulus of the particles, in turn, is expected to be proportional to the dilational modulus of fluid interfaces covered by core-shell particles [44].

We found an inverse relation between the dilational response of a particle covered air-water interface and the pH of the bulk phase. At pH 3 we found a maximum dilational modulus of 43 mN $m^{-1}$, which decreased to 27 mN $m^{-1}$ at pH 6 and to 18 mN $m^{-1}$ at pH 12 (data not shown). The decreasing dilational modulus indicates a decreasing bulk elastic modulus of the PNIPAM shell, the particle shell seems to becomes softer with increasing pH.

These results clearly show that the rheological properties of interfaces covered by core-shell particles can be tuned. The inverse relation between the dilational modulus and pH, underlines once more that steric interactions are responsible for the surface pressure created by our core-shell particles. For electrostatic interaction the opposite behaviour would have been expected.

### 7.2.4. Stability of particle stabilized dispersions

Dispersions of air and various oils in water were prepared with core-shell particles as sole interfacial stabilizers. Air bubbles could be stabilized by core-shell particles, while the hard PS particles did not yield any bubbles at all, even when high concentrations of electrolyte where present in the bulk. Upon storage, the bubble dispersions underwent phase separation, though, and disappeared in a time frame of 2-3 days. At all times bubbles remained spherical, showing that surface tension dictated the bubble shape. This observation indicates that stabilization is different from classical Pickering stabilization: it appears that core-shell particles adsorb at the bubble interface in a polymer like fashion, with the PNIPAM shell attached to the interface while the hard core probably predominantly reside in the water or air phase. This conclusion is further supported by our findings on the dilational response of air-water interfaces covered by core-shell particles.

For oil-in-water dispersions a remarkably different behaviour was ascertained. Core-shell particles were able to provide stability against phase separation for a variety of different oil-in-water emulsions. For polar oils it was found that the droplet surface undergoes an evolution from an initially partially covered to a close-packed interface. Once particles are jammed at the interface, phase separation is arrested. Jamming of the interface is apparent from the often non-spherical emulsion droplets which are formed by polar oil drops. The non-spherical droplet shapes suggest that the surface tension vanishes, as supposed to occur for Pickering emulsions stabilized by hard particles.

## 7.3. Performance of core-shell particles as interfacial stabilizers in comparison to hard particles

A remarkable property of the from us synthesized core-shell particles is their ability to adsorb at a variety of different fluid interfaces. No apparent energy barrier exists for interfacial adsorption of core-shell particles. This will be an advantage if low energy input processing methods are to be used for production of fluid dispersions. It also eliminates the need to add high concentrations of electrolyte to promote interfacial adsorption, as necessary for hard particles, and thereby ensures that particles in the bulk maintain colloidal stability (avoid flocculation).

The ability of core-shell particles to stabilized fluid dispersion depends on the type of fluid interface under consideration. At the air-water interface their behaviour does not resemble that of hard particles. In terms of dispersion stability and in terms of surface activity, their properties resemble that of PNIPAM-only microgels. In contrast, at the oil-water interface particles strongly anchor even at high surface pressures. The high rigidity of the hard core provides enough resistance to stop Ostwald ripening and

support non-spherical droplet shapes. The facile preparation and high stability of oil-in-water emulsions signifies that core-shell particles can combine the advantageous properties of soft particles, i.e., barrier free adsorption, with the ability of hard particles to form a colloidal armour around the oil droplet and stop phase separation.

## References


1. Santos, H.M., C. Lodeiro, and J.-L. Capelo-Martínez, *The Power of Ultrasound*, in *Ultrasound in Chemistry*. 2009, Wiley-VCH Verlag GmbH & Co. KGaA. p. 1-16.
2. Raut, J.S., et al., *Hydrodynamic cavitation: a bottom-up approach to liquid aeration.* Soft Matter, 2012. **8**(17): p. 4562-4566.
3. Rovers, T.A.M., et al., *Temperature is key to yield and stability of BSA stabilized microbubbles.* Food Hydrocolloids, 2016. **52**: p. 106-115.
4. Aveyard, R., J.H. Clint, and T.S. Horozov, *Solid particles as emulsion stabilisers*, in *Molecular Organisation on Interfaces*, G. Lagaly, Editor. 2002, Springer Berlin Heidelberg: Berlin, Heidelberg. p. 11-18.
5. Zeng, C., H. Bissig, and A.D. Dinsmore, *Capillary interactions among spherical particles at curved liquid interfaces.* Solid State Commun., 2006. **139**: p. 547.
6. Poulichet, V. and V. Garbin, *Ultrafast desorption of colloidal particles from fluid interfaces.* Proceedings of the National Academy of Sciences, 2015. **112**(19): p. 5932-5937.
7. Tcholakova, S., N.D. Denkov, and A. Lips, *Comparison of solid particles, globular proteins and surfactants as emulsifiers.* Physical Chemistry Chemical Physics, 2008. **10**(12): p. 1608-1627.
8. Binks, B.P., *Particles as surfactants - similarities and differences.* Current Opinion in Colloid & Interface Science, 2002. **7**(1-2): p. 21-41.
9. Gillies, G., M. Kappl, and H.-J. Butt, *Direct measurements of particle–bubble interactions.* Advances in Colloid and Interface Science, 2005. **114–115**(0): p. 165-172.
10. Park, J.I., et al., *Titelbild: A Microfluidic Approach to Chemically Driven Assembly of Colloidal Particles at Gas–Liquid Interfaces (Angew. Chem. 29/2009).* Angewandte Chemie, 2009. **121**(29): p. 5321-5321.
11. Salari, J.W.O., J. van Heck, and B. Klumperman, *Steric Stabilization of Pickering Emulsions for the Efficient Synthesis of Polymeric Microcapsules.* Langmuir, 2010. **26**(18): p. 14929-14936.
12. Israelachvili, J.N., *Chapter 13 - Van der Waals Forces between Particles and Surfaces*, in *Intermolecular and Surface Forces (Third Edition)*. 2011, Academic Press: San Diego. p. 253-289.
13. Preuss, M. and H.-J. Butt, *Direct measurement of forces between particles and bubbles.* International Journal of Mineral Processing, 1999. **56**(1–4): p. 99-115.

14. Eriksson, J.C., S. Ljunggren, and P.M. Claesson, *A phenomenological theory of long-range hydrophobic attraction forces based on a square-gradient variational approach.* Journal of the Chemical Society, Faraday Transactions 2: Molecular and Chemical Physics, 1989. **85**(3): p. 163-176.
15. Golemanov, K., et al., *Latex-Particle-Stabilized Emulsions of Anti-Bancroft Type.* Langmuir, 2006. **22**(11): p. 4968-4977.
16. Binks, B.P. and J.A. Rodrigues, *Inversion of Emulsions Stabilized Solely by Ionizable Nanoparticles.* Angewandte Chemie International Edition, 2005. **44**(3): p. 441-444.
17. Reed, K.M., *Wettability of solid particles in relation to particle-stabilised foams and emulsions*, in *Department of Chemistry*. 2011, The University of Hull.
18. Paunov, V.N., *Novel Method for Determining the Three-Phase Contact Angle of Colloid Particles Adsorbed at Air−Water and Oil−Water Interfaces.* Langmuir, 2003. **19**(19): p. 7970-7976.
19. Binks, B.P. and S.O. Lumsdon, *Pickering Emulsions Stabilized by Monodisperse Latex Particles: Effects of Particle Size.* Langmuir, 2001. **17**: p. 4540.
20. Du, Z., et al., *Outstanding Stability of Particle-Stabilized Bubbles.* Langmuir, 2003. **19**(8): p. 3106-3108.
21. Aveyard, R., B.P. Binks, and J.H. Clint, *Emulsions stabilised solely by colloidal particles.* Advances in Colloid and Interface Science, 2003. **100**: p. 503-546.
22. Gonzenbach, U.T., et al., *Ultrastable Particle-Stabilized Foams.* Angewandte Chemie International Edition, 2006. **45**(21): p. 3526-3530.
23. Binks, B.P. and T.S. Horozov, *Aqueous foams stabilized solely by silica nanoparticles.* Angew Chem Int Ed Engl, 2005. **44**(24): p. 3722-5.
24. Cervantes Martinez, A., et al., *On the origin of the remarkable stability of aqueous foams stabilised by nanoparticles: link with microscopic surface properties.* Soft Matter, 2008. **4**(7): p. 1531.
25. Lin, Y., et al., *Nanoparticle Assembly and Transport at Liquid-Liquid Interfaces.* Science, 2003. **299**(5604): p. 226-229.
26. Englert, A.H., et al., *Interaction forces between a deformable air bubble and a spherical particle of tuneable hydrophobicity and surface charge in aqueous solutions.* Journal of Colloid and Interface Science, 2012. **379**(1): p. 121-129.
27. Butt, H.-J., *A Technique for Measuring the Force between a Colloidal Particle in Water and a Bubble.* Journal of Colloid and Interface Science, 1994. **166**(1): p. 109-117.
28. Fielden, M.L., R.A. Hayes, and J. Ralston, *Surface and Capillary Forces Affecting Air Bubble−Particle Interactions in Aqueous Electrolyte.* Langmuir, 1996. **12**(15): p. 3721-3727.
29. Schuller, H., *Modellversuche zur Spreitung von Kolloid-Partikeln.* Kolloid-Zeitschrift und Zeitschrift für Polymere. **216**(1): p. 380-383.
30. Bykov, A.G., et al., *Dilational surface elasticity of spread monolayers of polystyrene microparticles* Soft Matter, 2014. **10**: p. 6499.

31. Aveyard, R., et al., *Compression and Structure of Monolayers of Charged Latex Particles at Air/Water and Octane/Water Interfaces.* Langmuir, 1999. **16**(4): p. 1969-1979.
32. Sheppard, E. and N. Tcheurekdjian, *Monolayer studies.* Journal of Colloid and Interface Science, 1968. **28**(3): p. 481-486.
33. Lenis, J., et al., *Mechanical Stability of Polystyrene and Janus Particle Monolayers at the Air/Water Interface.* Journal of the American Chemical Society, 2015. **137**(49): p. 15370-15373.
34. Danov, K.D. and P.A. Kralchevsky, *Interaction between like-charged particles at a liquid interface: Electrostatic repulsion vs. electrocapillary attraction.* Journal of Colloid and Interface Science, 2010. **345**(2): p. 505-514.
35. Pieranski, P., *TWO-DIMENSIONAL INTERFACIAL COLLOIDAL CRYSTALS.* Physical Review Letters, 1980. **45**(7): p. 569-572.
36. Subramaniam, A.B., M. Abkarian, and H.A. Stone, *Controlled assembly of jammed colloidal shells on fluid droplets.* Nat Mater, 2005. **4**(7): p. 553-556.
37. Preuss, M. and H.-J. Butt, *Measuring the Contact Angle of Individual Colloidal Particles.* Journal of Colloid and Interface Science, 1998. **208**(2): p. 468-477.
38. Deshmukh, O.S., et al., *Equation of state and adsorption dynamics of soft microgel particles at an air-water interface.* Soft Matter, 2014. **10**(36): p. 7045-7050.
39. Li, Z., et al., *Poly(N-isopropylacrylamide) microgels at the oil-water interface: adsorption kinetics.* Soft Matter, 2013. **9**(41): p. 9939-9946.
40. Brugger, B., B.A. Rosen, and W. Richtering, *Microgels as stimuli-responsive stabilizers for emulsions.* Langmuir, 2008. **24**(21): p. 12202-8.
41. Kawaguchi, M., Y.-i. Hirose, and T. Kato, *Effects of Temperature and Concentration on Surface Tension of Poly(N-isopropylacrylamide) Solutions.* Langmuir, 1996. **12**(14): p. 3523-3526.
42. Lee, L.T., B. Jean, and A. Menelle, *Effect of Temperature on the Adsorption of Poly(N-isopropylacrylamide) at the Air−Solution Interface.* Langmuir, 1999. **15**(9): p. 3267-3272.
43. Destribats, M., et al., *Soft microgels as Pickering emulsion stabilisers: role of particle deformability.* Soft Matter, 2011. **7**(17): p. 7689-7698.
44. Cohin, Y., et al., *Tracking the interfacial dynamics of PNiPAM soft microgels particles adsorbed at the air–water interface and in thin liquid films.* Rheologica Acta, 2013. **52**(5): p. 445-454.

# Summary

Many recent studies in interfacial science have investigated the use of hard particles, such as polystyrene (PS) or silica particles, for stabilization of aqueous foams and emulsions. Applying hard particles for stabilization of disperse systems is referred to as Pickering stabilization. Such particle-stabilized dispersion are characterized by an extraordinary high stability against coalescence and can completely stop Ostwald ripening. The high stability arises due to the formation of a jammed interfacial layer of hard particles which shows an elastic response to compression. A difficulty is the preparation of particle stabilized dispersion, as hard particles often experience a pronounced energy barrier for interfacial adsorption. Besides, the ability of hard particles to stabilize fluid dispersion depends on the affinity of the particles for the fluid interface. Being able to stabilize a certain fluid dispersion requires to find the right particle type or careful modification of the particles surface chemistry. Addition of other surface active substances to the fluid dispersion can completely impair dispersion stability as the particles affinity for the fluid interface might be altered.

Soft particles, such as cross-linked polymeric particles made of poly-N-isopropylacrylamide (PNIPAM), are also known as good stabilizers for emulsions. PNIPAM particles are intrinsically surface active, their adsorption onto fluid interfaces is barrier-free. They form densely covered interfacial layers which provide very good stability against coalescence and whose viscoelastic properties can slow-down Ostwald ripening. Soft particles are less specific with regards to the type of fluid interface they can adsorb to. PNIPAM particles can stabilized a variety of different emulsion types.

In this PhD thesis we prepared core-shell particles with a PS core and a PNIPAM shell to obtain particles which can combine the advantageous properties of hard and soft particles, namely, being intrinsically surface active at a variety of different fluid interfaces, strongly adsorb to the fluid interface and being able to completely stop Ostwald ripening. We investigated the interfacial properties of these core-shell particles with the aim to use them as sole stabilizers for foams and emulsions.

In Chapter 2 we focus on the use of entirely hard PS particles for stabilization of air bubbles. We show how ultrasound exposure to a dispersion of solid PS particles leads to the formation of air bubbles which are stabilized by a jammed interfacial layer of particles. The resulting particle-stabilized bubbles do not show any signs of coarsening over several weeks. We further show that particles are held at the fluid interface by capillary interaction which can be weakened by surfactant addition and lead to rapid bubble dissolution. The information over the structure and properties of bubbles stabilized by hard particles serve as comparison for fluid dispersion stabilized by core-shell particles as investigated in the other chapters of this thesis.

In Chapter 3 we describe the two-step synthesis of core-shell particles with a hard PS core and a soft PNIPAM shell functionalized with methacrylic-acid (MA). We obtain

core-shell particles with varying core/shell size ratios (radius core/radius shell) in the range of 0.04 up to 1.33 and of low polydispersity. We find that the soft PNIPAM shell provides steric barrier against particle aggregation and can ensure colloidal stability even at a very high electrolyte concentration of 300 mM NaCl, while charge-stabilized PS core particles aggregate at such high electrolyte concentrations. Despite the presence of the hard core, the core-shell particles show responsiveness to temperature, pH and electrolyte concentration. Especially pronounced is the effect of temperature. At temperatures of 60 °C the measured hydrodynamic radius of the core-shell particles is only slightly larger than the radius of the core particles, suggesting that upon heating most of the water is expelled from the PNIPAM shell. Addition of electrolyte in the range of 1 – 20 mM NaCl leads to a reduction of the particle radius, higher electrolyte concentration only result in a negligible size reduction. Lowering the pH up to pH 3 also leads to a particle size reduction.

In Chapter 4 we show that the prepared core-shell particles can adsorb at a variety of different fluid interfaces such as the air-water and decane-water interface, while the PS core particles do not adsorb under the same experimental condition. We find that core-shell particles are able to develop a high surface pressure of 26 – 27 mN $m^{-1}$ after adsorption from the bulk to the air-water interface. Further, we investigated the influence of the thickness of the soft PNIPAM shell on the ability of core-shell particles to adsorb to the air-water interface. We found that a shell thickness well above 100 nm ensures facile interfacial adsorption, while core-shell particles with smaller shell appear to experience a certain energy barrier for interfacial adsorption. The absence of a pronounced energy barrier for interfacial adsorption of core-shell particles with a thick shell also allowed it to easily produce bubbles and emulsion droplets stabilized by core-shell particles. The resulting bubbles still underwent Ostwald ripening. For oil-in-water emulsions of hexane and toluene, both of which have a relatively high solubility in the continuous phase, we find that core-shell particles can stop Ostwald ripening. The observation of very stable, non-spherical emulsion droplets suggest that next to their facile adsorption to the fluid interface, core-shell particles can perform in a similar way as entirely hard particles as interfacial stabilizers for emulsion droplets.

In Chapter 5 we spread a known amount of core-shell particles at the air-water interface and measure the surface pressure arising due to the presence of core-shell particles upon compression in a Langmuir trough. We obtain a pressure-area isotherm which can be interpreted as an equation of state. We find that core-shell particles can develop a finite surface pressure at a surface coverage as low as 0.05. The low-frequency dilational elastic moduli as inferred from the compression isotherm are comparable to the values as reported for entirely soft, PNIPAM particles without a solid core. The maximum surface pressure developed by core-shell particles upon

lateral compression is a function of the shell thickness. For core-shell particles with a large shell (with a shell dimension of 230 nm and 530nm) the maximum surface pressure upon compression in the Langmuir trough amounts to 29 mN $m^{-1}$ which is close to the surface pressure measured after spontaneous adsorption from the bulk onto the air-water interface. Core-shell particles with a smaller shell dimension of 167 nm yield a maximum surface pressure of 53 mN $m^{-1}$ upon compression, which is much higher than the value of 29 mN $m^{-1}$ measured after spontaneous adsorption to the air-water interface, but equal to the maximum surface pressure measured for the hard PS core particles upon compression in the Langmuir trough. The differences found for core-shell particles with thin and thick PNIPAM shells may be attributed to the different interfacial structures. Core-shell particles with a shell dimension of 167 nm as well as core particles are strongly aggregated at the air-water interface. We suppose that this aggregation gives rises to a more cohesive particle layer with a higher mechanical stability which can accordingly resist a higher surface pressure.

In Chapter 6 concerns the detailed investigation of the adsorption dynamics of core-shell particles at the air-water interface. Tensiometry is used to measure the dynamic surface tension of core-shell particle dispersions. The obtained data are converted into adsorption rates with the pressure-area relationship established in Chapter 5. We find that at short timescales $\Gamma$ is proportional to $t^{1/2}$ and the rate of particle adsorption onto the interface is proportional to the particle bulk concentration $c_\infty$. Our experimental data can be best described by the Ward and Tordai model. This confirms that at short timescale were the surface coverage is low, the adsorption of core-shell to the air-water interface is diffusion limited. At long timescales, the increased surface coverage prevents the insertion of new particles into the interface, particle adsorption rates are reduced. We also proof that despite their spontaneous adsorption to the air-water interface, core-shell particles do not spontaneously desorb again. Finally we show that the spontaneous adsorption of core-shell particles results in two populations of core-shell particles with different interfacial configuration. We presume that this dual interfacial structure is an elastocapillary phenomenon.

In Chapter 7 we summarize the most important findings of this thesis. We discuss the properties and performance of hard particles as stabilizers for the bubble dispersions we prepared by sonication. Thereafter, we discuss the properties of core-shell particles as interfacial stabilizers for bubbles and emulsion droplets. We especially focus on the differences between hard particles and core-shell particles with respect to interfacial adsorption, lateral interaction between particles at the interface and the ability to stop Ostwald ripening.

## Acknowledgement

The last years, during which the work leading to this thesis has been done, were the most exciting, informative and enjoyable in my whole life. This positive experience is to a large extent the result of the immense professional and moral support I have been getting by my colleagues, friends and family. The support of all of you was invaluable and helped me to finalize my doctoral thesis without much pain and hassle.

I would like to thank Dr Marcel Meinders who lead the project as part of which this research has been carried out. Thanks for giving me the possibility to join the team of foam experts. Thanks for always having an open door to walk in and discuss scientific and non-scientific issues. With your positive mind-set you have helped me to keep motivated throughout the project. Your critical view towards scientific results helped me to shape this thesis in the proper way. Unforgettable for both of us will be your citation to a certain book: the golden standard on particles at interface.

Many thanks also to Dr Hans Tromp. I appreciate your scientific reasoning and your out-of-the-box thinking skills. Many times you gave an important impetus to our scientific discussion and you were also the one who could tell when it is the proper time to finalize our team meetings. Thanks for your scientific advices, for critically reviewing my manuscripts and for being honest and fair. Your special way of humour, always combined with a hint of sarcasm, made me laugh a lot and is something I will always remember about you.

The third person who made an important professional contribution to this work is my promotor, Prof. Dr M.A. Cohen Stuart. Thanks for taking over the responsibility to be my promotor in the first place. It was a great honour to be guided by such an experienced and distinguished scientist. Thanks for sharing you immense experience with me. Especially noteworthy is your contribution in the last stage of the PhD, when you were the one who kept me motivated and pushed the work to an end. I will be always grateful to you.

An important contribution to my professional development was given by our regular discussion among the “foam project” members: Frederic, Tijs, Min, Franklin, Eric, Ruud and Guido. Thanks for the good times. It was amazing to explore and discuss all possible aspect of foam and interface science together with you. The entire range of scientific aspects regarding foam and interface science covered by our team was impressive and gave me the chance to get a broad overview of the field.

My gratitude also goes to my Fysko friends & colleagues who gave an important support throughout my PhD research. Mara, Josie, Anita and Renko: you were the first ones I got in touch when starting my work at Fysko and you paved my way throughout the PhD. Frans, it was a great pleasure to work with you during the colloid science practical course. Not only was it an invaluable professional experience to share and discuss my thoughts with you, but it was also great fun. Simeon, thanks for taking time to discuss scientific results and share you immense experience in interface science. Although I felt we only saw each other a couple of times during these many years, it made an important contribution. Hans, I want to thank you for taking time to discuss the fundamentals of colloid science with you. You were always friendly, welcoming and open to discussions; I admire that. Dmitry and Huanhuan: thanks for the infinite discussions on emulsion science and particles at interfaces. I wish you all the best for your academic careers. Helene and Jeroen, thanks for our discussions and sharing the newest success stories out of the colloid kitchen. Sabine, Yunus and Armando: it was a great experience to organize the PhD trip to California with you. Jacob: we do not only had a similar professional background, we also shared the same kind of humour. I enjoyed having you around. I wish you all the best and hope to see you together with your family in a free standing house soon. Gosia: my dear officemate and friend for so many years. It was great to share this time with you. I am happy that you found your next professional challenge already and wish you lots of exciting adventures with your family in the future. I could go on forever... Many thanks to: Anton, Antsje, Bert, Cecilia, Celine, Chris, Diane, Dirk, Duc, Esio, Evan, Frank, Gosia, Hande, Hanne, Hannie, Harke, Herman, Ilse, Inge, Jan Maarten, Jasper, Joanne, Johan, Joris, Joshua, Juan, Kamuran, Katarzyna, Lennart, Lione, Liyakat, Maarten, Marcel, Marleen, Merve, Mieke, Monika, Nadia, Natalia, Paulo, Peter, Prachi, Rahim, Ran, Remco, Rene, Rojman, Ronald, Ruben, Soumi, Surrender, Thao, Ties, Tingting, Willem and Wolf.
Fysko, it was great to be part of such a dynamic group!

My gratitude also goes to my friends and colleagues from Food Physics. Thanks to Harry and Miranda for the support during the experimental work at the Axis building. Harry, Miranda, Els, Erik, Leonard, Paul, Elke, Alev, Anika, Auke, Carsten, Claire, Jinfeng, Kun, Pauline, Vaida, Costas and Maria. Thanks all of you for supporting me in many different ways. It was great fun to work with you.

Thanks to all my friends who may not have been involved in my research, but which gave their support during the entire time of the PhD. Here is the result of the hard work which kept me busy during the last couple of years.

Vielen Dank an meine Eltern, Bärbel und Wolfgang, und an Tante Elvira, Onkel Detlef und Heike für eure Unterstützung während meiner gesamten Ausbildung und darüber hinaus. Ich bin überaus dankbar für alles was ihr für mich getan habt. Ihr habt nicht gefragt wie lange es noch dauert bis ich mit meiner Doktorarbeit fertig bin, sondern ihr habt allzeit fest damit gerechnet, dass alles zu einem guten Ende kommen wird.

Thanks to my family in Costa Rica and Colombia. Maria, Edgar, Sergio and Diana, Edgar Augusto, Ernesto, Lorena, Aura, Edgar Antonio and Shafik: thanks for your continuous interest in my work and thanks for all the support. Maria, my special gratitude goes to you for your extended trips to Netherlands during which you have been taking care of all of us.

The most important contribution to the successful completion of my PhD was made by my family.
Sofia Isabella and Hanna Amira: the two of you made me smile even during the gloomiest days. I am curious what you will remember about this time. It will be probably the gummy bears waiting in my office for you.
Indira: Thanks for your endless support in all different ways and thanks for taking care of our children at all times when I had to do the many “small” experiments during weekdays, in the evenings and in the weekends. Without you I could have not finished this thesis. To finish this book, it is our success story. I want to keep writing many more success stories with you. Where our path is going, we do not know yet, but as long as we are together, it does not really matter to me. Let us enjoy what is ahead of us.

## Scientific Publications

C Buchcic, RH Tromp, MBJ Meinders and MA Cohen Stuart, Assembly of jammed colloidal shells onto micron-sized bubbles by ultrasound, Soft Matter, 2015

C Buchcic, RH Tromp, MBJ Meinders and MA Cohen Stuart, Characterization of the multi-stimuli-responsive properties of polystyrene-poly(N-isopropylacrylamide) core-shell particles, Manuscript in preparation

C Buchcic, RH Tromp, MBJ Meinders and MA Cohen Stuart, Harnessing the advantages of hard and soft colloids by use of core-shell particles as interfacial stabilizers, Manuscript in preparation

C Buchcic, RH Tromp, MBJ Meinders and MA Cohen Stuart, Equation of state of core-shell particles adsorbed at the air-water interface , Manuscript in preparation

C Buchcic, RH Tromp, MBJ Meinders and MA Cohen Stuart, Adsorption dynamics and interfacial structure of core-shell particles at the air-water interface, Manuscript in preparation

## Overview of completed training activities

**Discipline specific activities**

European School on Rheology, Leuven, Belgium, 2013
Summer School "Enrico Fermi" on Physics of Complex Colloids, Varenna, Italy, 2012
Food Structure and Rheology, Wageningen, The Netherlands, 2012
Microbubble Symposium, Leeds, UK, 2011
Microscopy and Spectroscopy, Wageningen, The Netherlands, 2012
School Colloids&Interfaces, Max Planck Institute of Colloids and Interfaces, Potsdam, Germany, 2013
Foam summer school, University Paris Sud, France, 2013
Student Colloid Conference, Potsdam, Germany, 2013
Workshop on Dynamics of Fluid Interfaces, ETH Zürich, Switzerland, 2014
Course Particle Characterization, Augsburg, Germany, 2011
Training period, Surfactant and Colloid Group, University of Hull, UK, 2012
Short course on Rheology, Ede, The Netherlands, 2011
AFM Training course by Bruker, Karlsruhe, Germany, 2013

**General courses**

VLAG PhD week, Baarlo, The Netherlands, 2012
Information Literacy/Endnote, Wageningen, The Netherlands, 2011
Essentials of Scientific Writing and Presenting, Wageningen, The Netherlands, 2011
Course Scientific Artwork, Wageningen, The Netherlands, 2011
Course Intellectual property organized by Top Institute Food and Nutrition, Wageningen, The Netherlands, 2012
Project Management (TIFN Kickoff meeting), Wageningen, The Netherlands, 2011

**Optionals**

Preparation of Research Proposal, 2011
Organization PhD Excursion US, 2013
PhD Excursion, US, 2013
Group meeting Fysko, 2011- 2014
Work meetings TIFN, 2011 – 2015
Visit Nestle Research, Lausanne, Switzerland, 2013

The work described in this thesis was performed at the Laboratory of Physical Chemistry and Soft Matter at Wageningen University, The Netherlands.

The research described in this thesis was financially supported by the Top Institute Food & Nutrition, Wageningen, The Netherlands.

Financial support from Wageningen University and Top Institute Food & Nutrition for printing this thesis is gratefully acknowledged.

Cover design: Indira Moreno Echeverri

This thesis was printed by Digiforce, Vianen, The Netherlands.